The Space Cowboys

Glacies Nova: The Mars Expedition

2021 AIAA Space Design Competition

Faculty Advisor: Adam Nokes

Team Members: Ali Attarwala, Alexander Chiu, Kelly Heilman, Katherine Layton, Samuel Luttrull, Kalman Mahlich, Michael Martinets, Kristen Pallesen, Sreeteja Pampati

The University of Texas at Austin
Department of Aerospace Engineering and Engineering Mechanics

The Space Cowboys Members

Member	AIAA # & Signature	Member	AIAA # & Signature
 Ali Attarwala	1230177 *Ali Attarwala*	 Kalman Mahlich	1230083 *Kalman Mahlich*
 Alexander Chiu	1230066 *Alexander Chiu*	 Michael Martinets	1230061 *Michael Martinets*
 Kelly Heilman	1230110 *Kelly Heilman*	 Kristen Pallesen	1069820 *Kristen Pallesen*
 Katherine Layton	998846 *Katherine Layton*	 Sreeteja Pampati	1230400 *Sreeteja Pampati*
 Samuel Luttrull	998778 *Samuel Luttrull*	 **Faculty Advisor:** Adam Nokes	*Adam Nokes*

Table of Contents

List of Acronyms

3DOF	=	Three-Degree of Freedom
AIAA	=	American Institute of Aeronautics & Astronautics
ADCS	=	Attitude Determination & Control System
AIT	=	Assembly, Integration, & Test
C3	=	Characteristic Energy
CBE	=	Current Best Estimate
C&DH	=	Command & Data Handling
CER	=	Cost Estimating Relationship
CDF	=	Cumulative Distribution Function
COPV	=	Composite Overwrapped Pressure Vessel
DGB	=	Disk-Gap-Band (Parachute)
DOF	=	Degrees of Freedom
DSN	=	Deep Space Network
ECLSS	=	Environmental Control and Life Support System
EDL	=	Entry, Descent & Landing
ESA	=	European Space Agency
FPA	=	Flight Path Angle
GNC	=	Guidance, Navigation & Control
HGA	=	High Gain Antenna
IOC	=	Initial Operating Capability
ISS	=	International Space Station
ISRU	=	In-Situ Resource Utilization
IMU	=	Inertial Measurement Unit
LASSO-M	=	Low-Mass Acquisition System for Samples in Orbit of Mars
LGA	=	Low Gain Antenna
MAV	=	Mars Ascent Vehicle
MLE	=	Mars Landing Engine
MLI	=	Multi-Layer Insulation
MMOD	=	Micrometeoroid and Orbital Debris

MMRTG	=	Multi-Mission Radioisotope Thermoelectric Generator
MOCET	=	Mission Operations Cost Estimation Tool
MRN	=	Mars Relay Network
MRO	=	Mars Reconnaissance Orbiter
MSL	=	Mars Science Laboratory
NASA	=	National Aeronautics & Space Administration
NTO	=	Nitrogen Tetroxide
OSIRIS-REx	=	Origins, Spectral Interpretation, Resource Identification, Security, Regolith Explorer
PCEC	=	Project Cost Estimating Capability
PDF	=	Probability Density Function
PICA	=	Phenolic Impregnated Carbon Ablator
PLF	=	Payload Fairing
R&D	=	Research and Development
RAM	=	Random Access Memory
RCS	=	Reaction Control System
RFP	=	Request for Proposal
SPHERES	=	Synchronized Position Hold, Engage, Reorient, Experimental Satellites
SPURS	=	System for Production of Under Regolith Samples
SRC	=	Sample Return Capsule
SRP	=	Supersonic Retropropulsion
TGO	=	Trace Gas Orbiter
TPS	=	Thermal Protection System
TRN	=	Terrain Relative Navigation
TT&C	=	Telemetry, Tracking, & Control
USCM8	=	Unmanned Space Vehicle Cost Model, Eighth Edition
UDP	=	Universal Docking Port
USD	=	United States Dollars
VDC	=	Volts of Direct Current
WBS	=	Work Breakdown Structure

List of Figures

List of Tables

1. Executive Summary

In recent years, as the National Aeronautics & Space Administration (NASA) and private space companies have improved and expanded access to space, mission planners have begun setting their sights on Mars and beyond. One of the primary challenges of establishing a human presence on Mars is finding ample quantities of resources critical to sustaining life, such as water. Closer examination of the water currently on Mars could also provide new insights into the existence of past or present life on the red planet. Several robotic missions have already discovered and analyzed Martian ice deposits in-situ. However, retrieving an ice sample and returning it to Earth would further our understanding of the ice's chemical makeup because the capabilities of terrestrial labs far outpace anything that can be delivered to Mars using our current technology and resources. This paper presents a proposed architecture for a dedicated robotic mission to acquire and return Martian ice samples to Earth.

The name of this mission is *Glacies Nova*, which translates to "new ice" in Latin. The Terra Nova Expedition was one of the first expeditions to explore the Antarctic here on Earth. We wanted to evoke the spirit of exploring untouched lands, as we attempt to design the first mission to bring back ice from another planet.

Overall, the primary goals of this mission are threefold. First, the mission seeks to return ice core samples from Mars to Earth to increase our understanding of the chemical makeup of Martian ice deposits and the possibility of past or present life on Mars. Second, it is also meant to enhance our knowledge of the nature and history of water on Mars and the potential for its use as part of an In-Situ Resource Utilization (ISRU) system for future missions. Finally, this mission will help improve our familiarity with the Martian environment to pave the way for future crewed missions and an eventual self-sustaining human presence on Mars.

The specific requirements for the mission were provided by the American Institute of Aeronautics and Astronautics (AIAA). These requirements describe the design of a robotic system that can travel to Mars, extract ice core samples, and then safely return to Earth. The mission must return at least 2.5 kg of ice cores in a frozen state before December 31st, 2030. The end-to-end mission costs must also be less than $1 Billion USD in total.

Due in large part to these cost and time constraints, the mission architecture consists of a spacecraft launched as a single unit aboard a reusable Falcon Heavy rocket. The launch vehicle deploys the approximately 4400 kg spacecraft directly into a Mars intercept trajectory with a characteristic energy of up to 10 km^2/s^2. After separation from the launch vehicle, the spacecraft deploys its solar panels and spins up to dynamically stabilize itself for cruise.

The spacecraft is composed of the LASSO-M orbiter and a Mars entry aeroshell (which in turn contains the SPURS lander and descent stage). During transit to Mars, LASSO-M (Low-mass Acquisition System for Samples in Orbit of Mars) serves as a cruise stage and provides power, propulsion, GNC, and communications for the mission components stowed in the entry capsule. The orbiter itself has a dry mass of 518 kg and carries 1302 kg of propellant, providing a total ΔV capacity of 3.9 km/s. It is powered by a single main engine that runs on hypergolic monomethyl hydrazine and nitrogen tetroxide (MMH/NTO). A set of 12 monopropellant MMH thrusters provide attitude control and propulsion for minor maneuvers and station keeping. The orbiter is powered by two large solar wings that provide a total output of 2000 W at the mean orbital radius of Mars and is equipped with X-Band High and Low Gain Antennas for communications with Earth and other existing spacecraft in orbit around Mars. Attached to the side of the orbiter is the Sample Return Capsule (SRC), which stores the samples during transit back to Earth.

Just prior to arrival at Mars, pyro bolts are fired to separate the orbiter from the Mars entry aeroshell. The aeroshell performs direct EDL to its landing site on the surface of Mars while the orbiter diverts course above the Martian atmosphere and fires its main engine just enough to capture into a stable, highly elliptical orbit. The capture orbit is polar with its apoapsis situated above the Martian north pole so that the orbiter will spend more time in view of the lander and less time shadowed by Mars from Earth and the Sun.

Within the entry capsule is the SPURS (System for Production of Under-Regolith Samples) lander attached to a descent stage very similar to those which landed *Curiosity* and *Perseverance* on Mars. After bleeding most of its velocity via drag, the aeroshell deploys a parachute and jettisons its heat shield. Once its onboard radar has identified an acceptable landing site, the descent stage drops away from the aeroshell and delivers the lander to the targeted landing site in the Milankovič crater. The expected landing ellipse is 7x13 km and is located at a latitude of 55.1° N and a longitude of 146.6° W. Terrain relative navigation will allow the descent stage to avoid hazards within the target ellipse and set the lander down within reach of ice deposits that have been detected by instruments aboard current Mars orbiters. Past Martian missions such as *Phoenix* and *Odyssey* have confirmed the presence of shallow ice deposits in the region, allowing for easy access for our robotic drilling system. The selected landing site has ample sunlight in the early days of the mission, permitting the use of solar panels on the lander. The final sols of the mission period see decreased solar incidence, but during this time the lander stays in a low power sleep mode awaiting a window for launching samples to orbit. It will still be operable with the lower power output from its solar panels.

The lander consists of a hexagonal chassis made up of composite sandwich panels with a flat equipment deck on top. It stands on three legs made of telescoping aluminum tubes with honeycomb crush cores. Situated in the center of the deck is an insulated shroud that contains the Mars Ascent Vehicle (MAV), protecting it from damage during EDL and providing passive insulation to reduce the power needed to keep the propellant and electronics warm. The lander is equipped with two static solar arrays tilted 45° to the south to improve power generation at the lower solar angles during the later portions of the mission. Power from these arrays is stored in two lithium-ion batteries. It is also equipped with a set of three antennas – Ultra High Frequency (UHF), X-Band High Gain, and X-Band Low Gain – that allow the onboard computers to communicate with Earth via the Mars Relay Network (MRN) and the Deep Space Network (DSN).

The main function of the lander is to provide a platform for the sample acquisition and handling system. The system is equipped with a coring drill capable of drilling cylindrical cores 5 cm in diameter and 15 cm in length. The drill is based on the technology demonstrated by the rotary percussive drill on *Perseverance*. The drill is situated on a hand turret at the end of a 2 m long, 5 degree of freedom robotic arm, and can reach a total drilling area of approximately 6 m^2. The drill is equipped with an embedded temperature sensor, and its RPM is modulated to ensure that the drilling process does not generate enough heat to melt the ice and risk refreezing, which could lock the drill in place. Within the drill's coring bit is a sample tube held by a retention mechanism that allows the filled tubes to be inserted by a plunger into a designated transfer cradle, getting hermetically sealed in the process. The sealed samples are then stowed into the sample container by a second handling arm on the deck of the rover. The sample container is insulated by aerogel panels and is equipped with redundant vapor compression cooling loops for scenarios where active cooling is needed. Each sample has a mass of 270 g, meaning that a total of 10 cores need to be extracted to satisfy the 2.5 kg sample mass requirement. The sample container has slots for 12 tubes - space for the 10 required samples along with one for contingency and one for a witness tube, which is sealed without a sample inside to act as a control for any unexpected results.

While the lander is carrying out operations on the ground, the orbiter slightly lowers the periapsis of its elliptical orbit into the Martian atmosphere and gradually aerobrakes to lower its apoapsis. After approximately 6 months, it boosts its periapsis back up to a circular, 200 km altitude orbit. The use of aerobraking saves several hundred kilograms of

propellant, without which the single launch mission architecture would not be feasible within the budget constraints, as a more expensive launch vehicle (such as a Delta IV Heavy or Expendable Falcon Heavy) would be required.

Once ground operations are complete and the orbiter is in position, the sample container is launched from Mars aboard the MAV. The MAV is a two-stage solid fueled rocket capable of delivering just over 22 kg of payload to a 200 km circular orbit. It is equipped with a set of cold nitrogen gas thrusters that allow it to maintain attitude while in orbit. It is powered by a set of primary batteries that are not engaged until lander separation and has a small onboard UHF and low gain X-band communication system that allows it to coordinate with the orbiter for docking. The launch window is chosen such that the orbiter is above the horizon at launch and never loses line of sight of the MAV prior to docking. Once on orbit, the MAV maintains attitude while the orbiter maneuvers to rendezvous. The SRC on the side of the orbiter opens to reveal a docking adapter, which then mates with the complementary adapter on the front of the sample container. The SRC is like the capsules used in the *Stardust* and *OSIRIS-Rex* missions but scaled up by 50% to accommodate a larger payload. Internally, the SRC is modified to include optical sensors to facilitate docking as well as coolant reservoirs and tubing to support the active thermal control needed to prevent the samples from heating above their melting point during Earth entry.

Once docking is complete and the remainder of the MAV is jettisoned, the orbiter performs a trans-Earth injection burn and cruises back to Earth. The SRC remains open for the duration of this phase to allow the radiators surrounding the sample container to reject heat into space. The attitude of the spacecraft is controlled to keep the samples shaded from sunlight, except when maneuvers, communications, or other factors may require otherwise. During periods where the capsule must be exposed to solar radiation, active cooling remains available via the container's vapor compression loop, which helps maintain thermal control. As the spacecraft approaches Earth, the heatshield of the SRC closes and it is released on a direct entry trajectory. The remainder of the spacecraft diverts itself into a heliocentric orbit. The SRC enters the atmosphere, deploys its parachutes, and lands softly on the ground for retrieval. The batteries in the SRC allow for its locating beacon to broadcast for at least 24 hours after landing, giving crews ample time to find and recover the samples. The selected landing site will be near an Arctic research station such as Barrow Observatory in Northern Alaska. The landing is anticipated to occur in June 2030, when the average high temperature in the area is from 1-7°C (lows remain at or below freezing) and it receives nearly constant sunlight. There tends to be no snow cover in the region and precipitation probabilities (primarily for rain) remain below 12%. The significant passive

insulation on the capsule and close to freezing temperatures of the landing site are sufficient to keep the samples frozen from thermal inertia until they can be collected by the waiting research team and transferred to a terrestrial freezer. This site was selected over other possible arctic and Antarctic sites (such as Summit Station, Greenland or McMurdo Station, Antarctica) because the additional risks to successful recovery associated with extreme weather and high altitude outweigh the reduced chance of samples melting due to consistently freezing temperatures.

This development schedule is driven largely by the necessity of launching in 2026, as a later launch would not allow return of the samples prior to the deadline at the end of 2030. At submission of this proposal the mission would complete pre-Phase A conceptual design. Then, the mission will enter Phase A: Concept and Technology Development until the System Requirements Review in January 2022, and then proceed to Phase B: Preliminary Design and Technology Development leading up to a Preliminary Design Review in April 2023. In Phase C: Final Design and Fabrication, the orbiter, lander, MAV, aeroshell, and sample return capsule will all be manufactured in parallel for time efficiency. This phase will conclude with the Critical Design Review in Fall 2024. Finally Phase D: System Assembly, Integration and Test, Launch, and Checkout will conclude with the Fall 2026 Launch and the mission will move into Phase E: Operations and Sustainment.

This proposal also includes a detailed cost breakdown. Cost analysis is crucial to the mission because the stated budget for end-to-end mission costs is $1 billion (in fiscal year 2020 US dollars), quite restrictive for a mission of this magnitude. The main cost analysis was completed using NASA's Project Cost Estimating Capability. This analysis provides a full cost breakdown across the elements of NASA's work breakdown structure. For comparison, a Monte Carlo simulation using cost estimating relationships from Space Mission Engineering: The New SMAD is included that displays a range of values for mission element cost outcomes. The resulting cost estimate distribution is centered at a total mission cost of $934M USD with an 85.6% chance of remaining within the $1B USD budget. This low cost is achieved by pulling a significant portion of the mission technologies from heritage sources and designing the mission architecture around the use of only a single launch vehicle.

Finally, though the risks associated with various systems are discussed throughout the report, a risk analysis summary is included that identifies the most significant among them and spells out the mitigation strategies built into the spacecraft design and mission operations to reduce the chances that these will negatively impact the mission goals.

2. Mission Overview

This section discusses the overall needs and goals for the mission, as well as the high-level system requirements set out by AIAA's Request for Proposal. It also includes an overall mass budget that lists the top-level allocations for each of the major systems involved in the mission and spells out the current overall mission mass margin.

2.1. Need Statement and Goals

As stated in the RFP, retrieving a Martian ice core sample is a critical step towards the goal of establishing a human presence on Mars because it allows for more detailed analysis of Martian ice deposits. Water is the most crucial resource for sustaining life and is the cornerstone of any Environmental Control and Life Support System (ECLSS). It is also valuable as a potential source of propellant. As such, gaining a better understanding of the ice deposits already present on Mars allows future missions to potentially extract and utilize a valuable resource. Thus, the overall need that drives this mission is: To search for evidence of past or current life on Mars in the short term, and in the long term to establish a sustainable human presence beyond the Earth's influence.

This need leads to several key goals of the mission. The first and most important of these is the retrieve ice core samples from the Martian surface and return them in their original frozen state to Earth for study. This will allow scientists to greatly expand their understanding of the chemical makeup of the Martian environment and the potential history of life on Mars. Second, the mission desired to learn more about the nature of water on Mars and the practical aspects of its potential for use in future ISRU systems to support robotic or crewed exploration of Mars. Data gained from the extraction, handling, and examination of these samples will feed directly into the design of these future systems. Finally, the mission seeks to gain new knowledge about the Martian environment with the explicit goal of paving the way for future crewed exploration of Mars. The region in which we propose to land has been identified as a prime candidate for future crewed missions due in large part to the balance of solar availability and accessible water ice deposits. Thus, this sample collection lander would serve as a direct precursor to future human landings on the Martian surface. All environmental data collected would feed directly into the life support system design and science goals of such a mission. Together, accomplishment of these goals would mean that the Glacies Nova mission represents a leap forward in our scientific understanding of the Martian environment and a major step toward the most significant advance in human exploration since Apollo 11.

2.2. System Level Requirements

The following are the system level requirements as laid out in the AIAA Request for Proposal:

Table 2.2.A Overall System Requirements

REQ #	Requirement
SYS-001	The mission shall return no less than 2.5 kg of Martian ice in its frozen state.
SYS-002	The mission shall consist of a robotic system that can land on or near Martian ice deposits.
SYS-003	The robotic system shall be capable of performing drilling operations on the Martian surface with the express purpose of retrieving ice core samples.
SYS-004	The system shall extract samples that are at least 25mm in diameter and 100m in length.
SYS-005	The system shall be capable of storing ice core samples in their frozen state during surface operations.
SYS-006	The system shall accommodate safe transfer of the frozen ice samples to Earth-based laboratories.
SYS-007	End-to-end mission operations shall be defined including launch, transit to Mars, EDL, surface operations, ascent, and Earth return.
SYS-008	The end-to-end mission cost shall not exceed $ 1 billion USD (adjusted to FY 2020) including launch, design development test and evaluation, and flight unit costs for the mission.
SYS-009	Cost estimation for development of any advanced technology shall be carried out and included in the overall cost estimate.
SYS-010	The ice core samples shall be returned to Earth for scientific analysis no later than December 31, 2030.
SYS-011	The total fueled mass of the spacecraft (including LVA) shall not exceed 5312 kg.

2.3. Mass Budget

The top-level mass budget including the total masses of each spacecraft component and propellant is shown below. The current overall mass margin for the mission is 15.8%. While this value is low for a mission at this stage of development, the risk in this case is mitigated by the fact that there is room for growth in launch vehicle capability. The mass margin was calculated using the capacity of a fully reusable Falcon Heavy to a C3 of 10 km^2/s^2. However, with no additional modifications to the spacecraft or interfaces, it is possible to switch to a partially reused Falcon Heavy, flown in a configuration where the two side boosters are recovered but the center core is expended. Such a configuration has been used in the past for US government missions and would provide a performance increase at an additional cost of around ~$30M (as estimated from public information on SpaceX prices). The exact performance differences are not published, so they cannot reliably be quantitatively analyzed for this report.

Mars Sample Return Mission Mass Budget						
	Level 3	Level 2			Level 1	
	Breakdown	CBE	Contingency	Allocated		
1.0 Payload					19.3	
2.0 Ascent Vehicle					392.7	
3.0 Lander					394.2	
4.0 Landed Mass					806.2	
5.0 EDL System					1759.1	
6.0 Mass at Entry					2565.3	
7.0 Cruise Stage/Orbiter					518.7	
8.0 Spacecraft Dry Mass					3084.0	
9.0 Consumables					20.0	
10.0 Propellant					1302.3	
11.0 Injected Mass					4406.3	kg
12.0 Launch Vehicle Adapter					182.0	
13.0 Boosted Mass					4588.3	
14.0 Margin					723.7	15.8%
15.0 Total Launch Vehicle Capacity					5312.0	FH Reusable

Figure 2.3.A. Mission Overall Mass Budget

3. Mission Architecture

This section provides an overview of our design's architecture, including our concept of operations, sample collection path, landing location choice, planned trajectories, and timelines.

3.1. Concept of Operations

A graphical depiction of our proposed mission concept of operations is provided below in Figure 3.1.A. The mission timeline and corresponding Mars solar longitude is listed in Table 3.1.A.

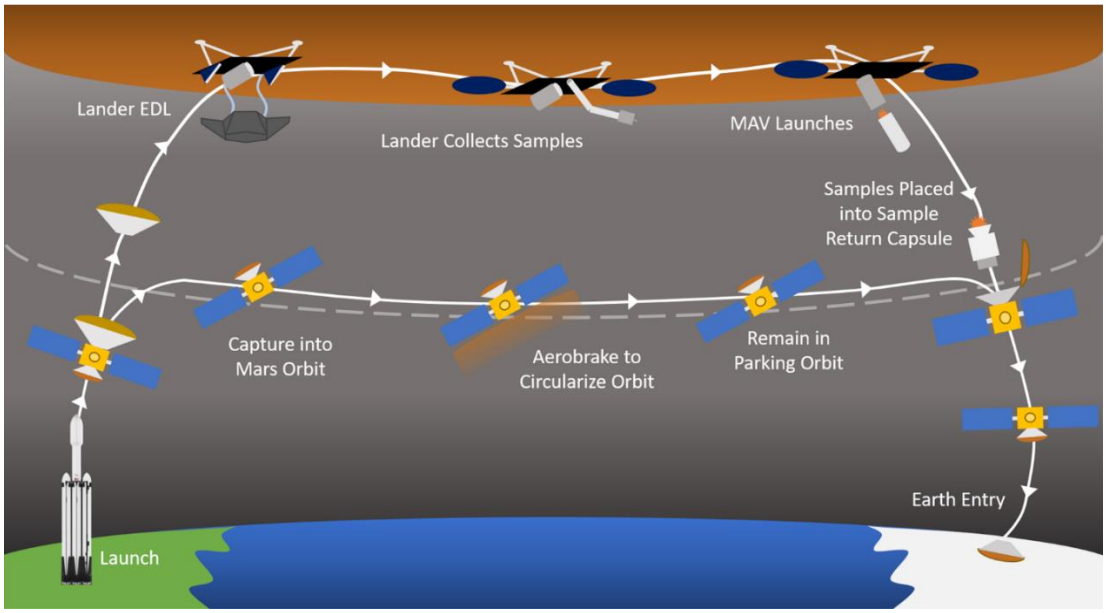

Figure 3.1.A. Mission Concept of Operations.

Table 3.1.A. Mission Timeline

	Dates	Mars Solar Longitude
Launch and Earth Departure	October to November 2026	--
SPURS Lands on Mars and LASSO-M Captures into Orbit	August to October 2027	146° - 178.5°
LASSO-M Aerobrakes to Circularize Orbit	Mars Arrival – April 2028	Mars Arrival - 295°
Sample Collection	Mars Arrival – January 2028	Mars Arrival - 235°
MAV Launch and Rendezvous	April 2028	295°
Mars Departure	August to September 2028	360° - 28°
Earth Arrival and Sample Return	May to June 2029	--

The mission begins with launch, where our spacecraft is sent into orbit packaged on a single launch vehicle. The spacecraft consists of the SPURS lander and descent stage, both stored within an aeroshell and mated to the side of the LASSO-M orbiter.

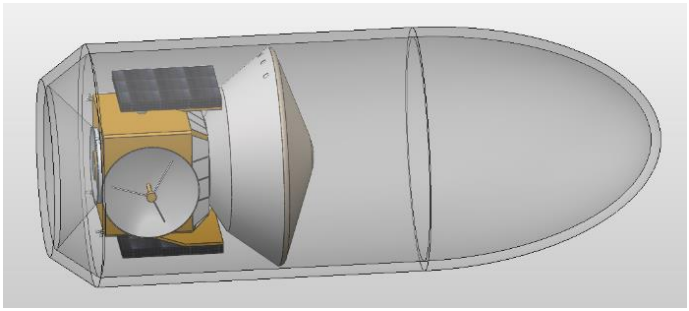

Figure 3.1.B. Spacecraft Launch Configuration Inside of Falcon Heavy PLF

The second stage of the launch vehicle performs trans-Mars injection and deploys the spacecraft directly on its intercept trajectory. After separation from the launch vehicle, the spacecraft deploys solar arrays and begins rotating at 2 rpm for spin stabilization during cruise. Throughout the journey to Mars, the orbiter acts as a cruise stage, performing trajectory correction maneuvers as needed with its thrusters.

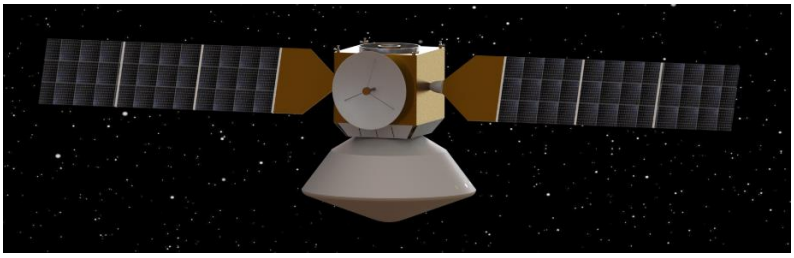

Figure 3.1.C. Spacecraft Outbound Cruise Configuration

The spacecraft enters Mars' sphere of influence on a direct course into the atmosphere. A few hours before entry, the orbiter separates from the aeroshell and diverts its course above the atmosphere.

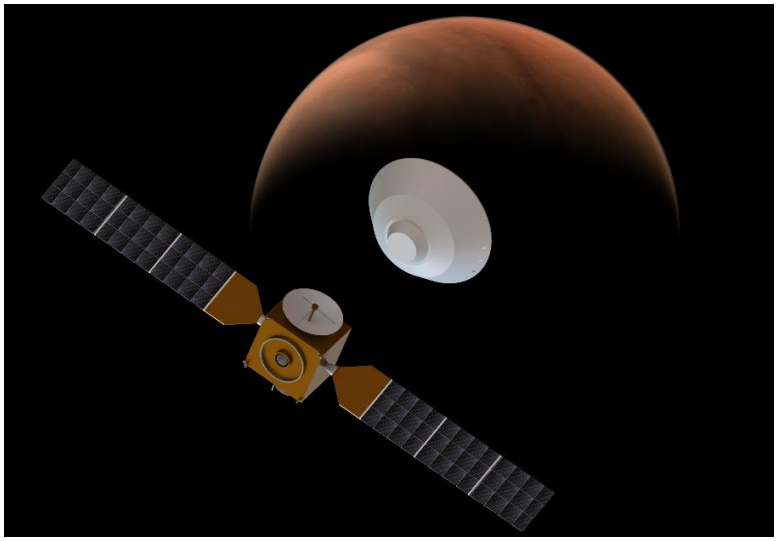

Figure 3.1.D. Spacecraft Separation at Mars Arrival

It then ignites its main engine and burns to capture itself into a highly elliptical orbit (slowing itself to just below escape velocity). The lander performs EDL with a descent stage like those used to land the *Curiosity* and *Perseverance* rovers, getting set down gently using a sky crane maneuver.

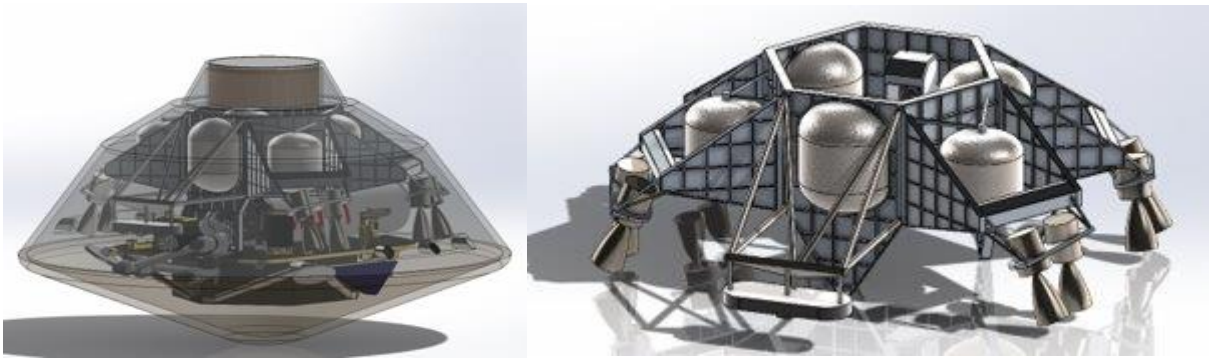

Figure 3.1.E. Stowed Descent Capsule (Left) and Descent Stage (Right)

Once safely on the surface, the lander begins surface operations, collecting samples and storing them in the sample container within the Mars Ascent Vehicle (MAV). During surface operations, the orbiter remains in space and uses drag from the upper layers of the Martian atmosphere to slowly lower its orbit periapsis. When its apoapsis is lowered sufficiently, the orbiter boosts its periapsis up out of the atmosphere to a stable 200 km circular orbit.

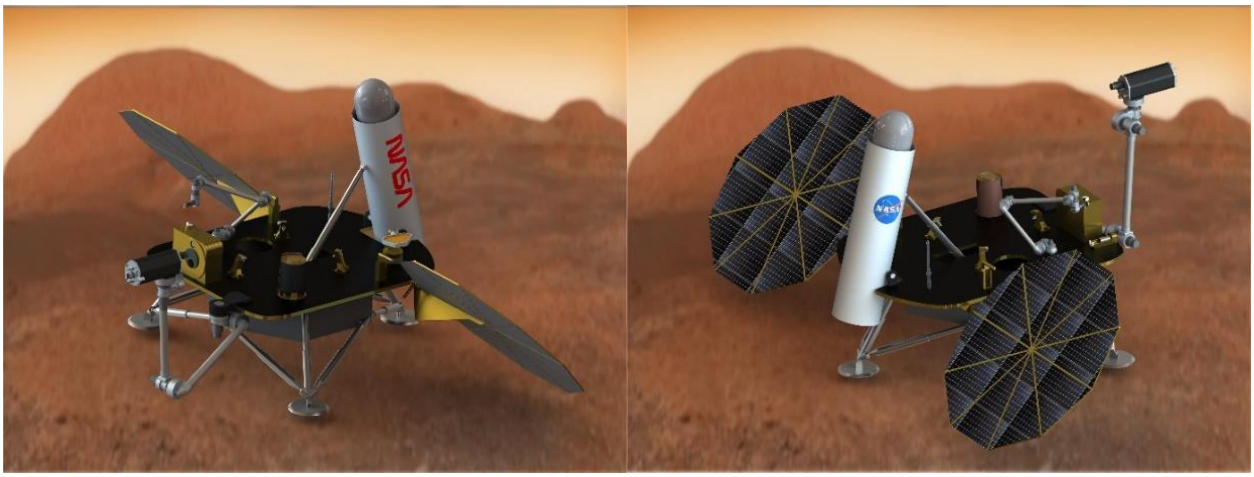

Figure 3.1.F. Lander in MAV launch configuration

Once all the necessary ice core samples are obtained, the MAV is sealed and launched from the lander platform. It then meets up with the orbiter and insert the sample container into the Sample Return Capsule (SRC). The spacecraft then enters a sleep period of low activity, preparing for an optimal return window to begin its transit back to Earth.

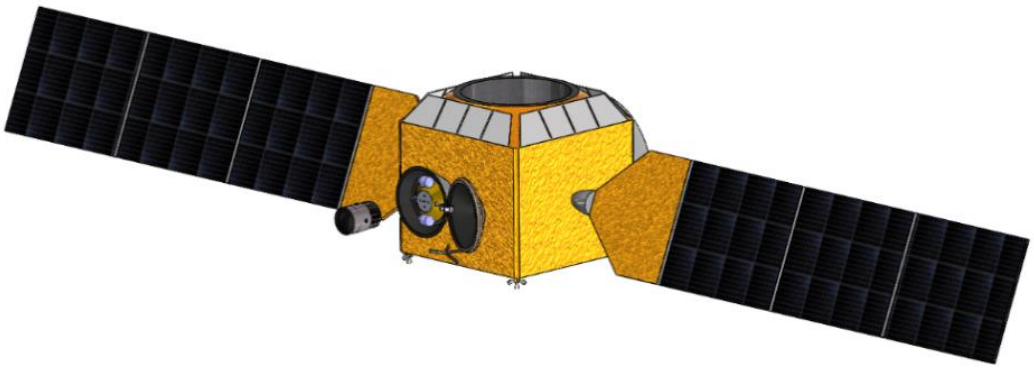

Figure 3.1.G. MAV Upper Stage Approaching Orbiter for Docking

When the return launch window is reached, the orbiter burns its main engine to perform a trans-Earth injection maneuver. The Earth return phase is carried out similarly to the original Mars transit phase, with onboard computers communicating with Earth and ensuring that the spacecraft remains on course. Upon arrival at Earth, the orbiter releases the SRC containing the sample container on an intercept course with the atmosphere and then diverts course into deep space. The SRC enters the atmosphere and lands near a research station to reduce the risk of samples melting before they can be collected and transferred to stable storage.

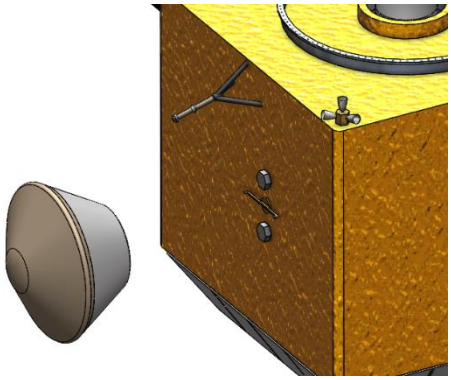

Figure 3.1.H. SRC Separation from Orbiter

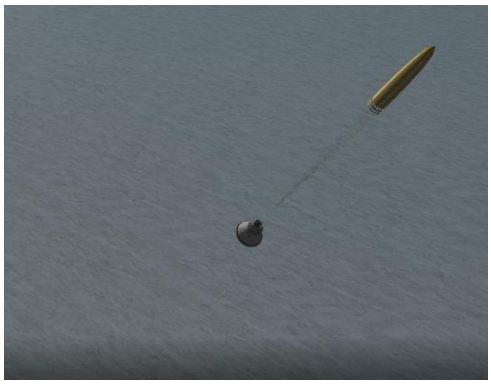

Figure 3.1.I. Parachute Deployment

3.2. Sample Collection Path

This section is intended to provide an overview of the path taken by the collected samples from their origin on Mars to their landing on Earth - the various subsystems referenced here are explained in greater detail in subsequent portions of the report.

First, the ice cores are extracted from the Martian surface by the lander's drill, mounted on the end of a robotic arm. A sample containment tube is situated inside of the drill's coring bit to receive the sample.

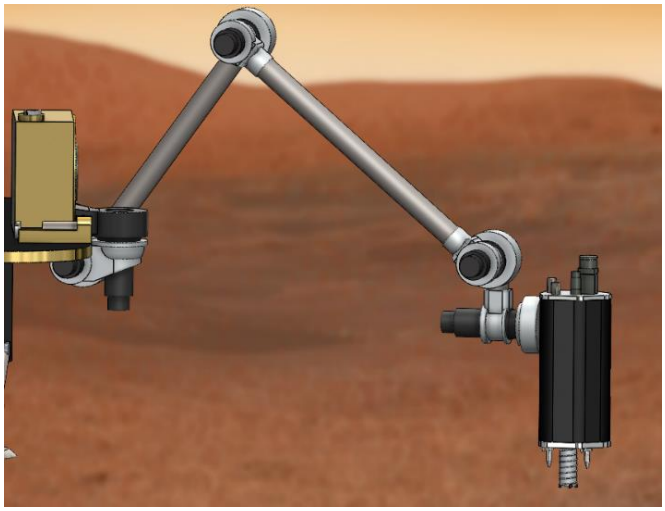

Figure 3.2.A. Sample Acquisition by Drill on Robotic Arm

The sample tube containing the ice core is then ejected from the end of the coring bit into a designated location for handling by the secondary onboard sample handling arm. During this phase, the tube is hermetically sealed and placed into the sample container (mounted in the nose of the MAV), which is equipped with both passive insulation and an active cooling system to maintain the samples in their frozen state. (For more detail on this process see Section 5.6.2 Sample Handling). Once all samples are loaded, the hinged lid on the top of the sample container

closes and seals. Shortly before the chosen launch window, the fairing is secured in place over the sample container on the MAV. The vehicle then rotates upright and launches off the surface of Mars, as shown in Figure 3.2.B.

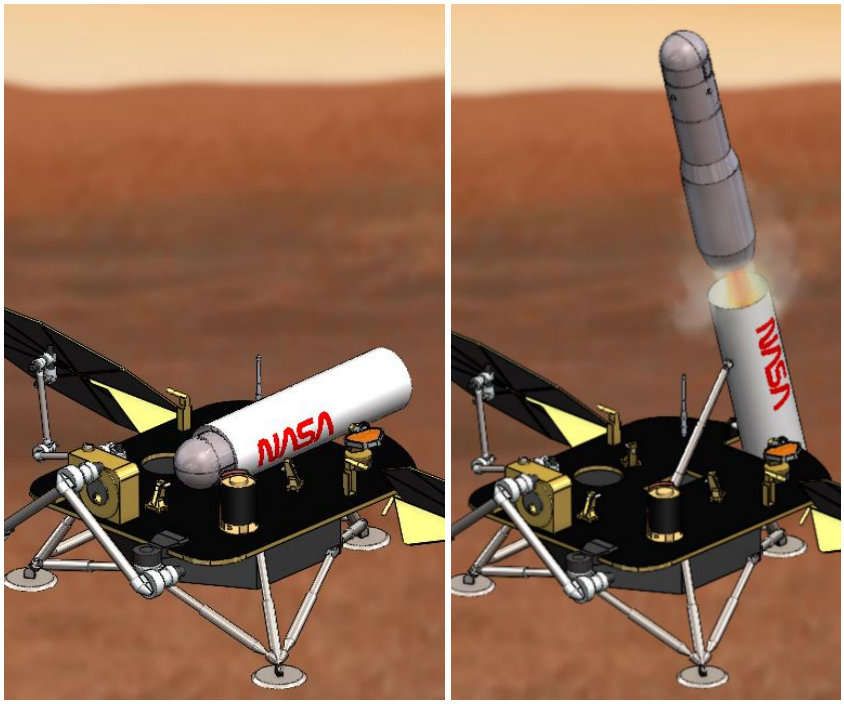

Figure 3.2.B. MAV with Samples in Nose Launches from Lander

Once the MAV is on orbit, the orbiter performs rendezvous to collect the samples. The payload fairing is jettisoned from the front of the MAV and the sample container is docked directly into the SRC, as shown in Figure 3.2.C.

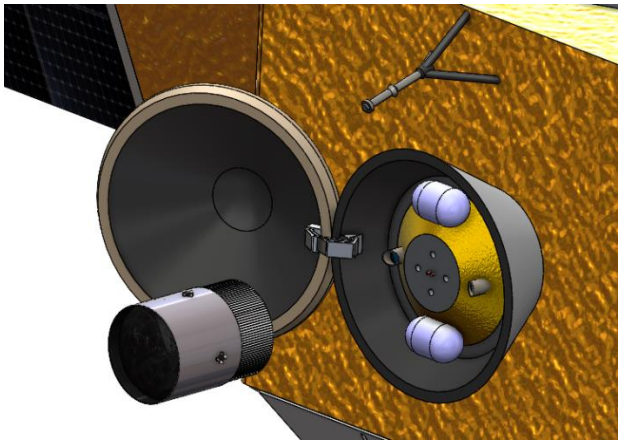

Figure 3.2.C. Samples Transferred from MAV to SRC on the Orbiter

The SRC remains open during the cruise back to Earth to allow the built-in radiators on the return capsule to keep the ice samples frozen. The orbiter performs trans-Earth injection and provides power to the sample capsule during the return trip. Cooling in space is primarily done passively by keeping the SRC shadowed from the sun, but the

active cooling system will start up if needed at any point (if, for example, a maneuver requires the spacecraft to assume an attitude where the SRC is exposed to direct sunlight).

Once the orbiter approaches Earth, the SRC holding the samples is closed and deployed on a direct entry trajectory. The active cooling system switches to an open-loop mode to prevent the samples from reaching their melting point during Earth EDL. The samples land under parachute near a research station and are retrieved by a field team awaiting their arrival.

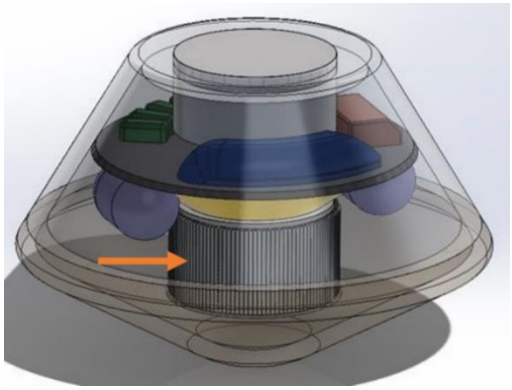

Figure 3.2.D. Samples Located in the SRC

3.3. Mars Landing Site Assessment

There are currently two main landing options on Mars available for this mission, mid-latitude and polar. Ice deposits are more abundantly available when landing in a polar region. However, doing so requires more complex power, thermal, and communication systems. The poles have extreme weather, and surface ice is contaminated with dust and frozen carbon dioxide (dry ice). Along with this extreme weather, the poles have a thinner atmosphere, making EDL much harder to accomplish. The matrix for this design decision is provided below in Table 3.3.A., which shows that a mid-latitude site is more ideal when considering ice quality, EDL success, sun exposure, cost, and overall risk.

Table 3.3.A. Mars Landing Site Decision Matrix

Mars Landing Site	Ice Wt. = 2x		EDL Wt. = 1x		Sun Wt. = 1.5x		Cost Wt. = 1x		Risk Wt. = 2x		Weighted Total
	U	**W**	U	**W**	U	**W**	U	**W**	U	**W**	
Polar	2	**4**	1	**1**	1	**1.5**	1	**1**	1	**2**	9.5
Mid-Latitude	4	**8**	4	**4**	4	**6**	3	**3**	3	**6**	27
Key: U = Utility Value, W = Weighted Value, 0 = Worst, 10 = Best											

A mid-latitude location still has drawbacks which need to be minimized when choosing a location. A mid-latitude site will not have ice deposits visible on the surface in most areas, due to the sublimation of surface ice in non-polar regions. The ice in the mid-latitude regions can be visible, or just inches below the surface. Choosing a site with visible ice, or minimal depth beneath the surface, is optimal.

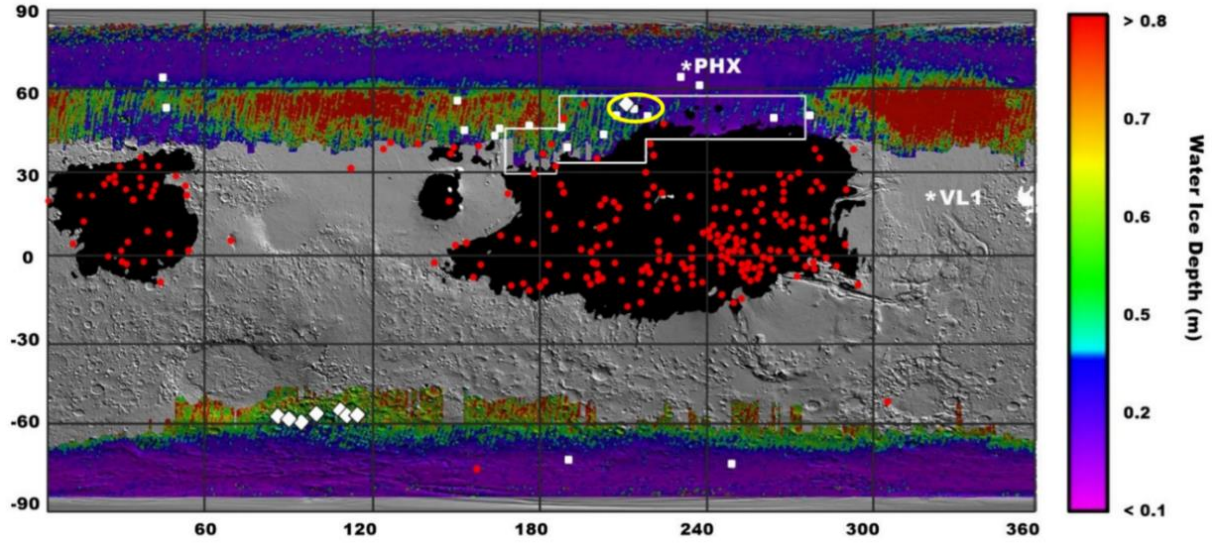

Figure 3.3.A. Mars Ice Treasure Map [1] and Available Ice Deposits [2]

By combining data from the Mars Climate Sounder instrument from MRO, the Thermal Emission Imaging System from Mars Odyssey and the Mars Global Surveyor, Figure 3.3.A. above shows a detailed ice map of Mars. Areas with cooler colors, like purple and blue, show where ice is less than one foot (30 cm) below the surface. Areas with warmer colors, like yellow and red, represent areas where ice is over two feet (60 cm) below the surface of Mars. The black areas on the map represent locations where a landing spacecraft would sink into fine dust. The outlined box seen in the northwest represents what NASA has identified as a prime area for future human exploration [1].

An ideal landing site for our mission will be just below where the Phoenix lander landed, as seen in Figure 3.3.A., at a latitude of about 55.1° N, as indicated by the yellow ellipse. This area has a crater with visible ice glaciers within it, and minimal ice depth throughout. This area has proven sites with ice visible just below the Martian surface, denoted by the white markers in the Figure above.

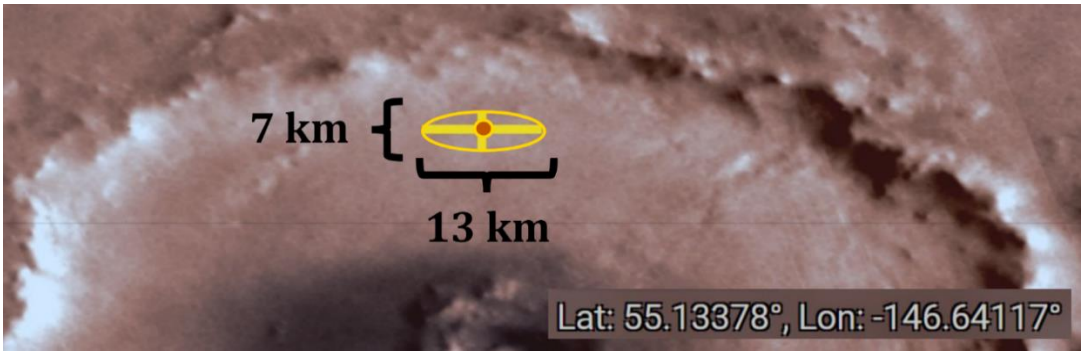

Figure 3.3.B. Mars Landing Site Ellipse

The chosen landing site for our mission is within the Milankovič crater, seen above in Figure 3.3.B., at a latitude of around 55.1° N and a longitude of 146.6° W. Our landing ellipse is 13 x 7 km, which is slightly larger than *Perseverance*'s ellipse of 7 x 6 km [3]. This crater's northern wall has visible glaciers within it, suggesting an abundance of ice in the area, which will minimize our risk of missing ice when drilling.

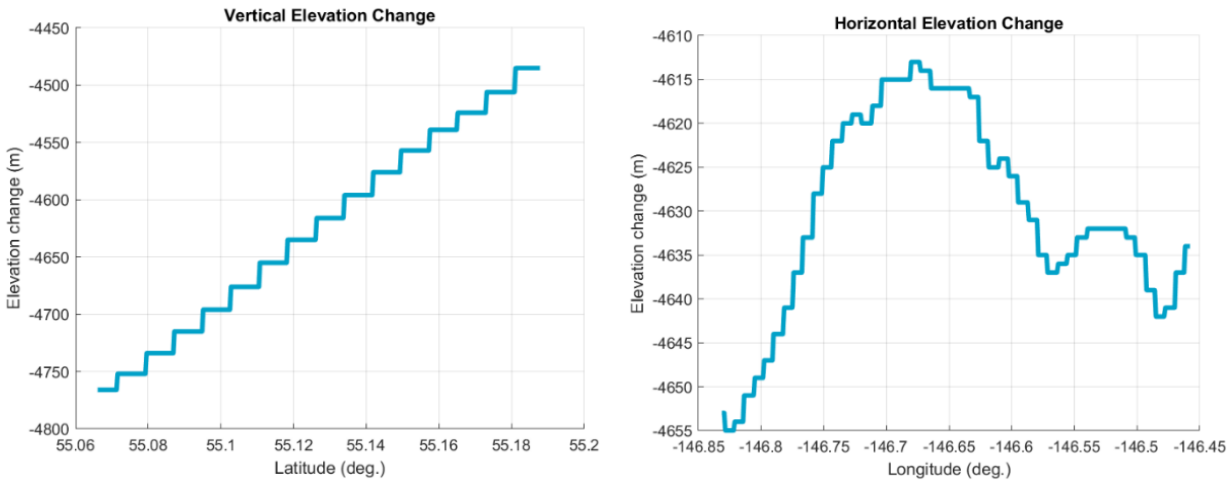

Figure 3.3.C. Vertical and Horizontal Elevation Change Near Landing Site

Figure 3.3.C seen above shows that the elevation change in our ellipse is not substantial. This flat region is ideal for EDL and Ascent. While relatively flat, the site has a degree slope in favor of the sun angle. This will allow our solar panels to be slightly tilted, optimizing sun exposure. While this is near a polar region, Phoenix was able to maintain power two months past its projected lifetime of 3 months using only solar arrays [4]. Our mission utilizes solar arrays, so this is the ideal landing location, when compared with other areas.

3.4. Trajectory Design

The Glacies Nova mission has four main trajectory phases: the outbound transfer from Earth to Mars, capture and aerobraking at Mars, the Mars parking orbit, and the inbound transfer from Mars to Earth. Each of the phases' maneuvers are performed by the orbiter. The trajectory design for the mission directly impacts other components of the mission, such as the required propellant mass, mission timeline, Mars season that the lander will be collecting samples, and the duration of transfer flights.

The total ΔV required for the orbiter over the full mission duration is 4.392 km/s, which includes 15% margin. The breakdown of this requirement, as well as the justification and timeline, are discussed in this section. All ΔV requirements in this section were calculated using equations from *Fundamentals of Astrodynamics and Applications* by David Vallado [5].

3.4.1. Outbound Transfer

The trajectory design is constrained by the Earth-Mars launch windows and the project requirement that the sample must be returned by December 31st, 2030. There are three launch windows that allow for a return to Earth prior to this date: 2024, 2026, and 2028. The 2026 launch window was chosen as the optimal option because of the timeline and ΔV requirements. Launching in 2024 is too soon to allow for enough time for R&D and spacecraft assembly prior to launch. Additionally, because the 2028 launch window is so close to the return deadline, it only allows for a Mars stay-time of 30 days and would require a return flyby of Venus to return in time. This would require additional thermal control complexity that would increase the mass of the Sample Return Capsule. The 2026 launch window does not have these problems, so it was chosen as the optimal launch window.

The specific range of outbound launch dates was determined from the following porkchop plots that show the V_∞ required for Earth launch and Mars arrival hyperbolic trajectories for the 2026 launch window. From Figure 3.4.1.A, the minimum V_∞ is 3.03 km/s to reach Mars, so the minimum C3 is 9.18 km^2/s^2. This requirement directly impacts the choice of the Falcon Heavy launch vehicle, which is discussed in Section 8. A maximum V_∞ = 3.16 km/s was selected for determining the outbound launch window and trip duration, which allows for a C3 = 10 km^2/s^2 for the launch vehicle.

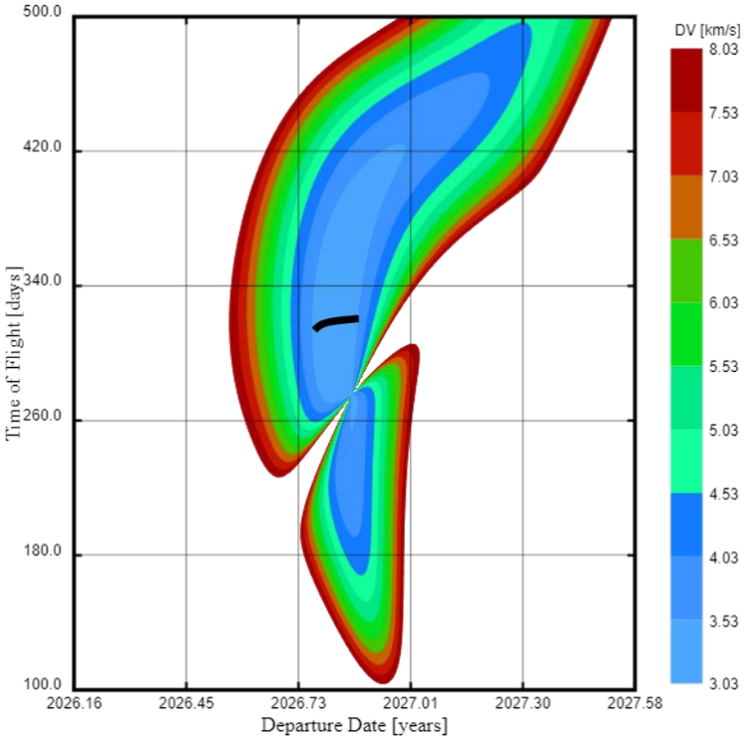

Figure 3.4.1.A. Porkchop Plot Showing V_∞ at Earth Departure (Black Indicates Launch Window) [6].

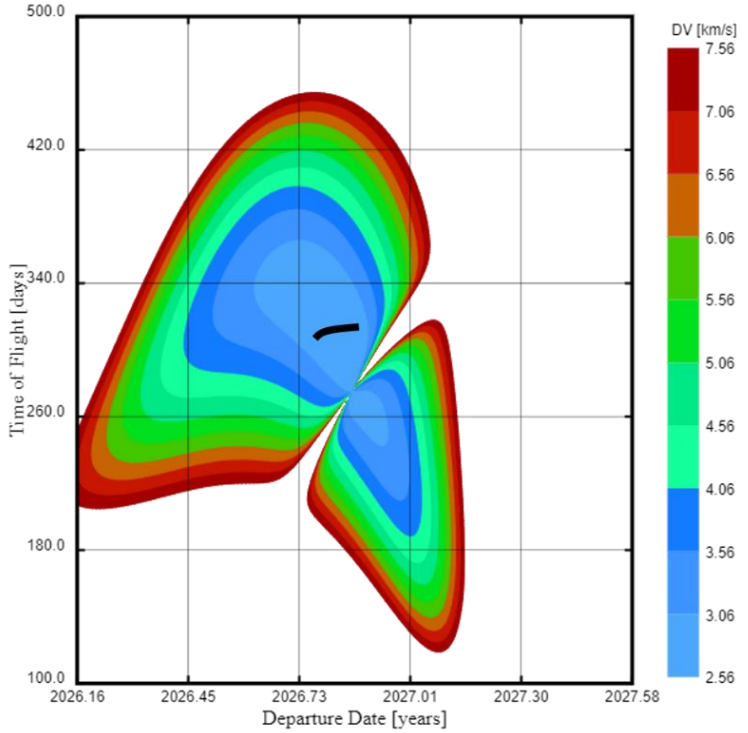

Figure 3.4.1.B. Porkchop Plot Showing V_∞ at Mars Arrival (Black Indicates Launch Window) [6]

For the Mars capture in Figure 3.4.1.B, there is a maximum of V_∞ = 2.75 km/s for the same dates and time of flights as the departure V_∞. The ΔV required for Mars capture depends on the capture orbit and is discussed in the next

section. Looking at both the outbound departure and arrival plots, the outbound departure launch window is October 18 to November 7, 2026, and the duration can range from 275 to 350 days. Therefore, the arrival dates range from August 17 to October 23, 2027.

Based upon MRO heritage, the ΔV allotted for course corrections during the outbound trajectory on the way to Mars is 30 m/s. This includes enough margin for the orbiter to correct itself if it is inserted into a slightly inaccurate outbound transfer [7].

3.4.2. Mars Capture, Aerobraking, and Parking Orbit

A trade study was carried out to determine whether a (1) purely propulsive capture into a circular orbit or a (2) propulsive capture into an elliptical orbit and aerobraking to circularize was the best method for our mission. Five factors were considered in the trade study: required propellent mass, cost, risk, delay of MAV launch, and amount of previous mission heritage. The trade study decision matrix is shown in Table 3.4.2.A. and shows the weights of the factors and both capture methods.

Decreasing propellant mass is very important due to the mission's tight mass constraints. Because we can only allow for one launch from Earth, and that launch includes the orbiter, EDL system, lander, and MAV, reductions in propellant mass help the mission stay under the mass limit. Because of its high importance, the propellant mass factor was weighted the heaviest in the trade study. Aerobraking saves 1.325 km/s of ΔV in comparison to a fully propulsive capture, which is equivalent to 880 kg of propellant.

Decreasing cost and risk are also very important. Aerobraking reduces cost, because it requires less propellant mass and thus a smaller launch vehicle, which is significantly more expensive than the operational costs of aerobraking maintenance. However, aerobraking involves more mission risk, due to the possibility that the Mars atmospheric density variations and/or the structural and thermal loading on the orbiter during periapsis passes causes mission failure. Because the mission requirements involve a tight budget, and there is already previous heritage for successful aerobraking at Mars, reducing cost outweighs the benefit of reducing risk for this mission.

Additionally, aerobraking takes around 6 to 7 months to complete, so there is a delay in the earliest the MAV can launch for rendezvous to April 2028. However, a fully propulsive capture would immediately be ready to rendezvous with the MAV at any time because it immediately reaches the desired circular parking orbit around

Mars. While aerobraking does have this disadvantage, the previous factors were more important for mission success as the MAV will not be able to launch until all samples are collected anyway. The heritage is the last and least weighted factor, as both aerobraking and a purely propulsive capture have successful heritage.

Table 3.4.2.A. Mars Capture Method Decision Matrix

Capture and Circularizing Method	Propellant Mass Wt. = 2x		Cost Wt. = 1.6x		Risk Wt. = 1x		Delay of MAV Launch Wt. = 1x		Heritage Wt. = 0.4x		Weighted Total
	U	**W**	U	**W**	U	**W**	U	**W**	U	**W**	
Aerobraking	9	**18**	7	**11.2**	5	**5**	4	**4**	8	**3.2**	41.4
Propulsive	2	**4**	2	**3.2**	8	**8**	10	**10**	10	**4**	29.2
Key: U = Utility Value, W = Weighted Value, 0 = Worst, 10 = Best											

The results of the trade study show that aerobraking is the best design option. Our mission uses a similar aerobraking method as MRO for Mars capture and circularizing. Once the orbiter reaches Mars, it performs a burn that is just enough to capture into the periapsis of a highly elliptical polar orbit. The periapsis altitude of this orbit is 430 km, and the orbit eccentricity is 0.92. Capturing into this orbit requires a ΔV of 919.5 m/s. Much like MRO, the orbiter will perform small burns at its apoapsis over the next 5 orbits to gradually lower its periapsis to an altitude of 140 km [8]. These five burns add up to be almost 15 m/s, and are called the aerobraking "walk in."

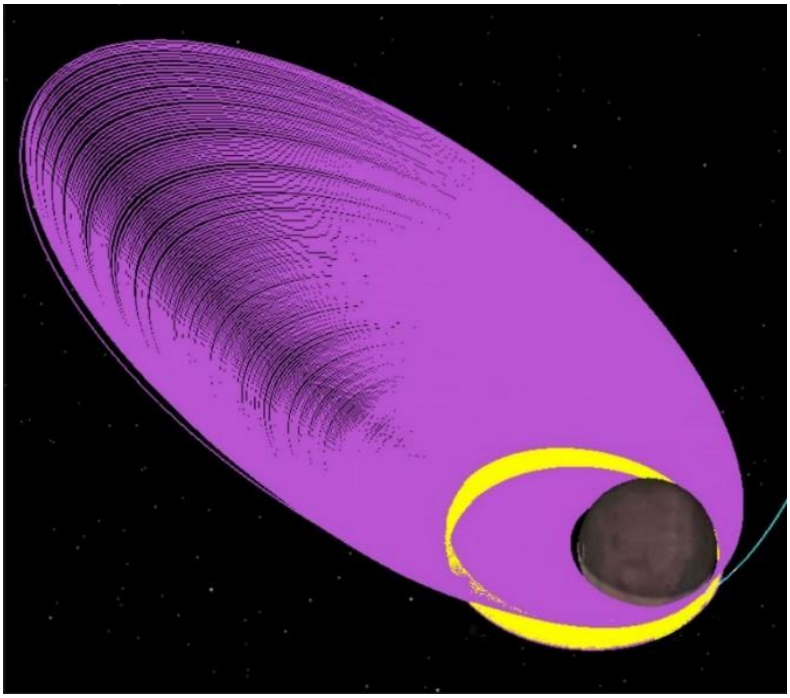

Figure 3.4.2.A. Orbiter Aerobraking Trajectory (Aerobraking in pink, solar conjunction pause in yellow).

Over the next 6 months and almost 200 orbits, the drag from the orbit passing through the Martian atmosphere lowers the apoapsis until it has an altitude of 200 km. A $\Delta V = 20$ m/s is allocated for the orbiter to make tiny burns at apoapsis to ensure that it passes at the correct altitude during the following aerobraking pass at periapsis. Because the atmosphere of Mars is highly variable, adjusting the orbiter's periapsis altitude for each pass is important so that the orbiter slows down enough but doesn't overheat or suffer structural damage from the atmosphere. Systems Tool Kit (STK) and the Mars Global Reference Atmosphere Model Version 3.8 (Mars-GRAM 3.8) were used to model the aerobraking duration and orbit shape.

Because fine tuning the orbit's periapsis altitude every pass is so critical, there must be constant communication between the orbiter and Earth for the full duration of the aerobraking. However, there is a solar conjunction between Earth and Mars from March 15-25, 2028, which causes a communications blackout as Mars passes behind the Sun. The aerobraking is not completed by the start of the solar conjunction, so the orbiter is pulled out of the atmosphere to a periapsis altitude of 200 km for March 10-30, 2028, to wait until communications are restored. This allows the orbiter to wait in a safe orbit around Mars while communications are paused. After the solar conjunction, the orbit periapsis is then lowered back into the atmosphere to resume aerobraking. These solar conjunction pausing maneuvers require a $\Delta V = 20$ m/s. Including the solar conjunction pause, the aerobraking is completed after about 6 months in early- to mid-April. The full aerobraking trajectory is shown in Figure 3.4.2.A. The aerobraking trajectory is shown in pink, while the solar conjunction pause is shown in yellow. After the orbit's apoapsis is lowered to 200 km, the orbiter then performs a burn to raise the periapsis out of the atmosphere to an altitude of 200 km, circularizing the orbit. This maneuver requires a $\Delta V = 24$ m/s and circularizes the orbit.

Because the aerobraking orbits are elliptical, the orbiter spends most of its time closer to its apoapsis. The orbit is polar, so the apoapsis is not in the shadow of the sun. This allows the solar panels of the orbiter to be in view of the Sun, Earth, and the lander for most of the orbit. This allows for smaller batteries on the orbiter because the solar panels are in direct view of the sun. If the apoapsis of the aerobraking was in the shadow of Mars, the power capacity of the batteries would need to be much larger. Additionally, because the lander is in the north hemisphere of Mars, the orbiter spends most of its time aerobraking in clear view of the lander for uninterrupted communications between the lander and Earth.

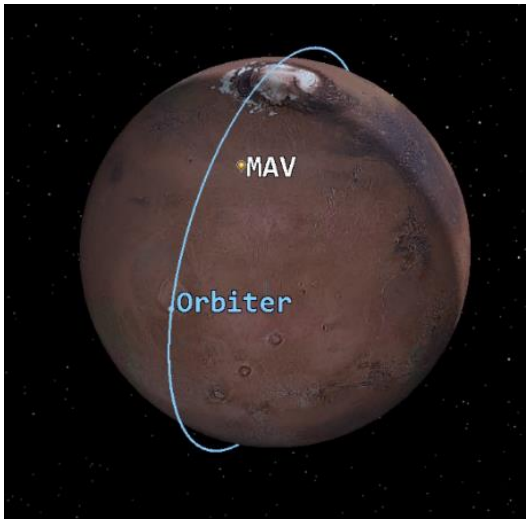

Figure 3.4.2.B. Parking Orbit at Mars Over Ten Days

Until the MAV is ready to launch to rendezvous with the orbiter in mid- to late-April 2028, the orbiter stays in this circular polar parking orbit with an altitude of 200 km. The parking orbit is shown in Figure 3.4.2.B, and the ground track of the orbiter is shown in Figure 3.4.2.C. Because it is polar, there is almost no nodal precession of the orbit, which allows for more MAV launch opportunities than a lesser inclined orbit. This allows for the orbiter to pass over the MAV twice a day, with one of those passes being northbound above the MAV. Because the lander lands with the MAV pointed north, the orbiter and MAV will only be able to rendezvous when the orbiter passes northbound overhead.

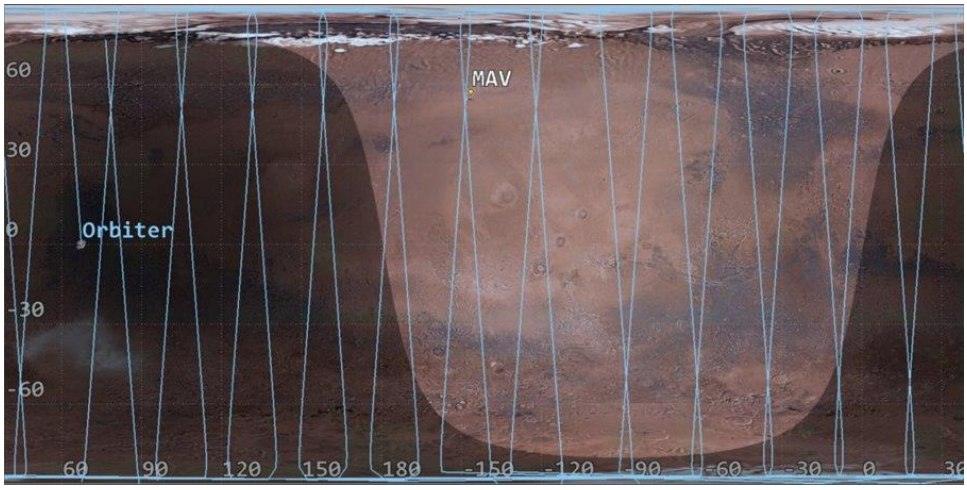

Figure 3.4.2.C. Parking Orbit Ground Track Showing the MAV at the Landing Site Location

The orbiter uses active control to rendezvous with the MAV. Before the MAV launches, the orbiter uses up to ΔV = 30 m/s to phase its orbit to match up with the MAV's launch trajectory. Thrusters on the orbiter are used for attitude control to align with the MAV. The orbiter then stays in the same circular parking orbit until it is ready to depart

Mars a couple months later. The orbiter has an additional ΔV = 20 m/s to station keep the parking orbit before the MAV launch and after rendezvous until departure.

3.4.3. Inbound Transfer

The inbound transfer launch window and duration are determined using the same method as the outbound trajectory window decisions. Unlike the outbound transfer, a type-1 trajectory was chosen for the inbound transfer to allow for a shorter flight duration back to Earth. This is important as it helps decrease the required time of flight and the risk of ice samples melting during return. As before, a lower V_∞ is chosen to decrease the required ΔV to insert into the inbound transfer. Additionally, a lower V_∞ for the Earth entry is important, as it helps the Sample Return Capsule not overheat during reentry, which would cause the samples to melt.

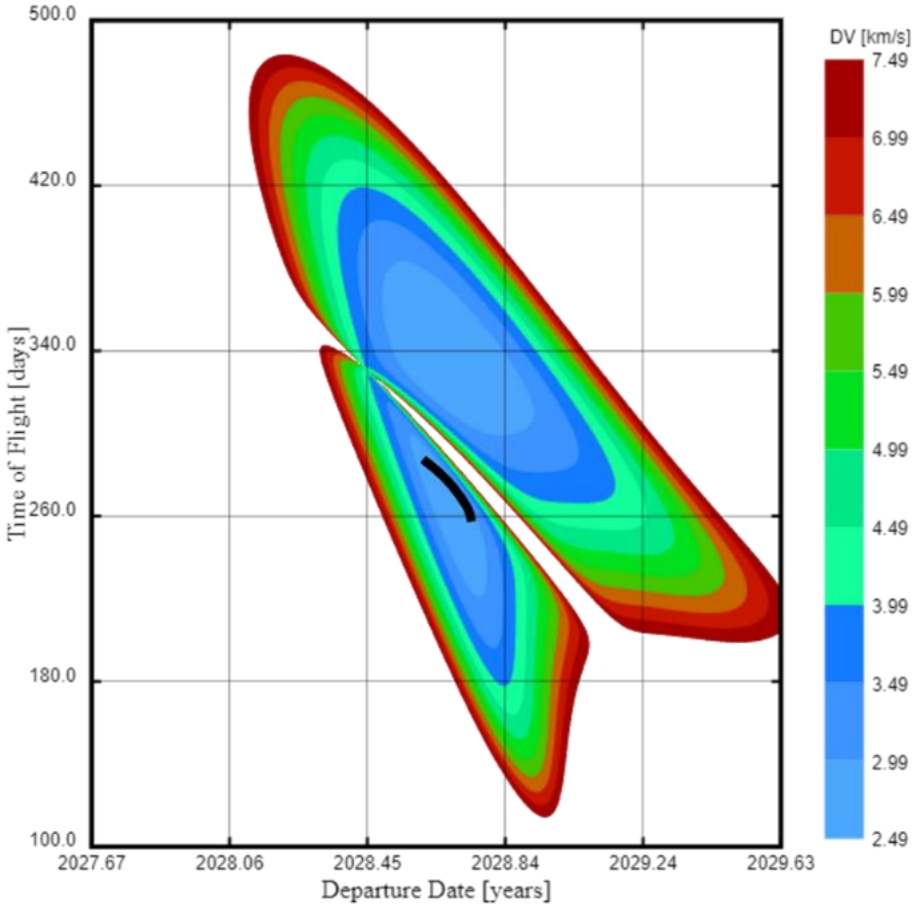

Figure 3.4.3.A. Porkchop Plot of V_∞ for Mars Departure (Black Indicates Launch Window) [6]

The maximum inbound departure V_∞ in Figure 3.4.3.A was chosen to be 3 km/s. From a 200 km parking orbit, this corresponds to a ΔV = 2.278 km/s. To determine the maximum V_∞ for the Earth entry, the maximum entry speed of the SRC was set to 12.9 km/s, the same as the OSIRIS-REx return capsule [9]. This corresponds to a maximum V_∞ =

7 km/s in Figure 3.4.3.B. Looking at both the outbound departure and arrival plots, the Mars departure launch window is August 1 to September 15, 2028, and the duration can range from 235 to 300 days. Therefore, the Earth arrival dates range from May 19 to June 18, 2029.

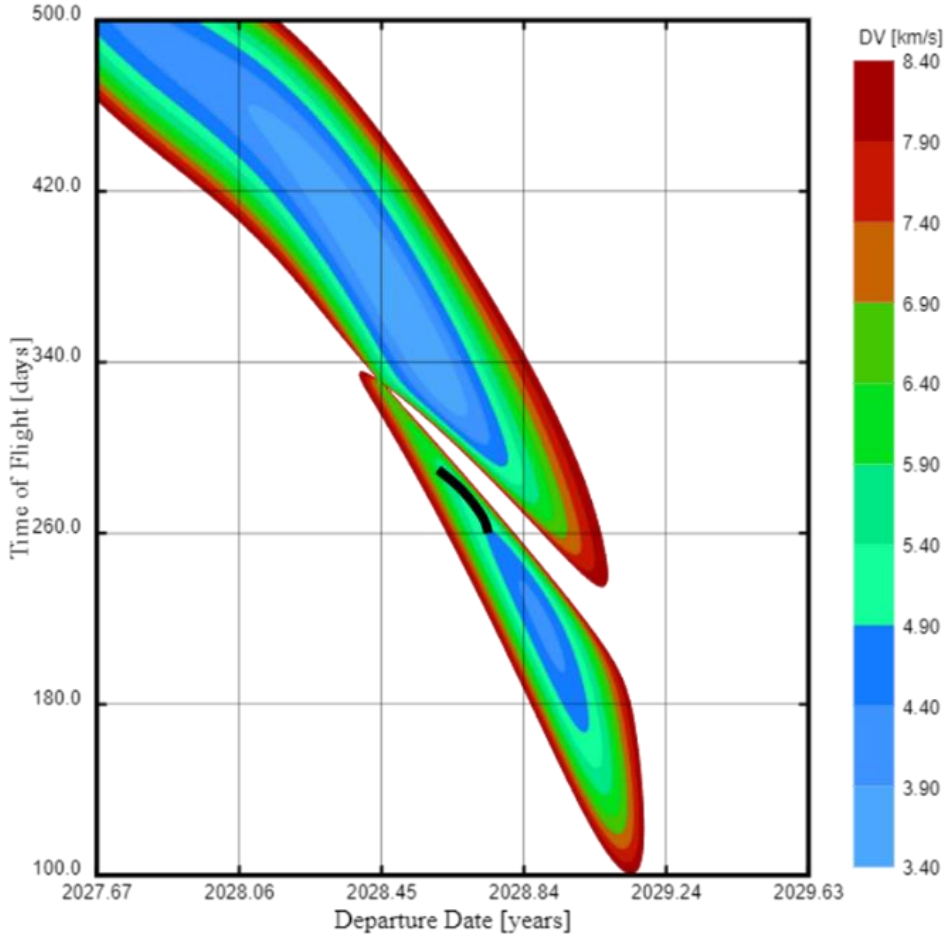

Figure 3.4.3.B. Porkchop Plot of V_∞ for Earth Arrival (Black Indicates Launch Window) [6]

Again, an additional 30 m/s is required for course corrections for the inbound transfer to ensure that the SRC will arrive at the correct landing location.

3.4.4. ΔV Budget

The following table lists the orbital maneuvers made by the orbiter in the four trajectory phases of the mission. The total required nominal ΔV for the mission is 3.407 km/s. There is an additional 15% of ΔV margin included, which is used in sizing the propellant mass.

Table 3.4.4.A. Nominal ΔV Budget

Orbital Maneuver	ΔV Allocated [m/s]
Outbound Transfer	**949.5**
Outbound Trajectory Correction Maneuvers	30.0
Mars Capture	919.5
Aerobraking	**79.4**
Aerobraking Walk In	15.0
Adjusting Periapsis to Correct Altitude	20.0
Pausing Aerobraking for Solar Conjunction	20.0
Aerobraking Walk Out	24.5
Parking Orbit	**50.0**
Station Keeping	20.0
Phasing to MAV Rendezvous	30.0
Inbound Transfer	**2327.8**
Mars Departure	2277.8
Inbound Trajectory Correction Maneuvers	30.0
Divert Orbiter to Deep Space at Earth	20.0
TOTAL	**3406.6**
TOTAL with 15% Margin	**3917.6**

4. LASSO-M Orbiter

The Low-mass Acquisition System for Samples in Orbit of Mars (LASSO-M) orbiter is the center of the space-based segment of the mission. It fills the role of the cruise stage for the lander, but instead of being expended upon arrival to Mars like *Curiosity* and *Perseverance*, it diverts and captures into Mars orbit, where it awaits the return phase of the mission. After this waiting period, it receives the sample container from the MAV and then performs the trans-Earth injection maneuver. It then reprises its role as a cruise stage on the return journey, providing guidance, navigation, power, and course corrections for the return capsule.

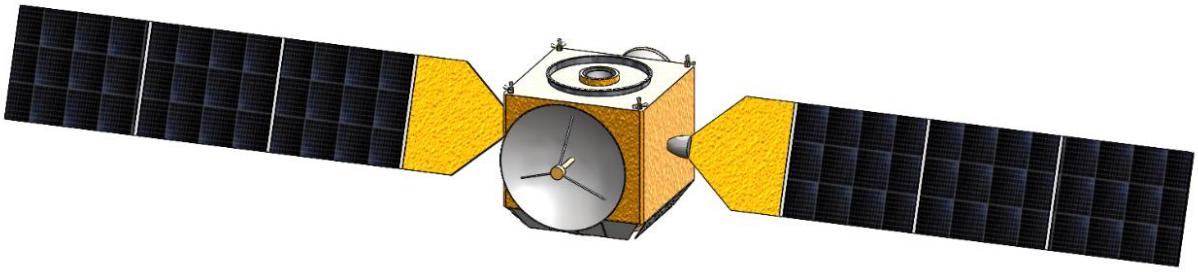

Figure 4.A. Front View of Orbiter

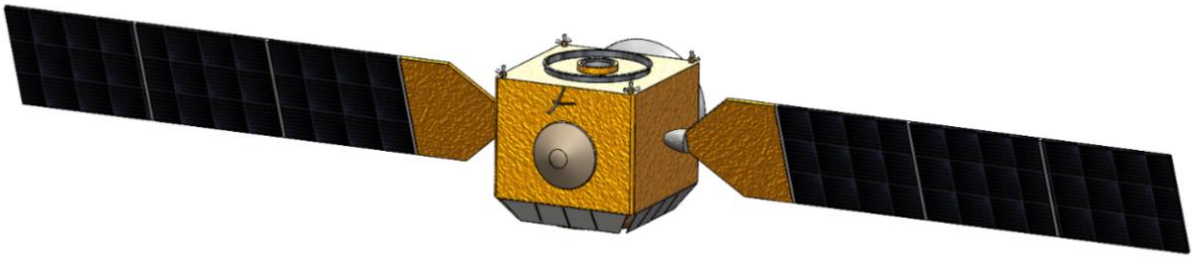

Figure 4.B. Back View of Orbiter

4.1. Requirements

Below are the requirements for LASSO-M's capabilities and subsystems. The main drivers of the orbiter design are the need for it to provide support for the ground segment during cruise and propulsion for the return trip in a package with as little mass as possible.

Table 4.1.A LASSO-M Orbiter Requirements

REQ #	Requirement
ORB-001	The orbiter shall allow for retrieval of ice samples in Mars orbit and facilitate storage and transportation back to Earth.
ORB-002	The orbiter shall be capable of performing an aerobraking maneuver to transfer from a highly elliptical capture orbit to a 200x200 km circular orbit in 6 Earth months or less.
ORB-003	The orbiter propulsion system shall provide a minimum of 3918 m/s of delta-V capacity.
ORB-004	The orbiter shall be capable of performing course correction maneuvers in deep space both with and without the mars aeroshell attached.
ORB-005	The orbiter power system shall be able to deliver a minimum of 1000 W of power for operation of spacecraft systems.
ORB-006	The orbiter shall include a structural and electrical interface with the sample return capsule prior to separation and Earth reentry.
ORB-007	The orbiter shall be placed in a heliocentric disposal orbit after completion of the mission objectives.
ORB-008	The dry mass of the orbiter, including the sample return capsule, shall not exceed 518.7 kg.
ORB-009	The orbiter shall be capable of communication with the Earth-based DSN as well as the lander, MAV, and other spacecraft in the Mars Relay Network.
ORB-010	The orbiter shall include a docking system capable of rendezvous, relative navigation, and docking with the MAV in Martian orbit in less than 8 hours after MAV launch.
ORB-011	The orbiter shall be capable of keeping propellants and electronics within acceptable operating temperature ranges.

4.2. Mass Budget

The orbiter has a total mass allocation of 1841 kg, including 1302.3 kg of propellant and a 20 kg blanket allocation for miscellaneous consumables as may be required by various onboard systems. The total dry mass allocation of the orbiter is 518.7 kg, of which 82.5 kg is reserved for the Sample Return Capsule. The propulsions system makes up an unusually large portion of the spacecraft dry mass because of the high delta-V requirements of Mars orbit insertion and Trans-Earth injection.

	Breakdown	CBE	Contingency	Allocated	
7.0 Cruise Stage/Orbiter					518.7
7.1 Propulsion		128.0	12.8	140.8	
7.1.1 Mass of Engines	7.3				
7.1.2 Mass of Thrusters	7.1				
7.1.3 Propellant Tanks	43.1				
7.1.4 Pressurant Tanks	41.4				
7.1.5 Pressurant	17.1				
7.1.6 Lines, Valves, Fittings, Regulators, etc	12.0				
7.2 ADCS		30.0	3.0	33.0	
7.3 Communications		35.0	3.5	38.5	
7.4 C&DH		20.0	2.0	22.0	
7.5 Power		84.2	12.6	96.8	
7.5.1 Solar Panels	40.7				
7.5.2 Batteries	15.0				
7.5.3 PMAD	18.5				
7.5.4 Wiring	10.0				
7.6 Structure		75.0	7.5	82.5	
7.7 Thermal Control System		19.6	2.9	22.5	
7.7.1 Surface Finishes	3.6				
7.7.2 Insulation (MLI)	3.5				
7.7.3 Radiators	11.3				
7.7.4 Heaters	1.2				
7.8 Sample Return Capsule		75.0	7.5	82.5	
9.0 Consumables					20.0
10.0 Propellant					1302.3
10.1 MMH				566.4	
10.1 NTO				735.9	

Figure 4.2.A. Orbiter Mass Budget

4.3. Structures and Thermal

The main orbiter chassis is a 2.2 m x 2.2 m x 1.8 m rectangular prism constructed out of graphite-epoxy sandwich panels with aluminum honeycomb core. The launch vehicle side of the orbiter (shown at the top in the images below) consists of the launch vehicle adapter interface ring as well as the shroud and aperture for the main engine nozzle. The opposite end consists of a skirt structure that interfaces with the connection ring on top of the Mars entry aeroshell. The two vehicles are mated at this joint using pyrotechnic bolts which fire to separate the two upon arrival at Mars. The outer surface of the chassis is covered in MLI to provide passive thermal control for the spacecraft's

interior, primarily to keep the propellant tanks at low temperatures to prevent hydrazine decomposition or boiloff of NTO. Active thermal control is available via several patch heaters placed on electronics as well as radiator panels flanking the skirt end of the orbiter (visible at the bottom in the left image of Figure 4.3.A).

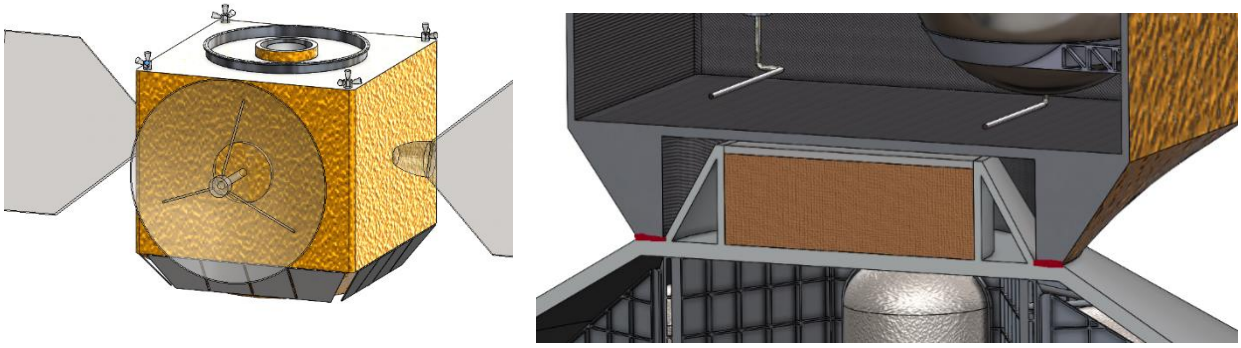

Figure 4.3.A. Orbiter Main Chassis (Left) and Cutaway Details of Interface with Mars Aeroshell (Right, Red Lines Represent Pyro-Bolted Interface)

4.4. Power

The orbiter power system architecture is heavily based on the European Space Agency's (ESA) Trace Gas Orbiter (TGO). The orbiter will be powered by a 13.33 m^2 solar array, which is expected to generate an average of 1333 W. Assuming a GaInP2/GaAs/Ge triple-junction solar array with areal density of 3.36 kg/m^2, this results in a total solar array mass of 44.8 kg. The orbiter with its solar wings deployed is depicted in Figure 4.4.A below.

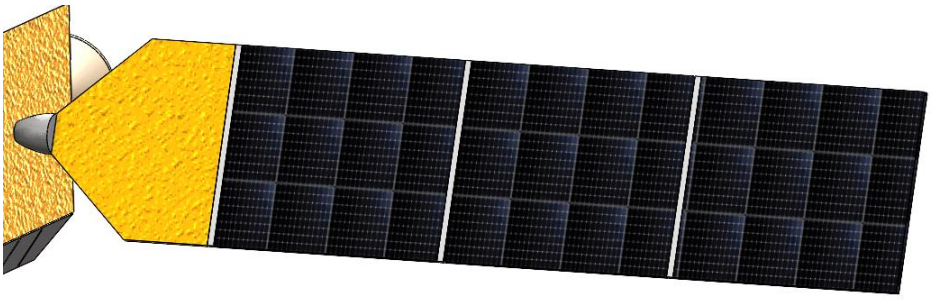

Figure 4.4.A. Solar Wing Deployed on Orbiter

Given two 90 A-hr lithium-ion battery modules and a 28 VDC spacecraft power bus voltage, a total of 5100 W-hr of energy storage capacity will be available for periods of increased power demand and during Mars eclipse. The power budget in Figure 4.4.B below details the allocations for each major orbiter subsystem. Estimates were initially based on power fractions provided in *Space Mission Engineering: The New SMAD* [10]and were subsequently adjusted to satisfy worst-case conditions during Mars eclipse, resulting in a healthy power margin of 24 percent.

Orbiter Power Budget					
	Level 2			**Level 1**	
	CBE	Cont.	Allocated		
1.0 Payload				300	
2.0 Spacecraft Bus (dry)				770	
2.1 Propulsion	90	9	99		
2.2 ADCS	100	10	110		
2.3 Communications	160	16	176		
2.4 C&DH	90	9	99		
2.5 Power	80	8	88		
2.6 Structure	30	3	33		
2.7 Thermal Control System	150	15	165		
2.8 Other (ECLSS, etc.)	0	0	0		
3.0 Spacecraft Allocated Power				1070	
4.0 Margin				263.3333333	
5.0 Total Power Available				1333.333333	Watts

Figure 4.4.B. Orbiter Power Budget

The cruise stage and orbiter will have four distinct power modes: sleep, orbit insertion, trajectory corrections and rendezvous, and return. During sleep mode, communications are maintained between the orbiter and ground stations on Earth for positional tracking. Only the thermal control and navigation systems are activated. Rechargeable batteries ignite thrusters to reorient the spacecraft during trajectory corrections and rendezvous maneuvers. During the return trip, primary batteries ignite main engines to perform the trans-Earth injection maneuver.

4.5. Propulsion

The orbiter main engine will be an R-42DM from Aerojet Rocketdyne. The spacecraft will also be equipped with 12 MR-106L thrusters (also from Aerojet Rocketdyne) to provide attitude control, course correction during cruise, and station keeping in Mars orbit. The properties of each are summarized in the table below:

Table 4.5.A. Thruster and Engine Characteristics. [11]

Characteristic	**R-42DM (main engine)**	**MR-106L**
Propellant(s)	Hydrazine/NTO	Hydrazine
Thrust	890 N	22 N
Specific Impulse	330 s	235 s
Mass (ea.)	7.32 kg	0.59 kg
Quantity	1	12
Purpose	Orbit capture, Trans-Earth injection	Station keeping, course correction, attitude control.

The main engine nozzle will be set into the body of the vehicle and shrouded to protect it from MMOD (see Figure 4.5.A below).

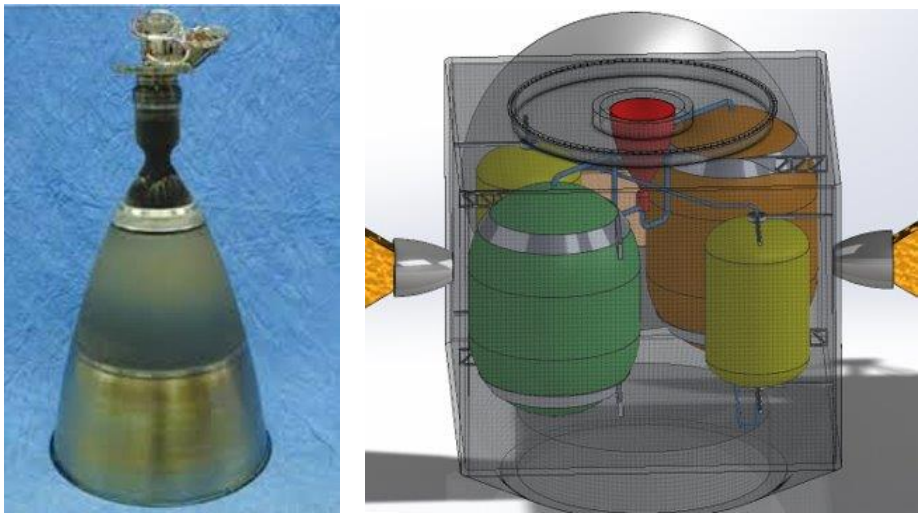

Figure 4.5.A. R-42DM Engine (Left) and View of Orbiter Propulsion System Internals (Right)

Propellant mass is sized from the ΔV requirements laid out in Table 3.4.4.A. The hydrazine tank is sized for an additional 75 kg for use as propellant by the RCS thrusters (the thruster configuration is shown in Figure 4.5.B below). The resulting total propellant load is 1302 kg, with 566 kg of hydrazine and 736 kg of NTO. All propellants are stored in titanium pressure vessels at 300 psi. Both propellant tanks contain surface tension-based propellant management devices to prevent the need for ullage motors or propellant settling maneuvers. The pressurant is 17 kg of helium stored in a titanium-lined graphite/epoxy COPV.

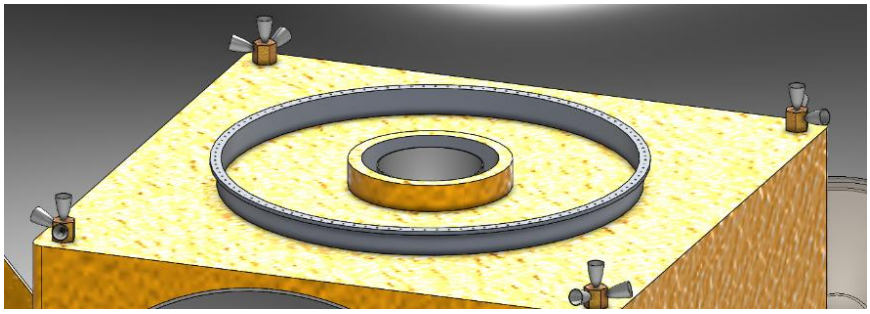

Figure 4.5.B. Orbiter Thruster Configuration with Main Engine Aperture in Center

4.6. Guidance, Navigation & Control

The mission will follow a GNC paradigm like those of past interplanetary missions. A nominal trajectory profile will be determined using a path planner prior to launch and loaded onto the spacecraft's computer system. After separating from the launch vehicle, a feedback control loop allows the spacecraft to make automatic corrections and adjustments to stay on course. A GNC block diagram is depicted below, in Figure 4.6.A:

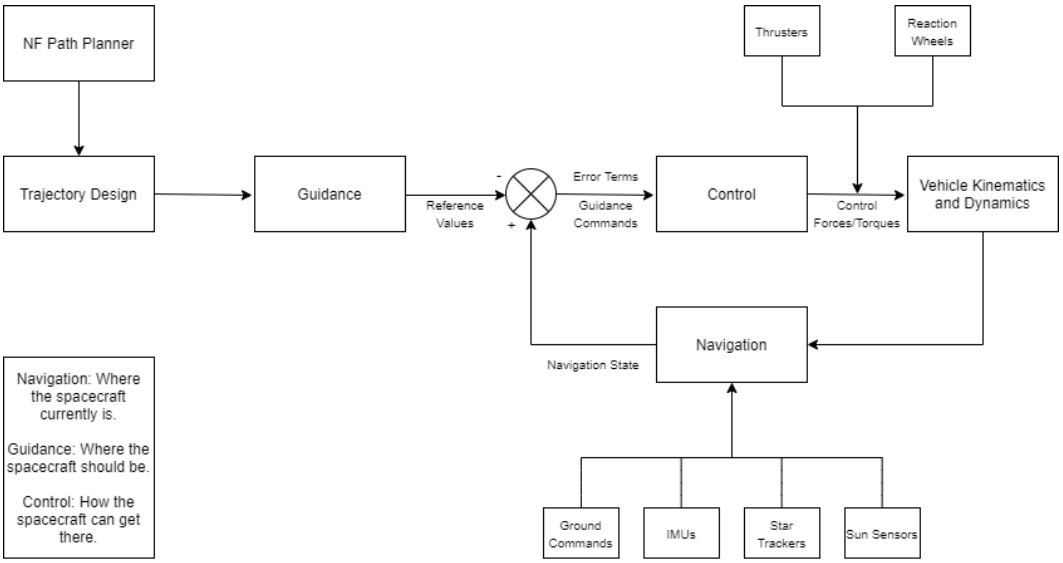

Figure 4.6.A. Block Diagram for the Spacecraft's GNC Framework

The cruise stage configuration of the spacecraft will be outfitted with IMUs, star trackers, and sun sensors, all of which provide readings used by the onboard computers to propagate a navigation state (translational and rotational). If this navigation state deviates from the desired trajectory, the system can correct itself with reaction wheels and Reaction Control System (RCS) thrusters.

In addition to automatic corrections, the system will be able to receive maneuver commands from Earth via its communication antennas. The DSN will also be tracking the spacecraft and receiving telemetry messages. If the navigation state propagated by the spacecraft's computers deviates too much, ground engineers can reset the onboard navigation state and command necessary course corrections. The following table lists the anticipated sensors and control devices for the system:

Table 4.6.A. GNC Sensors and Control Devices [12]

Name	Type of Device	Number (Backup)
Sun Sensors	Sensor	8 (8)
Star Trackers	Sensor	1 (1)
Inertial Measurement Units (IMUs)	Sensor	1 (1)
RCS Thrusters	Control Device	8 (4)
Reaction Wheels	Control Device	3 (1)

In addition to the GNC suite described above, a number of other sensors are also included to facilitate relative navigation and docking with the MAV. Radar ranging instruments allow the orbiter to determine relative position and velocity at longer ranges and guide itself in to rendezvous. Once the two are close, the orbiter commands the

MAV to reorient to optimal docking attitude and guides itself in to dock using optical sensors placed adjacent to the docking port in the SRC.

4.7. Command & Data Handling

The spacecraft's computer modules are perhaps the most critical components of the system, as they regulate and monitor the entire spacecraft throughout the course of the mission. Each of the subsystems for the spacecraft are governed by these modules, and as such, they must be extremely redundant and risk-tolerant to avoid any critical failures that could jeopardize the entire mission.

Electronics typically face extraordinarily harsh conditions when in space, as they are constantly bombarded with electromagnetic radiation that can flip bits and scramble data. All the electronic components and processors for this mission will be radiation-hardened to ensure reliability. Random Access Memory (RAM), which is typically necessary for computing, will be augmented with non-volatile flash memory, which allows the system to retain data without power. The VxWorks operating system, utilized by most deep space missions, is well known for its reliability and fault protection.

Given the impracticality of directly controlling the spacecraft during the mission (round trip communication times from Earth to Mars are several minutes), most of the processes and decisions made by the spacecraft will be autonomous. We foresee that with advancements in artificial intelligence and image recognition, the spacecraft will be capable of carrying out the mission with little to no operator interference. The table below lists the electronic components for the orbiter:

Table 4.7.A. Computer Components for the Orbiter

Name	Component
CPU	200 MHz BAE RAD750
RAM	512 MB
Flash Memory	20 GB
EEPROM	256 KB
OS	VxWorks

In the case of extreme events, however, the orbiter will still be able to receive messages from Earth and communicate with other spacecraft in the Mars Relay Network (MRN). Operators can send maneuver commands that the onboard electronics will receive and process. As the orbiter will have periods of time where it is on the far side of Mars, onboard storage allows it to store any messages or communications until it reaches its transmission window to Earth.

4.8. Communications

The orbiter is the mission component with the highest data uplink and downlink capacity from Earth. Its communications system needs to be capable of high throughout communication with DSN stations on Earth as well as the SPURS lander and other components of the Mars relay network. This goal is achieved by a set of X-band and ultra-high frequency antennas. The primary antenna is a 2-meter parabolic X-band High Gain Antenna (HGA) that transmits at 100 W of power. This provides a downlink capacity of 432 kbps to the 70-m DSN antennas on Earth at a 45-degree elevation. The orbiter also contains a set of X-Band Low Gain Antennas, used for lower throughput omnidirectional communications when the HGA cannot be pointed, and an Ultra High Frequency Antenna for shorter range communications with other spacecraft at Mars. The X-Band HGA, shown on the left of Figure 4.7.A. is the primary method of transmitting data to and from Earth. The right image is one of the orbiters LGAs, mounted on the same face as the SRC to support communications most readily with the MAV during docking.

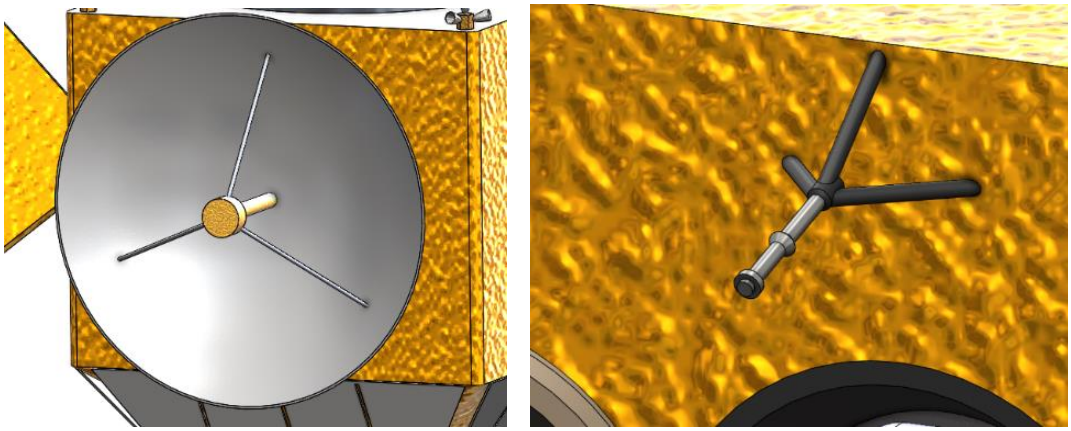

Figure 4.7.A. Orbiter HGA (Left) and LGA (Right)

A potential risk is loss of communication during a solar conjunction. Solar conjunction of Mars will occur between March 15 and March 25 of 2028, which coincides with the late aerobraking phase for all but the earliest launch dates in the launch window. As discussed in section 3.4.2 above, aerobraking will be halted for the duration of the conjunction if the two must overlap, thus preventing potential loss of mission due to the inability of operations personnel on Earth to monitor and modify the aerobraking orbits based on downlinked trajectory and atmospheric data.

The link budget for the downlink communication from the orbiter to Earth is shown below in Figure 4.7.B. This budget is for the case of the HGA transmitting data in the X-band to a 70m DSN antenna at an elevation angle of 45 degrees and pointing error of 5 degrees.

Link Budget for Mission Downlink					
Type of Link:	Downlink				
Channel:	X-Band				
Frequency:	8.5	GHz			
Wavelength:	0.03529412	meters			
Link	**Value**	**Units**		**Notes:**	
Power to Transmitter	100	W		*Power Source:*	Orbiter Power
Transmitter Efficiency	0.5			*Amplifier Type:*	TWTA
Transmitted Power	16.99	dBW			
Transmitter Antenna Gain	43.139	dB		*Transmitting Antenna Type:*	Parabolic
Signal Strength at Transmitter	60.128	dBW		*Transmitting Antenna Dimensions (m):*	2
Space Loss	-265.774	dB		*Distance from trans to rec (m):*	5.46E+10
Signal Strength Upon Arrival	-205.646	dBW			
Atmospheric Loss	-0.1	dB		*Assumed Elevation (θ)*	45
Signal Strength after Atmospheric Loss	-205.746	dBW		*Altitude of Ground Station (m):*	0
Pointing Loss	-5	dB		Avg Pointing Error (θ):	5
Signal Strength after Pointing Loss	-210.746	dBW		*Ant Half-power Beamwidth* (δ):	7.5
Receiver Antenna Gain	74.02	dB		*Receiver Antenna Type:*	Parabolic
RECEIVED POWER	**-136.726**	**dBW**		*Receiver Antenna Dimensions (m):*	70
Energy Per Bit: Eb	-193.715	dBW/Hz		*Bandwidth, B (Hz):*	500000
System Noise Density: No	-213.828	dBW/Hz		*System Noise Temp (K):*	30
Received Eb/No	20.113	dB			
Implementation Loss	-1	dB			
Link Margin (dB)	3.7	dB			
Required Eb/No	**17.413**	**dB**			
Required Bandwidth	432878.156	Hz			
Bit rate	**432878.156**	**bps**			

Figure 4.7.B. Link Budget

5. SPURS Lander and Sampling System

The System for Production of Under-Regolith Samples (SPURS) lander is at the core of the mission – it allows us to return samples from Mars and is the vehicle that can land on the planet and collect samples. While the form of the lander draws heavily from the *Phoenix* and *InSight* missions, and the sampling system is derived from that of *Perseverance*, the lander has been optimized within the mission's strict cost constraints to focus on the singular goal of obtaining, protecting, and launching samples into orbit.

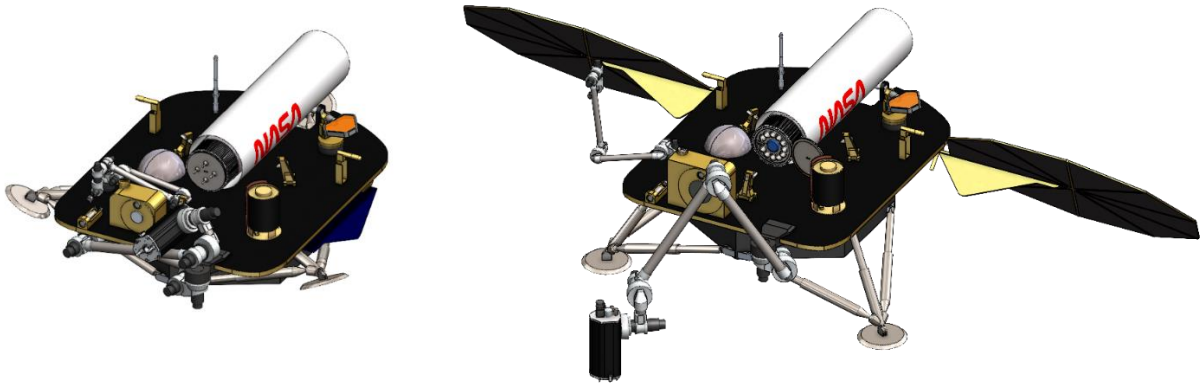

Figure 5.A. Stowed and Deployed Configurations of Lander

5.1. Requirements

Below are the requirements for the lander and its subsystems, including the entry, descent, and landing system discussed in Section 5.2.

Table 5.1.A Lander and EDL Requirements

REQ #	Requirement
LND-001	The lander shall be a robotic system capable of extracting, handling, and storing ice core samples on the surface of Mars.
LND-002	The lander shall be capable of carrying the Mars Ascent vehicle, and of providing the MAV a platform from which to launch into Mars orbit.
LND-003	The lander (not including MAV) shall have a total mass at landing of no more than 394.2 kg.
LND-004	The lander shall be capable of providing 300 W of electrical power for a duration no less than 2 hours during drilling operations.
LND-005	The lander shall be capable of sustaining critical systems in sleep mode at solar irradiances as low as 2.1 MJ/m^2/sol to await the MAV launch window.
LND-006	The lander shall contain a sample collection and handling system that allows for extraction of Martian ice core samples of at least 25 mm in diameter and 100 mm in length.
LND-007	The lander shall be capable of maintaining the ice core samples in their frozen state from collection until MAV launch.
LND-008	The lander shall be capable of hermetically sealing the ice core samples.
LND-009	The lander communication system shall provide uplink and downlink capabilities for commands and data to Earth at a bitrate sufficient to transfer video of critical drilling operations.
LND-010	The lander communication system shall be capable of receiving basic commands via an omnidirectional antenna for cases in which directed antennas cannot be operated.
EDL-001	The entry, descent and landing system shall be capable of landing no less than 806.2 kg on the surface of Mars.
EDL-002	The entry, descent, and landing system shall be capable of landing accurately enough to ensure access to ice deposits.
EDL-003	The entry, descent, and landing system shall allow for control of the lander's azimuth angle such that the forward side of the MAV faces within ±11.5° of true north.
EDL-004	The entry, descent, and landing system (including fueled descent stage and aeroshell) shall have a mass at launch of no greater than 1759.1 kg.

5.2. Mass Budget

The lander has a total mass allocation of 394.2 kg, approximately half of the total mass of the landed system (the other half is accounted for by the fully fueled MAV). A breakdown of the subsystem mass allocations is shown below. A breakdown is also shown for the descent stage discussed in Section 5.3 (Entry, Descent, and Landing)

	Breakdown	CBE	Contingency	Allocated	
3.0 Lander					394.2
3.1 Sampling System		120.0	12.0	132.0	
3.1.1 Core Drill and Bits	25.0				
3.1.2 Drill Arm	70.0				
3.1.3 Sample Handling Arm	20.0				
3.1.4 Sample Handling System Misc.	5.0				
3.2 Communications		24.2	2.4	26.6	
3.2.1 Low Gain/UHF Antennas	4.0				
3.2.2 High Gain Antenna	8.0				
3.2.3 Transponders	6.0				
3.2.4 Diplexers	1.2				
3.2.5 RF Switches, Cables, etc	5.0				
3.3 C&DH		25.0	2.5	27.5	
3.4 Power		74.0	11.1	85.1	
3.4.1 Solar Arrays	14.0				
3.4.2 Batteries	34.0				
3.4.3 PMAD	18.0				
3.4.4 Wiring	8.0				
3.5 Structure		75.0	7.5	82.5	
3.5.1 Vehicle Structure	60.0				
3.5.2 MAV Launch Tube	15.0				
3.6 Thermal Control System		20.0	4.0	24.0	
3.7 Other		15.0	1.5	16.5	

Figure 5.1.A. Lander Mass Budget

	Breakdown	CBE	Contingency	Allocated	
4.0 Landed Mass					806.2
5.0 EDL System					1759.1
5.1 Propulsion		167.9	33.6	201.5	
5.1.1 Mass of Engines	54.0				
5.1.2 Mass of Thrusters	40.0				
5.1.3 Propellant Tanks	28.9				
5.1.4 Pressurant Tanks	21.0				
5.1.5 Pressurant	8.0				
5.1.6 Lines, Valves, Fittings, Regulators, etc	16.0				
5.2 Propellant (Hydrazine)		350.0	0.0	350.0	
5.3 Structure		625.0	62.5	687.5	
5.3.1 Backshell	250.0				
5.3.2 Heatshield	225.0				
5.3.3 Descent Vehicle Strucure	150.0				
5.4 Mechanisms		119.0	23.8	142.8	
5.4.1 Parachute	58.0				
5.4.2 Parachute Deployment	11.0				
5.4.2 Bridle Lowering Sytem	50.0				
5.5 Communications		20.0	2.0	22.0	
5.6 C&DH		50.0	10.0	60.0	
5.7 ADCS		50.0	5.0	55.0	
5.8 Power		65.5	9.8	75.3	
5.8.1 Batteries	28.5				
5.8.2 PMAD	27.0				
5.8.3 Wiring	10.0				
5.9 Other		150.0	15.0	165.0	
6.0 Mass at Entry					2565.3

Figure 5.1.B. Descent Stage Mass Budget

5.3. Entry, Descent, & Landing

The mission requires an EDL system capable of delivering approximately 800 kg of payload to the Mars surface at altitudes of around –3000 m to –4000 m MOLA and a latitude of approximately 50-60 degrees north. The atmosphere in these high latitudes on Mars is thinner for some portions of the year due to freezing of atmospheric carbon dioxide. This effect will be particularly pronounced at our arrival time because past missions have seen the lowest atmospheric pressure around Martian solar latitudes of around 150° when Mars is around aphelion and the south pole is in near total darkness (see Figure 5.3.A) [13]. The solar latitudes of the possible landing times under the proposed mission architecture range from approximately 147° to 180°, during which Phoenix (PHX in Figure 5.3.A) measured mean atmospheric pressures as low as just under 750 Pa and Viking 1 (VL1) saw local values dip below 700 Pa. The EDL sizing simulations discussed in this proposal were conducted using a worst-case sea level pressure of 700 Pa, with appropriate scaling also applied to the density used in aerodynamic calculations. Though VL1 measurements drop below this value, the Viking 1 landing site was substantially further south than Viking 2 (VL2) and Phoenix. Both are closer in latitude than VL1 to this mission's chosen landing site and show good agreement with each other in their atmospheric variation measurements, in relation to which a 700 Pa minimum is conservative (neither observed a single day with mean pressure below 725 Pa).

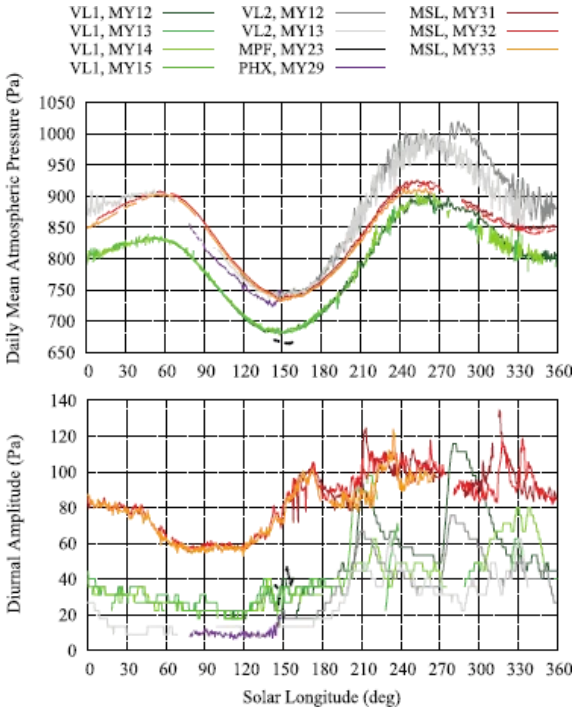

Figure 5.3.A. Local Atmospheric Pressure Variation at Mars Landing Sites [13]

The only heritage system capable of achieving the landed mass requirements needed for this mission is the combination parachute/sky crane system utilized to land the *Curiosity* and *Perseverance* rovers, both of which exceeded a landed mass of 900 kg [14]. Supersonic Retropropulsion (SRP) was considered as an alternative to parachute deceleration but was not selected due the outcome of the trade study summarized in the decision matrix below. The benefits of SRP would be minimal due to the relatively low ballistic coefficient of the vehicle (107 kg/m^2, compared to *MSL*'s 140 kg/m^2) and would come with increased risk to mission success (due to lack of current development) as well as schedule and cost. A primary benefit of SRP would be its potential for very high accuracy landing (on Earth, Falcon 9 has repeatedly demonstrated meter-level accuracy using SRP, albeit on suborbital trajectories), but this is lessened to some degree by the lack of a GPS-style navigation system on Mars. Moreover, the *Mars 2020* mission demonstrated the ability of the sky crane system to target an ellipse that falls well within the bounds needed for this mission's chosen landing site. An SRP system would also need to be more massive than a comparable parachute system, so it would be a poor choice for the overall mission mass margin. Reliance on aerodynamics to bleed off most of the spacecraft's energy during EDL leads to the concern of deteriorated performance due to EDL taking place at a low point in the pressure cycle at arrival as discussed above. However, the solar latitude during the arrival and EDL of the *Curiosity* rover was 150.7°, so the sky crane system has successful flight heritage under nearly identical atmospheric conditions [15].

Table 5.3.A. EDL System Decision Matrix

EDL System	Cost Wt. = 2.0x		System Mass Wt. = 1.0x		Landed Mass Capacity Wt. = 1.5x		Landing Accuracy Wt. = 1.5x		Risk Wt. = 1.75x		Weighted Total
	U	**W**	U	**W**	U	**W**	U	**W**	U	**W**	
Skycrane	8	16	7	7	6	9	8	12	8	14	58
SRP	4	**8**	3	3	10	15	10	15	4	7	48
Key: U = Utility Value, W = Weighted Value, 0 = Worst, 10 = Best											

Given these factors, it was determined that SRP is not necessary and does not make sense to use for this mission at such low ballistic coefficients. The resulting system is derived from a roughly 10% downscaled version of the MSL/Mars 2020 Sky crane EDL architecture, with some additional tweaks made to reduce mass as mission parameters allow. In particular, propellant load was reduced by 50kg and the parachute size was decreased from 19m to 16m, which are both possible due to the reduced landed mass and lower landing site altitude requirements.

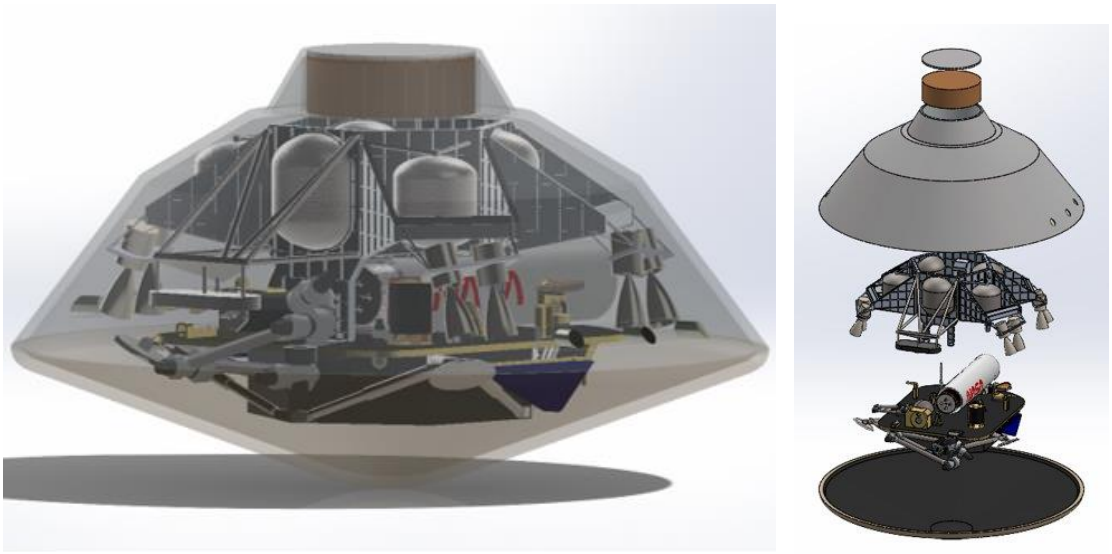

Figure 5.3.B. Stowed Configuration of Lander and EDL System

EDL occurs in multiple stages. First, the Mars entry aeroshell separates from the orbiter prior to orbital insertion and directly enters the Martian atmosphere. Prior to atmospheric entry, it ejects a set of 3 entry balance masses with a total mass of 75 kg to offset the center of mass and generate a lift to drag ratio of 0.15 (compared to MSL, which ejected 150 kg and generated a L/D of 0.24) [16]. It then enters the Martian atmosphere at approximately 6 km/s and slows from these hypersonic speeds through a controlled descent, accomplished by rotating the lift vector with onboard RCS thrusters. When parachute deployment conditions are reached, another set of masses are ejected to re-center the CG and the parachute is deployed after a brief time when oscillations have stopped. The heatshield is jettisoned when the vehicle slows to below Mach 0.8. While under parachute, the spacecraft's landing radar creates a 3-dimensional map of the terrain below and feeds this to the Terrain-Relative Navigation (TRN) system, which matches the radar data maps of ice deposits and hazard zones pre-constructed from orbiter data collected during the leadup to EDL by NASA's various Mars orbiters. This system allows selection of a precise landing site that will both provide a safe place for lander touchdown and ready access to the desired ice deposits. The TRN system incorporated into Mars 2020's EDL system allowed landing within 5 meters of the point selected while the rover was under parachute - this is ample accuracy to land on or near ice deposits visible in high-quality orbital imagery at the chosen landing site. Once a site is selected, the descent stage breaks away from the backshell and flies its generated trajectory to the selected site. This trajectory is designed such that when the sky crane is lowered, the lander will be oriented with the MAV's nose pointing to the north and the solar panels (after deployment) tilted to the south. The landing vision system on Mars 2020 was shown to be accurate at determining the attitude to an error

of less than 0.5°, and the landing engines are deeply throttleable and canted to provide full 6DOF control [17, 18]. Taken together, these allow for a trajectory design that will land well within the roughly ±11.5° clocking needed to ensure adequate power generation (defined as the angle which would create a 2% cosine loss at solar noon). Finally, the lander is gently set on the surface (at a speed of approximately 0.75 m/s) and the descent stage performs a flyaway maneuver.

Key features of the EDL system are specified in Table 5.3.B below:

Table 5.3.B. EDL System Specifications

Mass at Entry	2565 kg
Landed Mass	806 kg
Heatshield Diameter	4.5 m
Ballistic Coefficient	107 kg/m^2
Offset Masses	2 sets at 75 kg ea.
L/D Ratio	0.15
Parachute	16 m DGB
Propulsion	8x MLEs (3.6 kN and Isp = 225 s)
Propellant Load	350 kg
Power	Li-SO2 Primary Batteries
Communications	2x X-band LGAs
Navigation Sensing	Redundant IMU navigation, radar altimeter (post-HS separation)

5.3.1. EDL Simulation Results

A custom 3DOF simulation was built to model the EDL dynamics and determine appropriate parameters for the system. The simulation numerically integrates the equations of motion for the system in the various phases of the EDL sequence- approximate solutions such as the Allen Eggers equations are not suitable because the trajectory is not purely ballistic due to the lift generated by the CG offset. Some of the above specifications, such as propellant load and lift to drag ratio, were selected after iteration with this simulation. Table 5.3.1.A shows the initial entry conditions as well some key simulation results for a nominal EDL with the worst-case atmospheric assumptions discussed above.

Table 5.3.1.A. EDL Trajectory Simulation Results

Initial Velocity	6000 m/s
Initial Altitude	125 km
Initial FPA	16 °
Peak Deceleration	11.0 g
Peak Heating*	170 W/cm2
Maximum Dynamic Pressure	11.7 kPa
Propellant Usage	289 kg (61 kg Margin)
Touchdown Time	Entry + 410 s (6 m, 50 s)
Downrange Travel	593 km

Peak heating is difficult to estimate without intensive CFD analysis due to the transition to turbulent flow over the large aeroshell, but for this case, calculations were done assuming laminar flow over both our capsule and MSL. The disparity between the calculated value and measured value for MSL was then used to scale up the laminar estimate for our mission - the resulting value is what is reported here. The 289 kg of propellant usage quoted includes a minimum flyaway propellant of 52 kg (all engines at full throttle for 4 seconds). All 350 kg would be burned because the flyaway continues until the tanks are depleted.

Figure 5.3.1.A shows the overall profile of the vehicle from entry until landing. The vertical dotted line represents parachute deployment. The trajectory remains mostly straight (and velocity mostly constant) for much of the entry, but at an altitude of around 60 km it begins to bend upward as the capsule hits the denser lower atmosphere and the lifting body dynamics reduce the velocity and flight path angle. It coasts for some time at about 20 km, bleeding off a large amount of energy, and then slows enough to begin tilting downward toward parachute deployment.

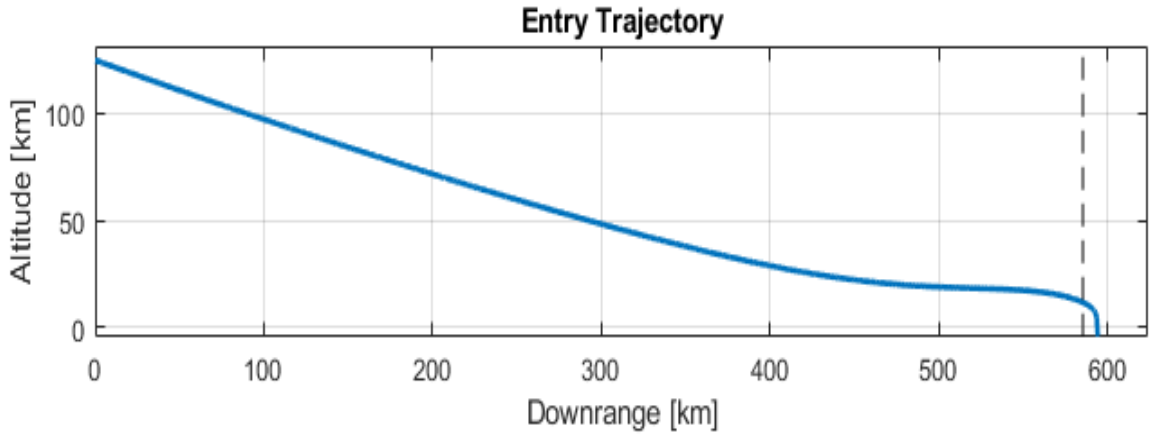

Figure 5.3.1.A. EDL Simulated Trajectory

Of primary concern is selecting a system and initial conditions that will result in parachute deployment within an acceptable set of bounds. DGB parachutes, of Viking and MSL heritage, have been designed and demonstrated to reliably deploy at Mach numbers of 1.8-2.2 and dynamic pressures of 500-750 Pa [19]. Figure 5.3.1.B shows the trajectory of the vehicle leading up to deployment in Mach-Q space (time increasing along the trajectory from top right to bottom left). The red lines represent the bounds for safe deployment. Parachute deployment in this scenario (at the end of the blue curve) happens safely within the acceptable bounds of the parachute design.

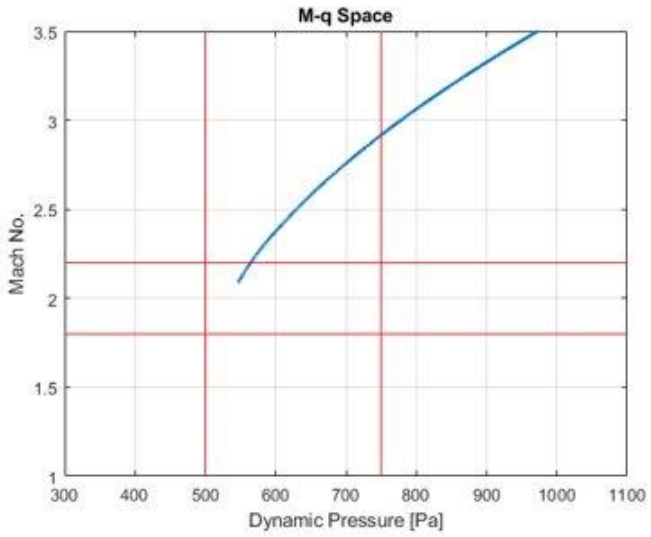

Figure 5.3.1.B Trajectory of Vehicle in M-q Space Leading to Parachute Deployment

The Figure below compares the simulated EDL trajectory in altitude-velocity space to those of MSL and Phoenix. The simulated Glacies Nova trajectory shows a blend of aspects from these two past trajectories. The overall shape of the curve with the 'flat' center, representing the region in which lift from the capsule is allowing nearly horizontal flight to bleed off velocity without dropping altitude, is remarkably like what was experienced by MSL - this is sensible because the EDL architecture is largely the same, though the upward curve on the MSL plot is slightly more pronounced due to the larger lift to drag ratio (even increasing in altitude at one point). However, the lower ballistic coefficient and slightly shallower entry angle cause the vehicle to begin to slow much higher in the atmosphere, similar to Phoenix.

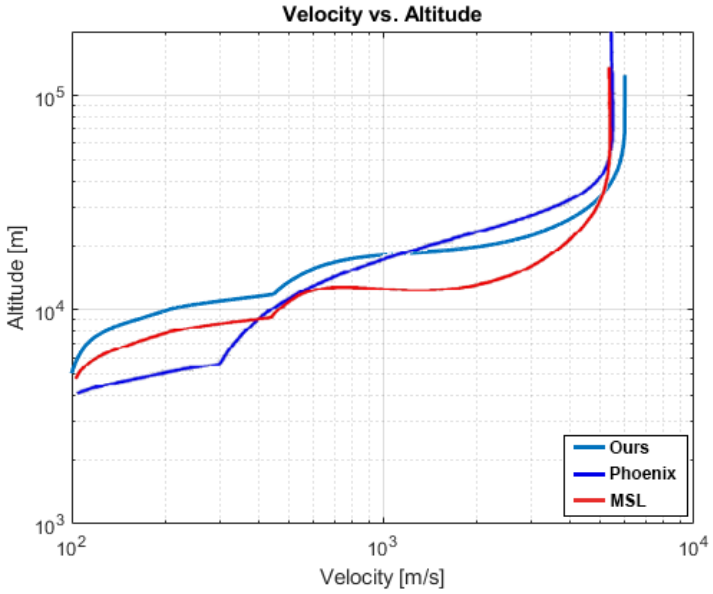

Figure 5.3.1.C Comparison of Simulated Trajectory to MSL and Phoenix [20]

5.4. Structures and Thermal

The main chassis structure of the lander consists of graphite/epoxy honeycomb sandwich panels to provide good stiffness and strength with little mass. A dark matte paint is applied to the panels to encourage absorption of solar energy (to aid in thermal control) and to prevent reflective glare from interfering with any imagery. An internal electronics box with thermal insulation and an assortment of heaters and radiators will keep science instruments and electronic components within their operating temperature ranges. The exterior of the chassis consists of mounting points for the solar panels, MAV erector system, landing legs, sampling system mechanisms, and other auxiliary sensors and components.

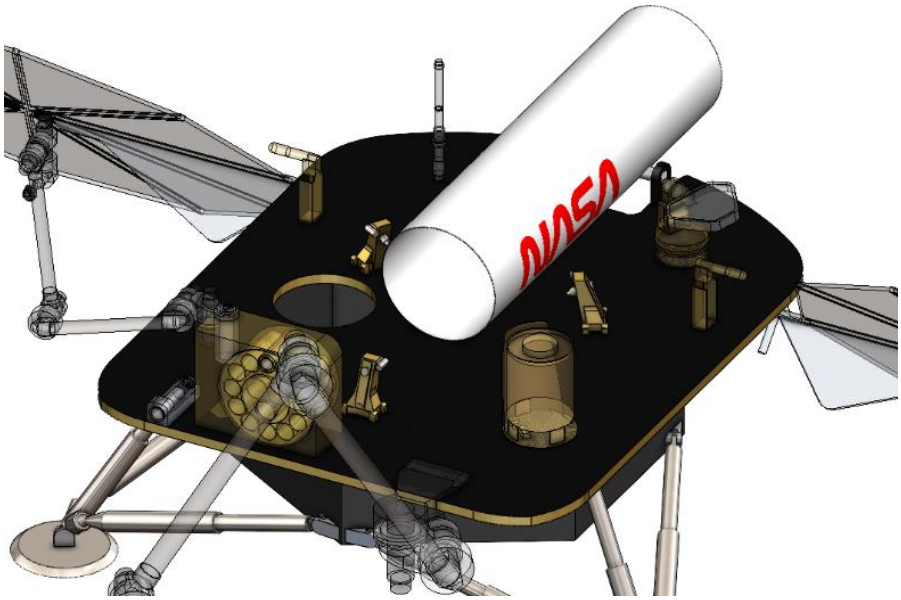

Figure 5.4.A. Main Lander Chassis

The legs of the lander are made of telescoping titanium tubing with aluminum honeycomb crush cores to absorb any excess impact energy on landing. Each consists of three legs - one central leg and two supporting side legs that attach to the base of the central leg with a ball and socket type joint. All legs are hinged at their connection points to the chassis. The landing feet are attached on hinges at the base of the central legs. This system provides a strong, stable base for the lander while still allowing the legs to be stowed up beneath the heatshield for cruise and entry. After the heatshield is jettisoned during the parachute descent, the legs are lowered and locked into place.

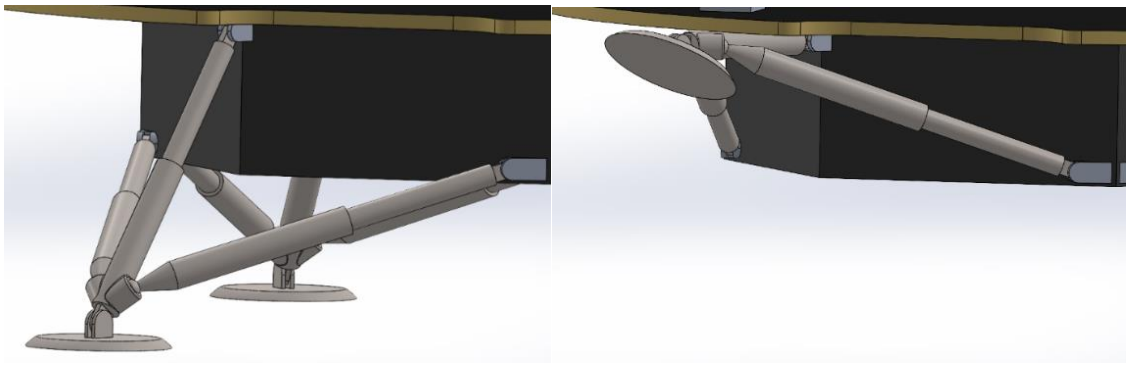

Figure 5.4.B. Landing Legs in Deployed (Left) and Stowed (Right) Configurations

The deck of the lander also includes a shroud to protect the MAV from damage due to debris during landing and shield it from Martian dust storms. The shroud is made thin insulated aluminum tube and is attached to the deck via a motorized hinge system that allows it to rotate upward, positioning the MAV for launch. The shroud is positioned over one of the landers legs so that the center of mass of the MAV stays within the stable base of the lander after it is lifted- as a result, the shroud is only able to rotate to an angle of 85° from the deck. It is pointed so that the MAV will be facing north at liftoff, and any launch azimuth offset due to landing error can be easily corrected after launch by the MAV's TVC system. This leg configuration has the additional benefit that there is not a leg obstructing the ground area in front of the lander where the sampling drill operates. Concealed inside the shroud are power and data umbilicals that allow the lander to transfer data and electricity to the MAV systems prior to launch. The bottom end of the shroud is open to allow the MAV exhaust to vent out of the back.

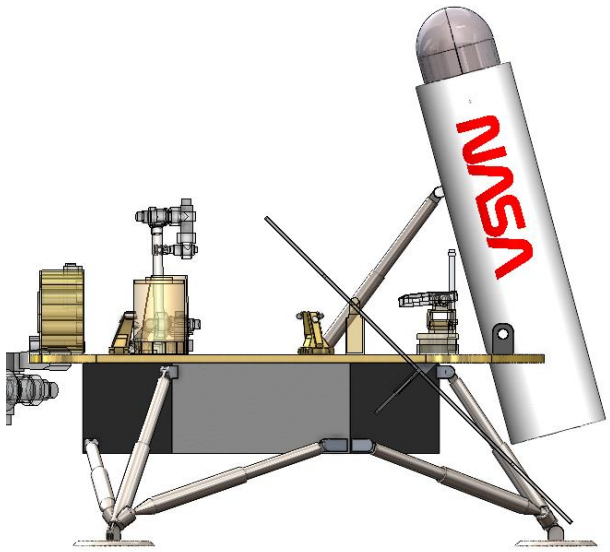

Figure 5.4.C. Side View of MAV in Shroud Upright on Lander Deck

5.5. Power System

The choice of power system has numerous implications for operations on the Martian surface. Factors such as landing site, maneuverability, thermal control methods, and potential science return are all influenced by the power source selected for the lander. Since solar panels and radioisotope thermoelectric generators (RTGs) have both been utilized in planetary missions successfully, a trade study was performed to select between these two alternatives.

The design factors evaluated during this trade study were (1) fuel efficiency, (2) mass, (3) cost, (4) reliability, and (5) risk. A successful return of ice core samples would be more desirable than spending the lowest possible budget, which means risk and reliability should be assigned a higher weight than cost. However, cost remains a primary driver of design decisions that prioritize the use of pre-existing technologies. Therefore, cost was awarded the second-highest weight. An RTG was used for the *Curiosity* and *Mars 2020* missions, and there is substantial documentation that affirms the reliability of RTGs in general [21] [22]. The Pu-238 fuel used in RTGs is highly regulated, scarce, and expensive, which makes fuel efficiency paramount [21]. Mass was given a higher weight than fuel efficiency because mass savings lower overall costs and provide a higher margin for system design evolution. Since the *Glacies Nova* mission will be unmanned, safety was not a consideration of the trade study.

Power system failure modes were analyzed to compare risk for these alternatives. Unlike solar panels, RTGs can generate consistent power in almost any Martian environment [23]. Because an RTG-powered lander would not require access to sunlight, a dust storm would pose more danger to a solar-powered lander. However, most Martian dust is easily displaced by gusts of wind, and severe dust storms are a rare occurrence. Moreover, a tilted array has the additional benefit of minimizing airborne dust accumulation from the Martian atmosphere. In the event of a severe dust storm, the lander could enter sleep mode to conserve its power and "wait out" the turbulent weather. Following such a storm, gravity and gusts of winds would gradually dislodge dust deposits and restore power functionality to the lander. Although power failure is less likely for an RTG, the risks of using solar panels are easily mitigated. Therefore, solar panels remain a viable alternative for surface power.

Prolonged exposure to the harsh Martian environment would present additional risks for surface operations. Contact with abrasive atmospheric dust and extreme temperature fluctuations would gradually cause solar cell degradation and thermal fatigue, thereby reducing the performance of the solar array. However, the shorter timeline of this mission would drastically reduce the impact of such incremental changes. Furthermore, an RTG-powered system

would experience similar performance reductions due to the steady decay of its radioactive core, which means opting for a solar-powered system does not introduce undue risk to the mission.

A decision matrix was developed utilizing the methodology described above, where each system was scored according to the assigned weightings and scaled values. The decision matrix is shown below in Table 5.4.A.

Table 5.5.A. Surface Power Source Decision Matrix

Surface Power Source	Fuel Efficiency Wt. = 1x		Mass Wt. = 2x		Cost Wt. = 2.5x		Reliability Wt. = 3x		Risk Wt. = 3x		Weighted Total
	U	**W**	U	**W**	U	**W**	U	**W**	U	**W**	
Solar Panels	4	**4**	4	**8**	10	**25**	8	**24**	8	**24**	85
RTG	1	**1**	3	**6**	1	**2.5**	10	**30**	10	**30**	69.5
Key: U = Utility Value, W = Weighted Value, 0 = Worst, 10 = Best											

The available electrical power produced by the solar array would be a function of several factors. The most important of these are the landing site latitude and time of year on Mars, which affect the incidence angle of the sunlight shining on the array and the amount of time sunlight is available per sol [24]. Low incidence angles at high latitudes, reduced solar intensity near Mars aphelion, and short periods of daylight during a Martian Winter would reduce the available amount of electrical power produced by the solar array. Other factors affecting array output would include shadowing of the array from the masts and antennas, the amount of dust in the Martian atmosphere, and dust deposition and accumulation on the array. The solar energy required to maintain the lander's thermal health would vary with latitude (i.e., landing site) and time of year [24]. During the Martian Winter there would be a higher demand for heat to maintain the lander's components within acceptable thermal limits, but there would be less total energy available from the solar array for the reasons discussed above.

Since the MMRTG costs around $109 million USD for production and deployment, it is likely that RTGs would be prohibitively expensive given the $1 billion mission cost constraint [25]. This coupled with higher efficiency and lower mass enables solar panels to edge RTGs for missions having stricter mass requirements, cost constraints, and shorter timelines. This led to the selection of solar panels over RTGs for the *Glacies Nova* mission.

5.5.1. Power System Architecture

The power system utilizes the same UltraFlex solar arrays used by the Mars *Phoenix* and *Insight* landers. The solar arrays have total surface area of 6.9 m^2 and will be tilted 45 degrees towards the sun. This will help offset cosine

losses arising from low solar insolation at the high latitude landing site. The stowed and unfurled configurations of the lander solar arrays are shown below in Figure 5.5.1.A.

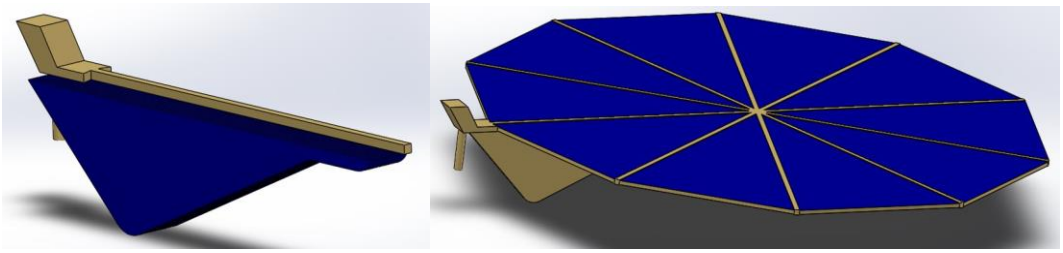

Figure 5.5.1.A. Lander Solar Arrays Stowed (Left) and Deployed (Right)

Once the lander reaches the Martian surface, the solar arrays deploy and tilt towards the sun to capture sunlight and initiate power generation. Of the available energy per sol, approximately 600 Watt-hours will be needed to excavate ice core samples. The remainder of the available energy would be needed for the lander's engineering functions, including communications and thermal control. The power budget in Figure 5.5.1.B shows the breakdown of power estimates for each of the major lander subsystems during its science operations phase. Power allocations were estimated with power fractions provided in *Space Mission Engineering: The New SMAD*, resulting in power margins for science operations and sleep mode of 27 percent and 9 percent, respectively [10].

Lander Power Budget

Science Operations	Level 2			Level 1	
	CBE	Cont.	Allocated		
1.0 Payload				0	
2.0 Lander Bus (dry)				330	
2.1 Propulsion	0	0	0		
2.2 ADCS	0	0	0		
2.3 Communications	54	5.4	59.4		
2.4 C&DH	27	2.7	29.7		
2.5 Power	30	3	33		
2.6 Structure	9	0.9	9.9		
2.7 Thermal Control System	180	18	198		
2.8 Other (ECLSS, etc.)	0	0	0		
3.0 Lander Allocated Power				330	
4.0 Margin				90	
5.0 Total Power Available				420	Watts

Lander Power Budget

Sleep Mode	Level 2			Level 1	
	CBE	Cont.	Allocated		
1.0 Payload				0	
2.0 Lander Bus (dry)				77	
2.1 Propulsion	0	0	0		
2.2 ADCS	0	0	0		
2.3 Communications	12.6	1.26	13.86		
2.4 C&DH	0	0	0		
2.5 Power	7	0.7	7.7		
2.6 Structure	2.1	0.21	2.31		
2.7 Thermal Control System	48.3	4.83	53.13		
2.8 Other (ECLSS, etc.)	0	0	0		
3.0 Lander Allocated Power				77	
4.0 Margin				7	
5.0 Total Power Available				84	Watts

Figure 5.5.1.B. Lander Power Budget for Science Operations (left) and Sleep Mode (right)

The lander will have three distinct power modes: drilling, charging, and sleep. For drilling core samples, it is expected that the lander will encounter a maximum power draw of 150 W for two hours of drilling. After the samples have been collected, the lander enters charging mode to capture sunlight during peak solar incidence and charge the batteries for night hours. When no sunlight is available, the lander enters sleep mode and utilizes its energy reserves to supply survival heat. Sleep mode could also potentially occur if sufficient dust accumulates on

the solar arrays. However, the vertical tilt of the arrays would prevent sizeable clumps of dust from accumulating on their surface. Moreover, wind gusts should help mitigate the accumulation of statically charged dust sticking to the panels. The lander will have two 30 A-hr rechargeable lithium-ion batteries, which provide a total of 1680 W-hr of energy capacity. Assuming 95% conversion efficiency and 50% depth of discharge, this amounts to 39.8 kg of battery mass. The energy capacity of the batteries is sufficient to enable drilling operations and active thermal control of ice samples once they have been collected and transferred to the storage container.

To account for changes in solar availability during the mission, a MATLAB script was written to calculate the power output of the arrays. This calculation required the following inputs: the tilt of Mars on its axis, landing site latitude, solar array tilt angle, distance from Mars to the sun, solar cell efficiency, and degradation factors. To be conservative, it was assumed that 40 percent of the arrays would be covered with dust and that Mars remained at its furthest point from the sun. Given these assumptions, when the lander arrives at Mars close to 150 solar longitude, its solar arrays will produce 420 W. This satisfies the power requirement for the lander to fulfill its science operations during the first half of its Martian stay. By the time the ascent vehicle takes off from the lander close to 300 solar longitude, cosine losses due to lower solar incidence amount to a fivefold reduction in the solar array power output [26]. However, this is acceptable because much less power is required to operate the active cooling system and maintain other engineering functions while the ascent vehicle awaits its launch window. The lander will enter sleep mode for this portion of the mission and will draw from its ample energy reserves, enabling functionality during dismal solar irradiances as low as 2.1 $MJ/m^2/sol$ [26].

5.6.Sample Collection and Containment System

As the primary mission goal is the return of ice core samples to Earth, it is of critical importance that the sampling system is robust and well defined. The sample collection path on the ground begins at extraction by the rotary percussive coring drill. The sample, already contained in its tube, is then transferred to the onboard sample handling system which seals the tube and secures it into the actively cooled sample container. Once samples are collected, the sample container is enclosed in the top of the MAV for launch to orbit.

5.6.1. Core Drilling System

The selection of the drilling architecture was driven by three main design considerations. First, the drill shall be able to carve through a variety of difficult terrain to make it to the ice beneath the surface. Second, the system shall be power efficient as to not drain more power than the onboard power supply can provide. Finally, the system shall be

capable of utilizing temperature tracking to throttle the drill's rpm as to not melt ice [27]. We considered lots of heritage in terms of extraterrestrial core drills and determined that the *Perseverance* scientific arsenal would give us the best starting point. We modified parts of the system as needed to meet our objectives.

Perseverance is equipped with a coring drill (amongst many other drilling instrumentation) capable of extracting cores 1 cm in dimeter and 5 cm in length. Such core dimensions do not meet our 2.5 cm by 10 cm minimum core requirements, so the drill will need to be scaled up. However, at these minimum core dimensions, a total of 59 samples would be needed to reach the other requirement of 2.5 kg of ice to be returned to Earth. And it was determined that the ascent vehicle could not fit more than about a dozen samples in the payload bay. Because of these constraints, the final ice core dimensions were chosen to be 5 cm in diameter and 15 cm in length. The drill itself measures 40 cm in length, but only the first 15 cm will be capable of core extraction with a hollow barrel. Past the 15 cm mark, the drill barrel can no longer hold material. The updated design of the coring drill is shown in Figure 5.6.1.A below. This represents the first major change to the *Perseverance* core drill. The drill housing and its sample retention plunger system remain unchanged.

Figure 5.6.1.A. Updated Coring Drill

The second modification will be on the drill material itself. Our drill needs to be able to carve through any surface material (soil, rock, sand) as well as the ice beneath the surface. Tungsten carbide drills offer great durability and strength as well as the ability to drill through ice, making the material an excellent choice for our mission [28]. Finally, all instrumentation located on the robotic arm of *Perseverance* except for the coring drill will be deleted to save mass and money. The rest of the system will remain unchanged. The robotic arm will be 7 ft long with 5 degrees of freedom and will be mounted directly on top of our Lander. When fully extended, the arm measures 2 m long, which allows the lander to drill holes in a sweep radius of about 2 m. This represents a total drillable area of ~

6 m^2 which is more than enough to perform many drilling operations as shown in Figure 5.6.1.B. below. In order to obtain all of our samples, a drilling area of 3 m^2 would be sufficient. So even if half of this area is deemed unfit for drilling (rocks, obstructions, etc.), the system can still operate nominally, and the mission can be completed.

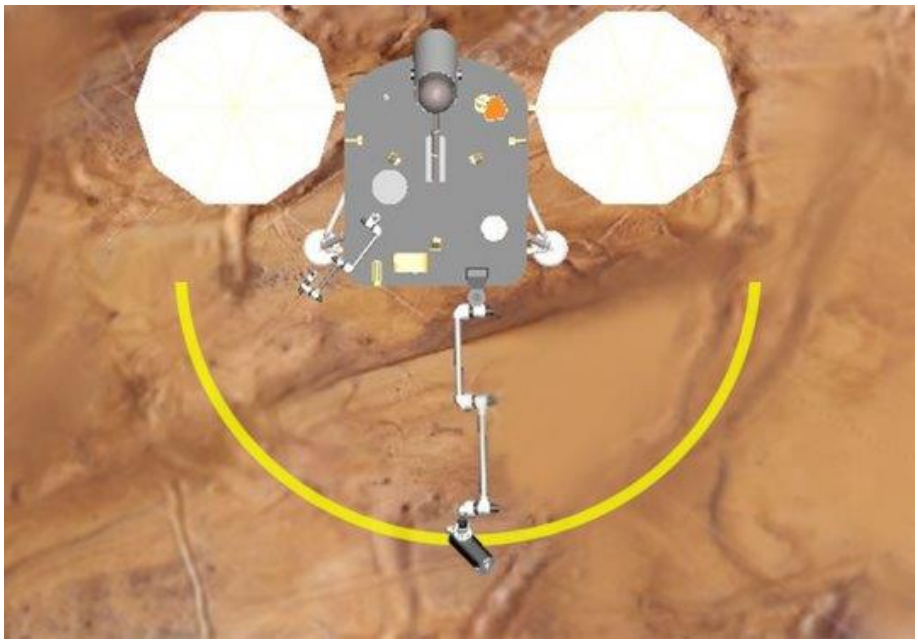

Figure 5.6.1.B. Robotic Arm Sweep Radius

Before choosing this specific drilling method, a trade study was conducted regarding which ice core drilling system would be best suited for our mission. For background information, Robert L. Staehle's "Mars Polar Ice Sample Return" design proposal was utilized to better understand different methods to extract ice cores from Mars' surface [29]. This cable-driven drilling system follows a very similar approach to drilling for ice cores on Earth.

Table 5.6.1.A. Ice Drilling System Decision Matrix

Ice Drilling System	Mass Wt. = 2x		Power Wt. = 2x		Reliability Wt. = 2.5x		Cost Wt. = 3x		Risk Wt. = 2x		Weighted Total
	U	**W**	U	**W**	U	**W**	U	**W**	U	**W**	
Cable Drill	3	**6**	4	**8**	10	**25**	7	**24**	3	**6**	69
Perseverance Drill	9	**18**	7	**14**	1	**2.5**	7	**30**	8	**16**	80.5
Key: U = Utility Value, W = Weighted Value, 0 = Worst, 10 = Best											

From the above trade study, it was concluded that simply modifying the *Perseverance* drill for the mission specific purposes would be the most optimal route in developing a drilling system. Staehle's most prominent design flaws were related to the mass budget specified for our system and the difficulty of integration and automation of earth ice

core extraction techniques on Mars. However, the *Perseverance* system is easily within the mission specified mass budget and is also a well-researched and tested system for coring samples on Mars.

The first failure mode for the each of the drilling systems results from potential refreezing of melted ice on the drill bit. If the drill is left frozen for extended amounts of time, such as a long night, there may be issues in restarting the drill for operational purposes. However, this mode can be mitigated by throttling the RPM of the drill. This would result in larger power draws within the specified power budget. The Staehle Drill, however, would perhaps experience a more serious problem of refreezing water on the coring system due to its manual rather than robotic design. This system would be more difficult to manage due to the depth that the drilling operations take place.

The next failure mode of discussion is related to mechanical failure. The *Perseverance* drill may experience certain terrain or environmental conditions that could result in wear and tear or material fatigue. However, this is an expected outcome of performing drilling operations in cold environments and the materials selection is integral in preventing total system failure. Therefore, regarding the *Perseverance* drill, this failure mode can be mitigated due to the high rigidity and low coefficients of thermal expansion of tungsten carbide. However, Staehle's drilling system is a highly mechanical system lacking autonomy. As a result, there are more potential areas that may be damaged resulting in a system failure, such as the cabling system to extract cores. A singular system that can be controlled autonomously and has a history of integration with current lander or rover technology would be the most beneficial in preventing mechanical failure.

Compared to our heritage, we had to upscale the drill diameter almost by a factor of two to meet our core size requirements. Consequently, we also needed to ensure that the new power draw was still in accordance with our power budget. However, according to Mellor's general considerations for drill system design, the torque requirement of our system does not increase by much [30]. This is because the two main factors that dictate torque required are drill diameter and drilling speed (depth speed not rpm speed). The graph below plots torque over drill diameter for three different drilling speeds: 0.5 in/rev, 0.1 in/rev, and 0.01 in/rev. Here, the unit in/rev simply means that for every 360-degree rotation, the drill is pushed down by a certain vertical distance measured in inches.

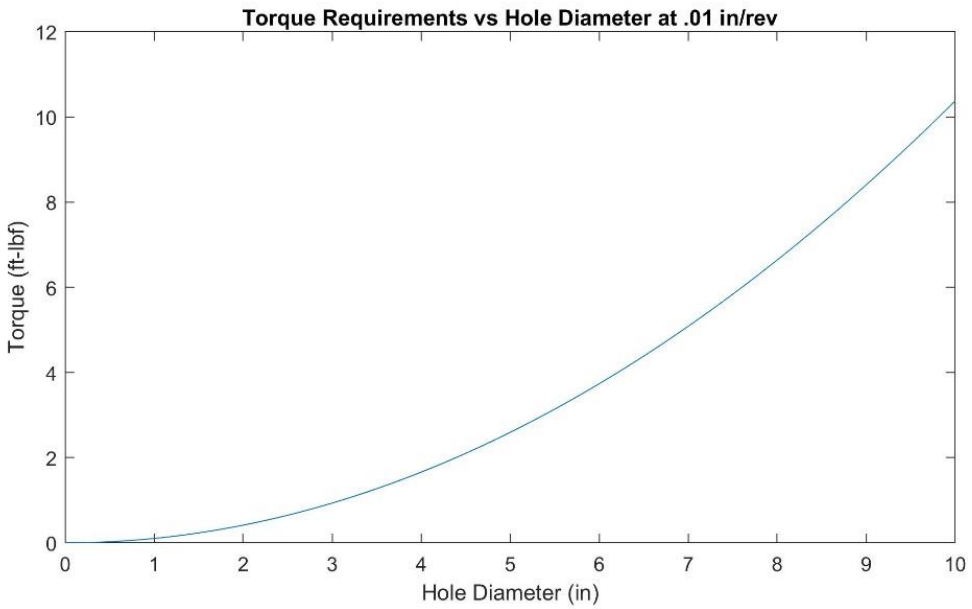

Figure 5.6.1.C Torque Requirement [29]

The graph above shows that as drill diameter increases, the required torque also increases. It is important to note that as the digging speed of a drill increases, the torque requirement also increases. In terms of drill diameter, our drill coming in at 5 cm is still considered small enough as to not increase the torque significantly on the exponential curve. In terms of drilling speed, if we choose a low drilling speed, we can expect the torque requirement to remain low. A drilling speed of 0.01 in/rev was chosen as the optimal solution. While this is a slow drilling speed, it is necessary as increasing the drilling speed would also increase torque requirements exponentially on the motor. The calculations in the chart above show that the new torque requirement would increase to 0.2 ft-lbf, from *Perseverance*'s 0.1 ft-lbf. This is still very reasonable and can be achieved with a slightly bigger or more powerful motor. Moreover, a slow drilling speed would also keep temperature increases to a minimum, which would be a safe way to limit the drill's rpm while keeping ice cold. We expect power consumption to be about 1.5x from *Perseverance*, so 150 W from 100 W. This remains in line with our power budget. The actual process of core extraction will be identical to the way *Perseverance* collects rock samples, except our cores will be 15 cm long. Ice on Mars is located between the surface and 10 cm below the surface underneath the soil. Utilizing the 40 cm long drill barrel, ice cores can easily be extracted from the landing site. If visible ice was in our drilling sweep radius, the robotic arm can simply drill pure ice cores directly from the surface. Moreover, the process can be repeated in the same location for a second core by lowering the drill into the hole and extracting another core. Extracting a third core from the same hole will not be possible as that would require a 45 cm drill barrel. The drill can first use a

regular bit to drill out a hole in the soil to access the subsurface ice. It can then swap to the coring bit from the drill carousel and drill one or two cores from the hole before needing to repeat the process.

During the drilling process, temperature readings are taken using a thermal imaging camera and embedded temperature sensors in the drill bit to prevent melting the samples. These readings will allow us to control the RPM of the drill to prevent melting or breaking of the ice core samples during the extraction process [31].

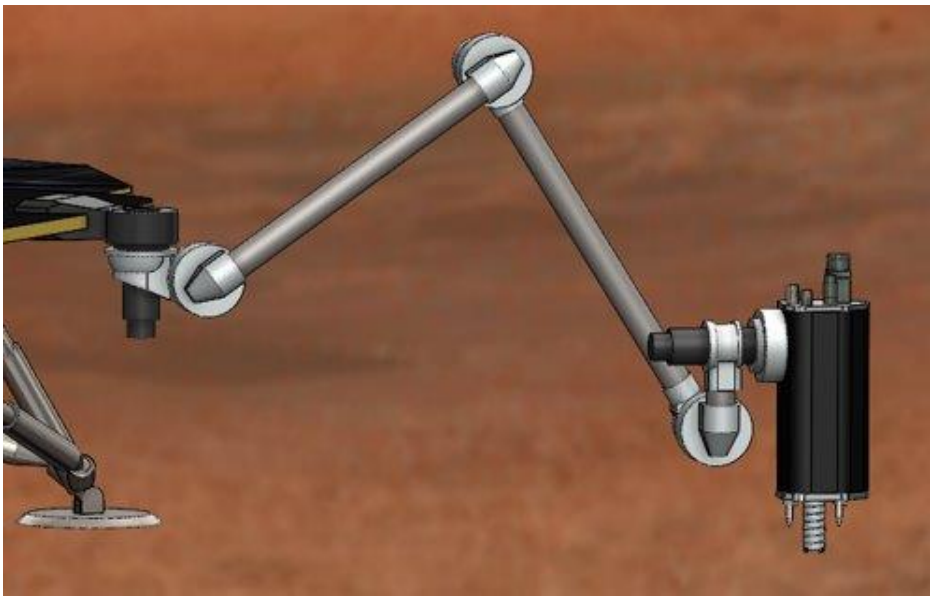

Figure 5.6.1.D. Drilling on the Martian Surface

5.6.2. Sample Handling

After the ice sample cores are extracted from the ground, the lander's sample handling system is responsible for places them into the sample container in the MAV to store until MAV launch off the surface of Mars. The major components of the sample handling system are the drill arm, the handling arm with a grip claw, the cap and tube dispensers, and the pass-off cradle. Both the drill arm and the handling arm have five degrees of freedom, allowing them to manipulate the samples, tubes, and caps effectively.

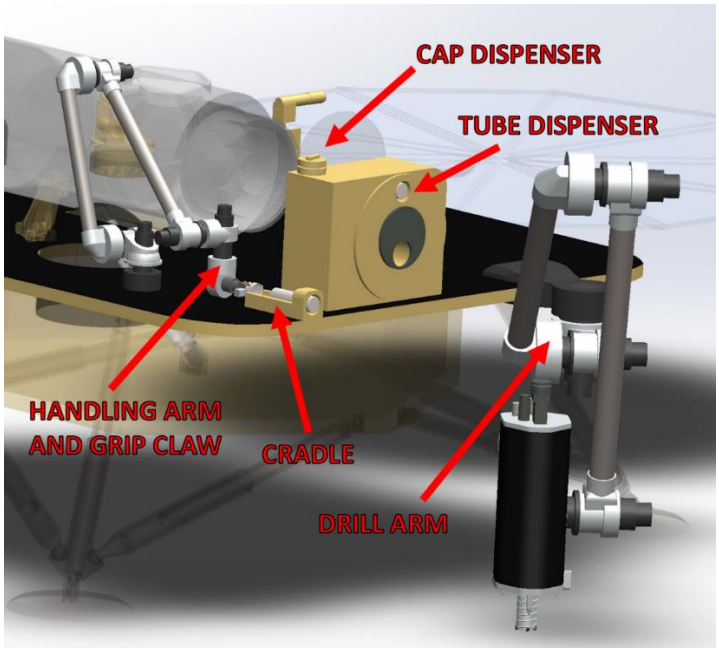

Figure 5.6.2.A. Sample Handling System Components

The following paragraphs describe the process of the sample handling of the ice core sample from extraction to final storage. First, after the lander successfully lands on the Martian surface, the drill arm moves out of its stowed position underneath the lander. It rotates to align with the tube dispenser and extracts a tube from the tube carousel, as shown in Figure 5.6.2.B. The tube stays inside the drill bit during the sample extraction, so the ice core will be inside the sample tube at the end. The drill arm then rotates to position the drill over the ground where the ice core will be collected. The drill then drills the core out of the ground, putting a sample into the sample tube in the drill shaft.

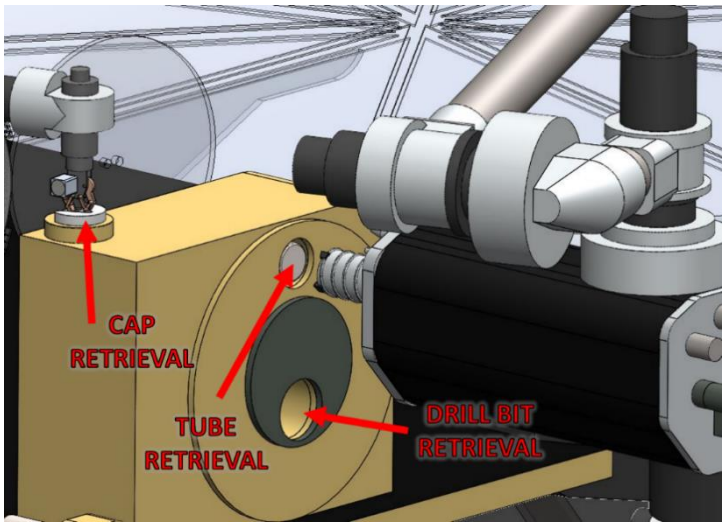

Figure 5.6.2.B. Sample Tube and Cap Retrieval

Next, the handling arm removes a cap from the cap dispenser by gripping the cap's handle and pulling the cap out, also shown in Figure 5.6.2.B. The handling arm then rotates down to place the cap in the back of the cradle and does not let go of the cap handle. The drill arm then rotates to position the drill bit at the front of the cradle, and the drill plunger pushes the sample tube containing the sample into the cradle. In doing this, the sample tube is pressed onto the cap, creating an airtight seal, as shown in Figure 5.6.2.C. (in the Figure the drill is shown backed out from the cradle ring for clarity, but during the real sample transfer process the bit would be pressed forward into the round receptacle in front of it).

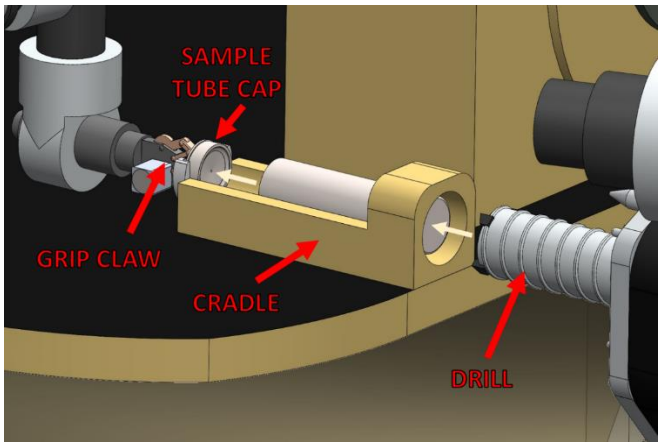

Figure 5.6.2.C. Sample Hand-Off Between Arms in the Cradle

Once the sample tube is capped, the handling arm, still gripping the sample tube's cap, lifts upwards to pull the sample tube out of the cradle, as shown in Figure 5.6.2.D. The handling arm then rotates around and positions the sample tube into the sample container, which is discussed further in the following section. Once the sample tube clips locks into place, the handling arm releases from the tube cap, and this process is repeated for the rest of the samples.

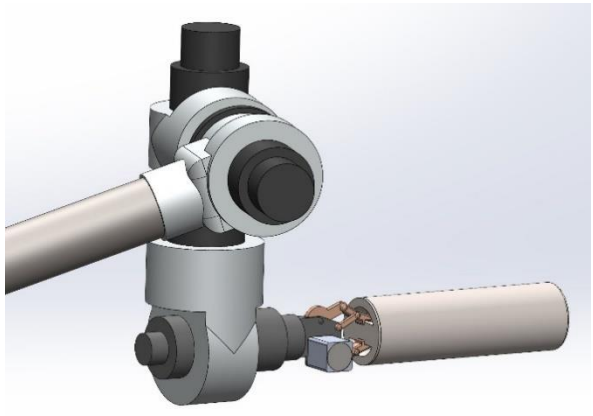

Figure 5.6.2.D. Handling Arm Lifts the Sample Tube Out of the Cradle

For the witness tube, the sample handling process is the same, except the drill does not collect a sample. Instead, the drill arm simply extracts the last sample tube straight from the tube dispenser and places it directly into the cradle, capping the empty sample tube. It is then placed into the sample container by the handling arm like the rest of the tubes. The sample container is discussed in section 5.8.

The original design of the *Perseverance* rover utilizes the drilling robotic arm both for sample extraction and transfer. To ensure a more efficient sample handling process, two robotic arms will be used, each for the function of extraction and transfer, respectively. Using two robotic arms allow for the samples to be placed into sample tubes, capped, and then placed into the sample container. If only one arm was used, the necessary complexity of the arm would be much greater than the two simpler ones. Additionally, to ensure the samples do not melt while exposed to warmer temperatures, the drilling and sample handling will take place during the Martian night. If the sample handling took place during the daytime, the sample could potentially heat up in direct sunlight and melt before being placed into the sample container.

The sample tubes and caps allow the arms to manipulate the samples and keep them from being exposed to the atmosphere while they are stored in the sample container in the MAV nose. The tube is 170 cm long, with an ID of 5 cm and an OD of 5.2 cm. They have an aluminum coating on the outside and a titanium nitride coating on the inside. This allows the samples to fully fill the inside but stay lightweight. The caps are also made of an aluminum exterior and a titanium nitride interior. Each cap has a handle that the handling arm's grip claw can grab securely.

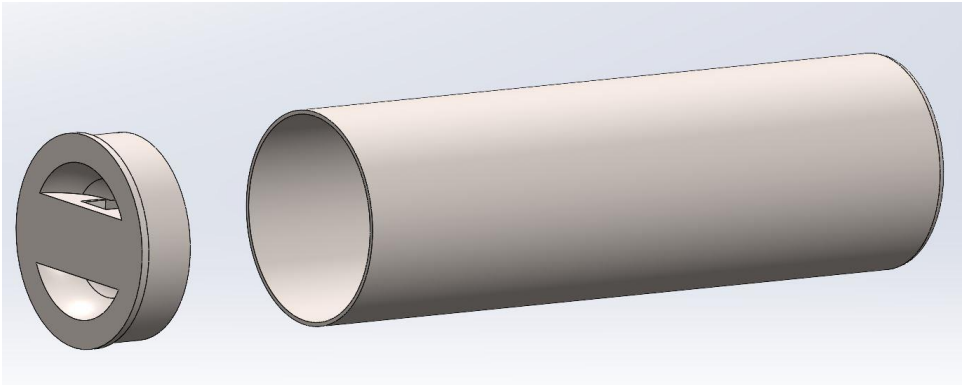

Figure 5.6.2.E. Sample Tube and Cap

The drill arm is the largest of the two arms and is located on the front of the lander. In order to save development cost, it is a direct copy of *Perseverance's* five degree of freedom drill arm. It has a total reach of 2.1m, and the drill is mounted on its hand turret.

The sample handling arm utilizes the same technology as the drill arm at a 60% scale, modified to have slightly different wrist joints. The new joints at the wrist allow the handling arm to fit and maneuver between fixed locations within the space on the lander in front of the sample container. Because the handling arm's movements are repetitive between the cap dispenser, cradle, and one of the 12 sample tube holes in the sample container, the handling arm is fully automated. Each of these locations is a set point that the five motors on the handling arm can rotate to without new live instructions from engineers. This decreases the amount of time needed to communicate movement commands back and forth with the lander, and thus decreases the amount of time that the sample spends outside of the ground before it reaches the sample container. The sample handling arm also retrieves the MAV fairings from their stored location on the lander and places them on the front of the MAV before launch.

The grip claw is attached to the end of the handling arm and is made of aluminum. The claw as a small motor that opens and closes the fingers, and another wrist motor rotates the claw itself. The grips on the claw are designed to fit snuggly onto the sample tube caps to ensure that the cap and sample tube will not fall out of the grip. The grip shape is shown in Figure 5.6.2.F.

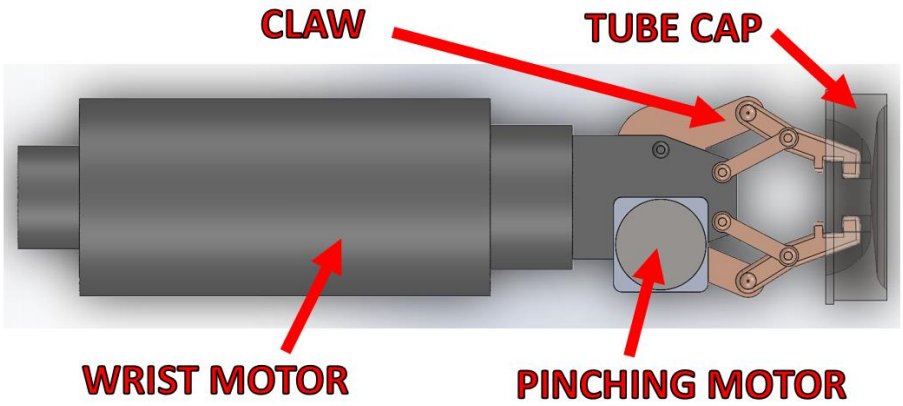

Figure 5.6.2.F. Handling Arm Claw

The tube and cap dispensers are located in the same part. They hold the sample tubes and caps from mission launch, through cruise and EDL until they are needed for sample collection. There are 13 cylinders in the sample tube carousel in the tube dispenser, allowing one to be empty during launch and descent so that there is not a tube exposed to the open air. The one hole located at the top of the dispenser is large enough for the drill bit to fit into. A clip is located at the base of the sample tubes, which the drill locks onto so that the tube stays in place during tube

extraction and drilling. When a new tube is needed for the next sample, the tube dispenser carousel rotates so the next sample tube is in the top hole. This is shown in Figure 5.6.2.G.

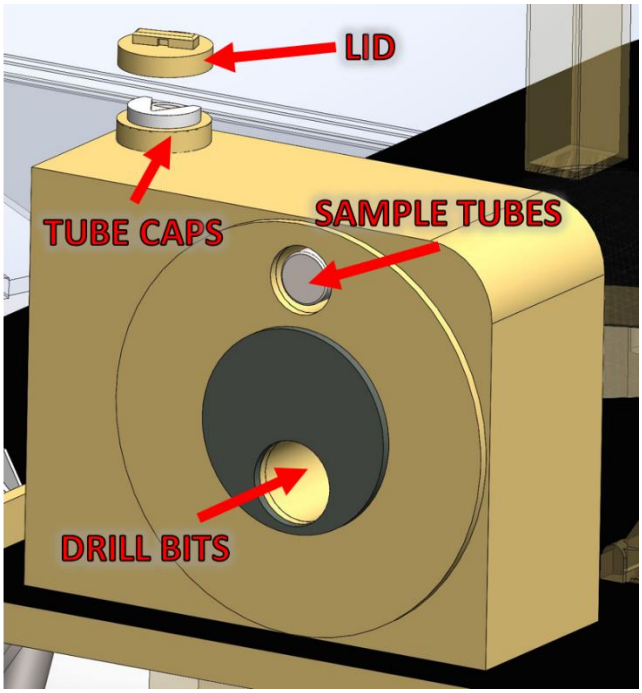

Figure 5.6.2.G. Tube and Cap Dispenser

The cap dispenser is located on the side of the tube dispenser and holds all 12 caps inside. During launch, cruise, and EDL, a cap dispenser lid covers the dispenser so that the caps stay secure inside. This lid has the same handle as the caps themselves, so the handling arm can remove the lid before sample handling begins. The cap dispenser itself holds the sample caps stacked on top of each other vertically, with a spring that pushes them to the top of the dispenser. To remove a cap, the handling arm grips the handle on the top cap and pulls it out horizontally allowing the other caps to be pushed upwards. The handling arm places the lid back onto the cap dispenser in-between sample collection to protect the caps. The cap dispenser is also shown at the top left Figure 5.6.2.G.

The sample transfer cradle allows the sample to be passed off from the drill arm to the handling arm reliably. It is located next to the tube and cap dispenser. The body of the cradle is a half-cylindrical cavity made to fit the sample tubes. At its front is a ring which matches the outer diameter of the coring bit. The opposite end contains a receptacle that allows the handling arm to position a cap securely in place. Once a sample has been collected, the drill rotates and positions the end of its bit within the ring. The internal plunger then drives the sample tube out into the cradle, pressing it into the cap and creating a hermetic seal.

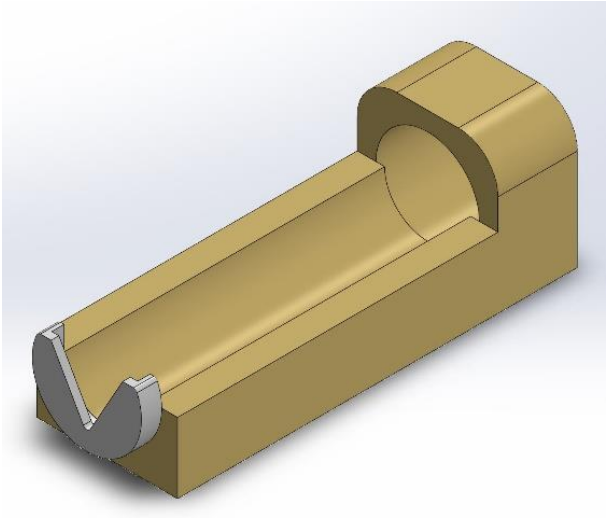

Figure 5.6.2.I. Sample Transfer Cradle

5.6.3. Sample Container

The samples must be maintained in a frozen state from collection until retrieval on Earth. For certain phases of the mission, such as during Martian nights and while shaded by the orbiter during cruise, passive insulation is enough to keep the temperature of the sample container sufficiently low. During Martian days and at times during return where it is impossible to shade the sample capsule, however, an active cooling method is required to ensure the samples never reach their melting point. Because power is limited by solar irradiance at Mars, energy efficiency is a major factor in the selection of a cooling system. Thermo-electric cooling and vapor compression cycles were both considered as candidates for this system. While thermo-electric systems have stronger spaceflight heritage, our analysis of each system determined that in our application a vapor compression system provided savings of approximately 200-300 W of electrical power. Due to power restrictions on the lander, it was decided to utilize a vapor compression cycle because of this significantly higher energy efficiency.

Table 5.6.3.A. Sample Cooling System Decision Matrix

Sample Cooling System	Mass Wt. = 2x		Power Wt. = 2x		Reliability Wt. = 2.5x		Cost Wt. = 3x		Risk Wt. = 2x		Weighted Total
	U	**W**	U	**W**	U	**W**	U	**W**	U	**W**	
Vapor Compression Cycle	8	**16**	8	**16**	10	**25**	8	**24**	8	**16**	97
Thermoelectric Cooler	4	**8**	2	**4**	8	**20**	6	**18**	8	**16**	66
Key: U = Utility Value, W = Weighted Value, 0 = Worst, 10 = Best											

The most common failure modes for a vapor compression cycle are related to compressor failure and refrigerant leakage. Oil lubricants require refrigerant to properly circulate through the system and maintain compressor operation. Therefore, refrigerant leakage can result in compressor failure and inadequate cooling. Thermoelectric coolers neither require refrigerants nor lubricants due to their reliance on the Peltier effect. However, simply adopting an oil-free scroll compressor and utilizing a parallel system will mitigate these failure modes while circumventing the significantly higher power demands associated with thermoelectric cooling systems. Finally, oil-free scroll compressors allow for operation in the microgravity environment of the sample return capsule.

The sample container is cylindrical in shape with a diameter of 370 mm and height of 210 mm (not including the docking lances on the lid). It contains space for 12 ice core samples 5 cm in diameter and 15 cm in length. The outer surface is wrapped in radiators that reject heat as part of the integrated cooling loop. A set of docking lances and plumbing connections on the lid interface the container with the return capsule during cruise back to Earth.

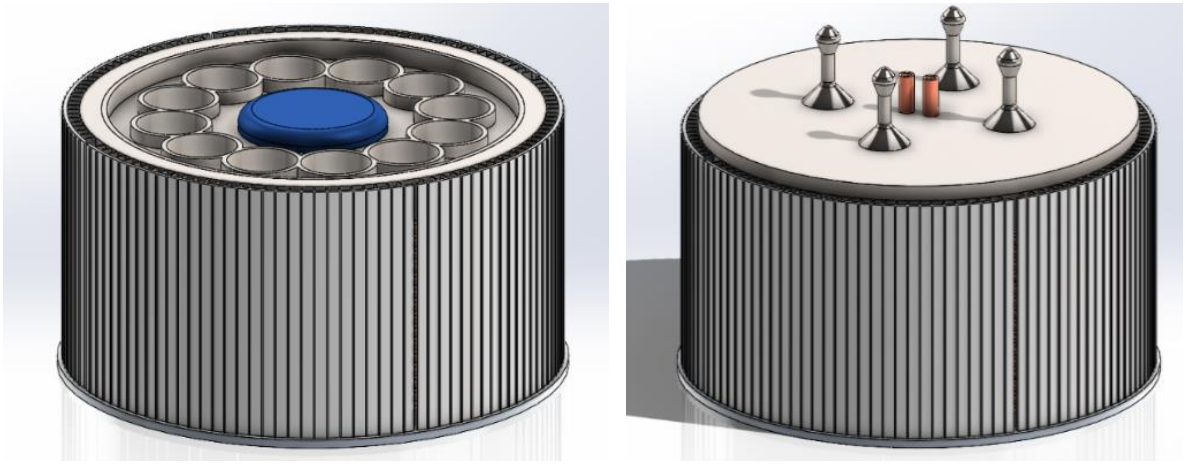

Figure 5.6.3.A. Sample Container With and Without Lid

The sample container is essentially a vapor-compression freezer laid out in several annular sections. At the center is the compressor assembly. The system utilizes a pair of compact oil-free scroll compressors to reduce potential contamination of the coolant which could clog lines and deteriorate cooling performance (there are two compressors because each one runs on an independent loop, as detailed below). On both sides of the sample tubes is a set of evaporator coils. The coils are contained in separate sealed chambers and immersed in heat transfer oil to facilitate the transfer of heat from the walls of the sample tubes and into the coolant. The inner and outer coils are two independent fluid loops to ensure the other can continue to provide cooling if the other begins leaking coolant. All of this is surrounded by a layer of aerogel insulation to prevent intrusion of heat from the external components or

environment. The outer surface of the container is wrapped in condenser coils, which in turn are in contact with radiators that reject the heat from the container. The condenser coils are laid out in a double helix, again with two separate and independent lines for fault tolerance (each helix is in a loop with one of the two evaporators).

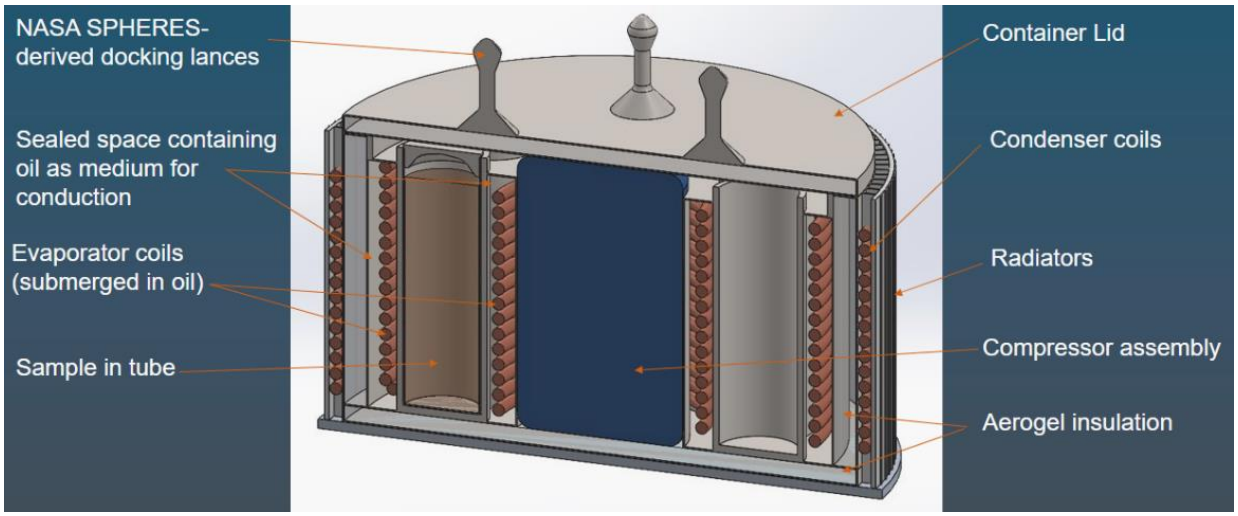

Figure 5.6.3.B. Sample Container Cross-Section and Components

5.7. Command & Data Handling

Much like the orbiter, the lander's electronics must be redundant and robust. The lander's computer modules share many of the orbiter's characteristics: radiation-hardened, with hardware redundancy in the form of multiple computers and software redundancy with built in fault tolerance. The Table below lists the specifications of the electronics that are part of the lander:

Table 5.7.A. Computer Components for the Lander

Name	Component
CPU	200 MHz BAE RAD750
RAM	256 MB
Flash Memory	1GB
EEPROM	256 KB
OS	VxWorks

The key differences between the electronics aboard the lander and the orbiter lie in the quantity of memory needed. The lander utilizes less RAM, as aside from communications, it has little need for processing power when compared with instrument-packed landers. As such, it requires less flash memory as well. It shares many of the hardware and software redundancies, however, to ensure that no critical computer failures can cripple the system.

5.8. Communications

Communication between the spacecraft and lander and Earth depends on establishing a telecommunications system that is capable of transmitting signals to and from Earth. The lander depends on receiving signals from Earth to carry out its missions, and it also needs to be able to relay information back to Earth to assist engineers in making sure that the lander functions properly, in the case of any system failures or just to guide the mission effectively.

Communications take place in the X-band in order to allow utilization of the Deep Space Network's (DSN) full range of antennas. The X-band low gain antenna (LGA) is primarily used for receiving commands and any other low-bitrate information from Earth (on the order of 10 bps). The steerable X-band high gain antenna (HGA) is capable of higher throughput direct to earth communications- uplink speeds are at least 3000 bps and downlink at least 800 bps through the DSN 70m antennas [32]. In addition to the direct to Earth communications, the lander contains a 400 MHz ultra-high frequency (UHF) antenna that allows communication with the Martian Relay Network at speeds of several megabits per second.

There is risk at certain times of the Martian day that the antennas may be shadowed by the lander solar arrays, disrupting communications. The LGA and HGA are both positioned at the back end of the lander such that will not be shielded by the solar panels during prime communication windows; this is the end of the lander that will be facing to the south on Mars, and as a result will have the least obstructed transmission path to and from the DSN on Earth.

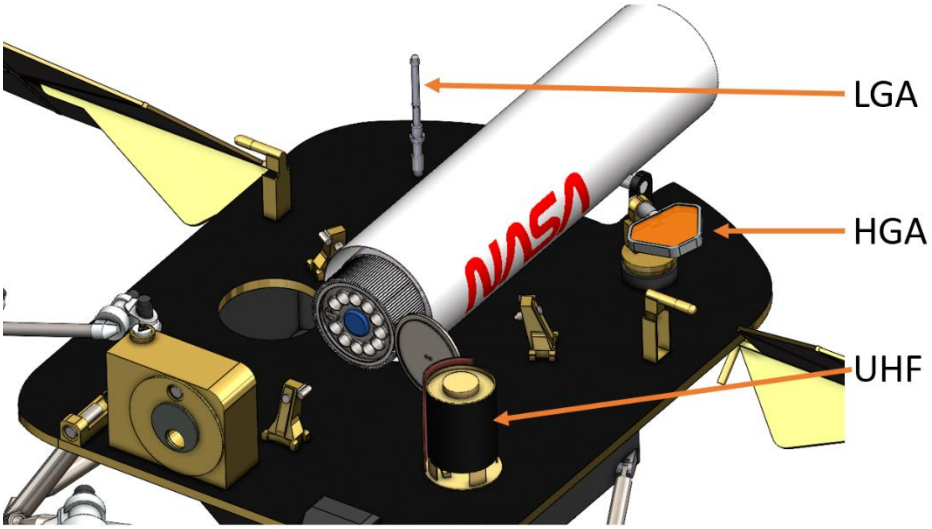

Figure 5.8.A. Lander Antennas

6. Mars Ascent Vehicle

The Mars Ascent Vehicle (MAV) is an important aspect to the sample return mission and is particularly challenging because there is no flight heritage for launching any vehicle off Mars. This vehicle must safely deliver a payload to low Martian orbit as well as allow for rendezvous and docking with the waiting orbiter to hand off the samples. This vehicle must be light and compact enough to fit within the descent aeroshell and land on the surface of Mars. It must also be able to be reliable operated after many months of being stored dormant in Martian surface conditions. An image of the complete design concept is shown in Figure 6.A below:

Figure 6.A. MAV Assembly and Exploded View

A summary graphic of the MAV internal design is shown in Figure 6.B. The design has a first stage diameter of 457 mm, second stage diameter of 381 mm, and an overall length of 2.27 m. The payload capacity of the vehicle to its

target 200 km circular orbit is approximately 22.1 kg, ample capacity to carry the sample containment system (mass allocation of 19.3 kg, including contingency) with the requisite 2.5 kg of ice cores,

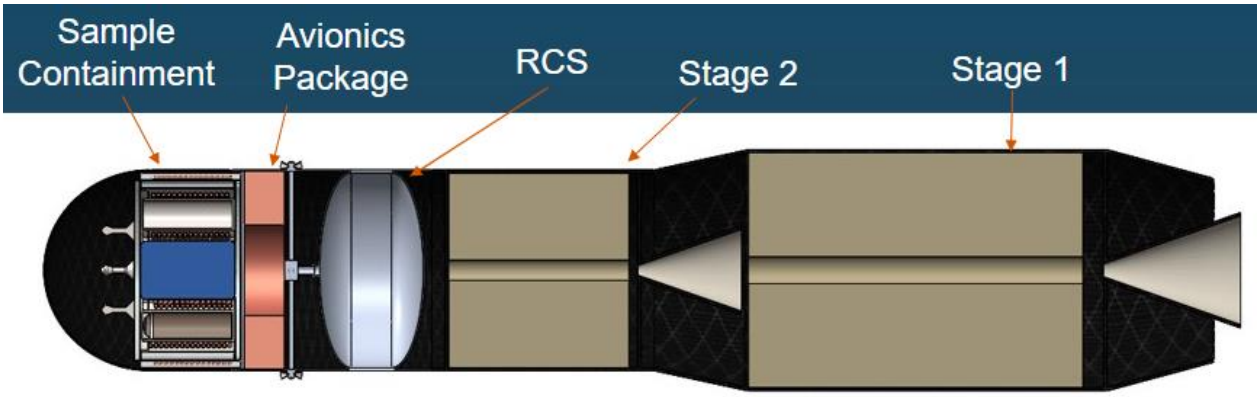

Figure 6.B. MAV Cross-Section

6.1. Requirements

The requirements for the MAV are driven by its main mission to bring the samples from the Martian surface to low Martian orbit. This must be a short amount of time to prevent the need for the MAV to contain its own power generation systems, as well as to allow the samples to be kept frozen by passive insulation and thermal inertia until being passed to the orbiter.

Table 6.1.A. MAV Requirements

REQ #	Requirement
MAV-001	The MAV shall be capable of delivering a payload of 22 kg to a 200 km circular Martian orbit.
MAV-002	The MAV shall have the ability to operate independently for up to 8 hours post separation from the lander.
MAV-003	The MAV shall be capable of communication and relative navigation with the orbiter to facilitate docking operations.
MAV-004	The MAV shall maintain its propellants above their minimum storage temperature to prevent embrittlement or cracking.
MAV-005	The MAV shall have the ability to maintain a constant set attitude on orbit for docking operations.
MAV-006	The MAV fairing shall be capable of closing around the sample container in the Martian environment and ejecting in space to reveal the docking adapter.

6.2. Mass Budget

The following is the mass budget for the MAV subsystems. The vast majority of the mass is propellant, and most other systems must be kept very lightweight.

	Level 3	Level 2			Level 1
	Breakdown	CBE	Contingency	Allocated	
1.0 Payload					19.3
1.1 Sample Containment System		17.5	1.8	19.3	
2.0 Ascent Vehicle					392.7
2.1 Propulsion		339.0	17.0	356.0	
2.1.1 Stage 1 Structure	32.2				
2.1.2 Stage 1 Propellant	214.6				
2.1.3 Stage 2 Structure	12.0				
2.1.4 Stage 2 Propellant	80.2				
2.2 ADCS (RCS Thrusters)		12.0	1.8	13.8	
2.2.1 Nozzles	0.5				
2.2.2 Tank and Plumbing	3.5				
2.2.3 Cold Gas	8.0				
2.3 Communications		6.0	0.6	6.6	
2.3.1 Low Gain/UHF Antennas	1.4				
2.3.2 Transponders	3.0				
2.3.3 Diplexers	0.6				
2.3.3 RF Switches, Cables, etc	1.0				
2.4 C&DH		1.5	0.2	1.7	
2.5 Power		5.4	0.5	5.9	
2.5.1 Batteries	2.6				
2.5.2 PMAD	1.8				
2.5.3 Wiring	1.0				
2.6 Structure		8.0	0.8	8.8	
2.6.1 Upper Section Skin	6.0				
2.5.2 Payload Fairing	2.0				

Figure 6.2.A. MAV Mass Budget

6.3. Propulsion

Two options were considered for the MAV propulsion architecture- a single stage hybrid fueled design as well as a two-stage solid design. The hybrid vehicle would provide more efficient propulsion, lower overall mass, and fewer separation events. Solid propellants are less expensive, more easily stored for extended periods, have much more significant spaceflight heritage, and result in an overall simpler system. A weighted decision matrix summarizing these factors was generated, and is presented in Table 6.3.A below:

Table 6.3.A. Method of MAV Propulsion Decision Matrix

Method Of Propulsion	Total Wet Mass Wt. = 2x		Thrust Wt. = 1x		Simplicity Wt. = 1.5x		Payload Mass Wt. = 2.5x		Cost Wt. = 1.5x		Weighted Total
	U	**W**	U	**W**	U	**W**	U	**W**	U	**W**	
Hybrid	6	**12**	4	**4**	4	**6**	6	**15**	4	**6**	43
Solid (2-Stage)	5	**10**	7	**7**	8	**12**	6	**15**	8	**12**	56
Key: U = Utility Value W = Weighted Value 10 = Best 0 = Worst											

Based upon this trade study, a two-stage solid-fueled MAV design was chosen. The decreased cost and schedule risk brought about by the decreased complexity and more substantial flight heritage of solid fuels are critical given the restrictive cost and time constraints of the mission.

Both the first and second stage motors are derived from the Northrop Grumman STAR 15G motor and have an I_{sp} of 280 s, a propellent mass fraction of 0.85, and an actuated nozzle for thrust vector control [33]. The adaptation of existing solid motor designs with significant spaceflight heritage (primarily as kick stages) reduces to cost and risk associated with the MAV propulsion system.

Modeling done by NASA to develop MAV requirements concluded that a vehicle lifting off Mars would require approximately 4115 m/s of ΔV to reach a 100 x 500 km elliptical orbit, after considering all appropriate losses (atmospheric drag, gravity, TVC cosine losses, etc.) [4] The MAV target in our proposed mission is a 200 km circular orbit, which has a nearly equivalent (in reality, slightly lower) specific energy. Thus, application of a 5% margin on top of this Figure produces a safe requirement for initial propulsion system design. MAV launch is slated to take place at a solar latitude of approximately 300°, which is near the point in the Martian year at which atmospheric density is the highest (See Figure 5.3.A) [13]. This does not have an appreciable impact on ΔV requirements, however, because drag losses only account for ~1% of the initial requirement. While atmospheric pressure variations are incredibly consequential for slowing down the vehicle from hypersonic speeds during EDL, they sit well within margin of error for MAV performance calculations – largely due to the small pressures involved and the fact that the MAV moves relatively slowly in the lowest and thickest portions of the atmosphere, thus experiencing little drag loss. Table 6.3.B provides a summary of the propulsion system mass and ΔV breakdown between the two stages- the ΔV was split evenly between the two stages in order to minimize the mass of the overall vehicle. (Note the total mass column represents the motors alone, and not the entire vehicle)

Table 6.3.B. MAV Propulsion System Breakdown

	Propellant Mass (kg)	Casing Mass (kg)	Total Mass (kg)	ΔV contribution (m/s)
Stage 1	214.6	32.2	246.8	2161
Stage 2	80.2	12.0	92.2	2161
Total	**294.8**	**44.2**	**339.0**	**4322**

6.4. Structures and Thermal

The MAV structure is made from lightweight graphite/epoxy composites. The outside is covered in a white, thermally resistant paint. The nose section of the vehicle, which contains the sample container, consists of two

fairing halves, which are stored next to the MAV through the entire mission until the MAV is ready to launch. The sample handling arm retrieves the fairings and places them on the front of the MAV, securing them into place. After the MAV launches and before rendezvous with the orbiter, the fairings are jettisoned via a pyrotechnic mechanism on orbit to reveal the docking adapter.

The section directly behind the fairings is a thin airframe that houses the RCS tank and avionics. The remainder of the rocket is the two motors, which are housed in filament wound casings and connected via more pyrotechnic staging mechanisms that allow them to be jettisoned in flight as their fuel is spent.

Small patch heaters are contained in the avionics bay to keep batteries and other sensitive components within their acceptable temperature ranges. There are also heaters placed on the propellant casings to prevent the propellant temperature from dropping so low that it experiences cracking or embrittlement. Insulation surrounding the MAV in its shroud on the lander assists in controlling the propellant temperature.

6.5. Power

The ascent vehicle will have two distinct power modes: sleep and ascent. The only power draw during sleep mode is temperature monitoring and thermal control, which is powered by the orbiter power system during cruise and the lander power system while on Mars. After disconnecting from the lander, the MAV will be powered by onboard lithium sulfur dioxide (Li-SO_2) primary batteries containing 720 W-hr of energy. This will allow the MAV system about 8 hours of operation post-separation. The process of launch and orbital rendezvous will nominally take approximately 2 hours, allowing a margin for error. The power budget for ascent vehicle subsystems is shown below in Figure 6.5.A, utilizing power allocation estimates from *Space Mission Engineering: The New SMAD* [10].

Ascent Vehicle Power Budget					
	Level 2				
	CBE	Cont.	Allocated	Level 1	
1.0 Payload				19.8	
2.0 MAV Bus (dry)				77.22	
2.1 Propulsion	9.9	0.99	10.89		
2.2 ADCS	10.8	1.08	11.88		
2.3 Communications	16.2	1.62	17.82		
2.4 C&DH	8.1	0.81	8.91		
2.5 Power	9	0.9	9.9		
2.6 Structure	2.7	0.27	2.97		
2.7 Thermal Control System	13.5	1.35	14.85		
2.8 Other (ECLSS, etc.)	0	0	0		
3.0 MAV Allocated Power				97.02	
4.0 Margin				19.404	
5.0 Total Power Available				116.424	Watts

Figure 6.5.A. MAV Power Budget

6.6. Other Systems

The MAV contains a cold gas RCS system and a high-pressure nitrogen tank for on-orbit maneuvering and attitude determination and control. The vehicle is controlled by an onboard redundant avionics package and includes both inertial guidance and set of small star trackers for attitude determination. A lightweight X-band communications system that allows communication with the lander and orbiter (but not directly to Earth) during flight. The MAV flight profile is designed such that it is always visible to the orbiter during ascent and rendezvous, allowing more detailed relative navigation data to be gathered by the orbiter's radar tracking instruments and then beamed to the MAV for docking guidance,

6.7. Ascent Trajectory and Orbiter Rendezvous

After final trajectory plans are uploaded and commands are received from mission control, the shroud on the lander will pivot to the upright position and the MAV will perform system checks prior to launch. It will transfer to internal power then ignite the first stage engine and lift off out of the shroud. The launch will take place when the orbiter is making a northward pass over the lander in its polar orbit, shortly after it is visible above the horizon. This allows the most direct trajectory possible for the MAV, reducing the amount of time before docking during which it must rely on its limited internal power systems. This trajectory will also ensure that the two vehicles remain within line of sight of each other at all times from launch to docking.

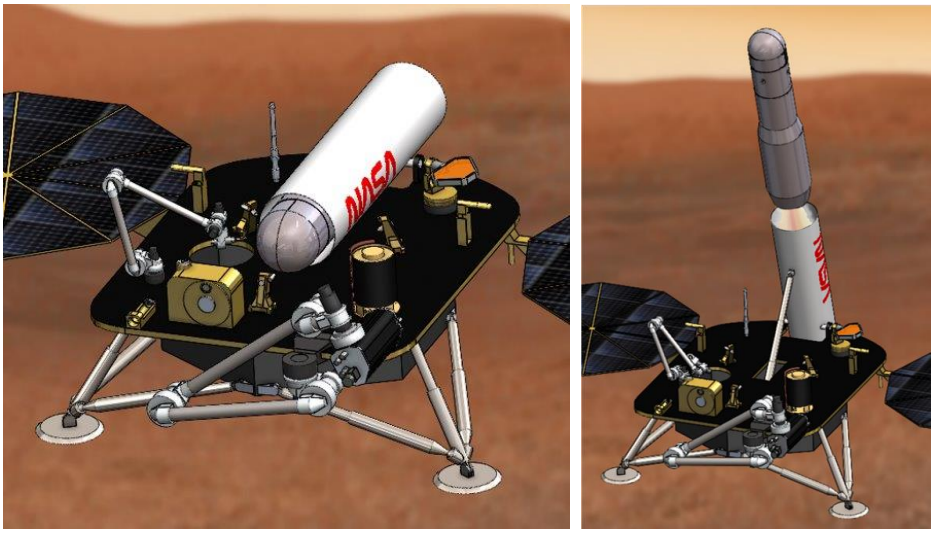

Figure 6.7.A. MAV Launch Sequence

As the first and second stage expend their fuel, they are jettisoned to reduce the vehicle mass. About 60 minutes from launch, the remaining pieces of the MAV (including the sample container) will rendezvous with the orbiter. The MAV maintains attitude while the orbiter uses its thruster to complete the docking sequence guided at first by

its radar instruments, and then by optical docking cameras once the vehicles are in proximity. The two vehicles dock using the docking adapter on the front of the sample container, reveled by jettisoning the payload fairing. The remainder of the MAV jettisoned once docking is complete, finishing the handoff of the samples to the orbiter.

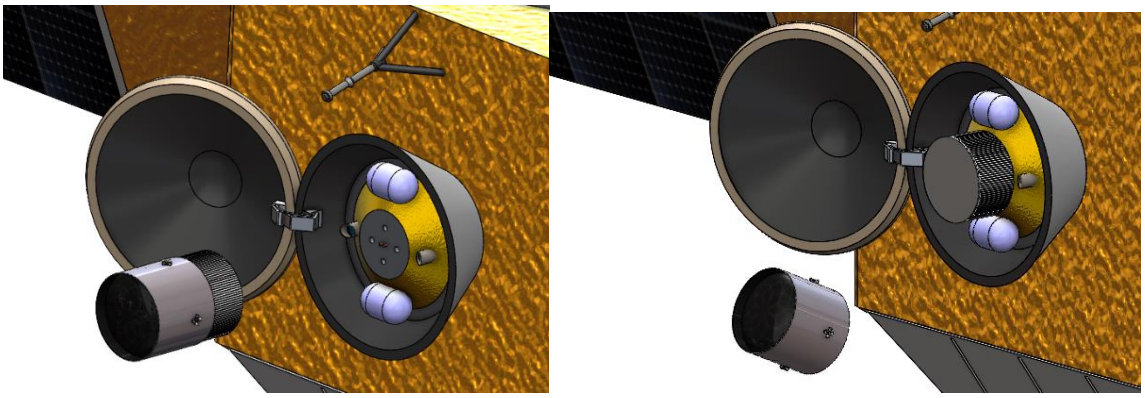

Figure 6.7.B. Staged MAV Approaching Orbiter (left) and Jettisoned after Docking with SRC (right)

7. Sample Return Capsule

The samples are stowed in a sample return capsule (SRC) derived from *OSIRIS-Rex* and *Stardust* heritage [9]. The capsule profile is a 70-degree sphere-cone aeroshell with a PICA heatshield and SLA on the back shell for thermal protection, scaled up 50% from the sample return capsules of these previous missions to accommodate the larger sample container and thermal control system.

Figure 7.A. SRC in Open and Closed Configurations

7.1. Requirements

Below are the requirements for the SRC:

Table 7.1.A. SRC Requirements

REQ #	Requirement
SRC-001	The SRC shall be capable of landing safely on Earth after reentry speeds of up to 12.9 km/s.

SRC-002	The SRC shall not allow the samples to melt at any point between receiving them from the MAV and collection by crews on Earth.
SRC-003	The SRC shall operate a locating beacon for at least 24 hours after landing to aid teams in recovery.
SRC-004	The SRC shall provide electrical and fluid interfaces to the sample container in order to facilitate active cooling

7.2. Operations

The sample return capsule begins the mission closed and attached to the side of orbiter and stays in this configuration until the MAV launch and rendezvous sequence. When the MAV and loaded sample container are en route, the hinge mechanism opens the heatshield to reveal the docking adapter to which the sample container attaches directly. The heatshield remains open throughout the duration of the return cruise phase in order to allow operation of the radiators on the sample container.

Just prior to separation and Earth entry, the heatshield closes and seals. Because the radiators on the sample container cannot operate with the heatshield closed, the cooling system switches to an open loop scheme during reentry and landing where heat is rejected by venting heated refrigerant overboard into the wake of the capsule. The SRC contains additional coolant reservoirs to facilitate cooling during this phase.

Once the heatshield is closed, the capsule is separated from the orbiter via a pyrotechnic mechanism that also imparts a small amount of rotation to keep the capsule passively stabilized until it hits the atmosphere. It performs reentry and then lands under its parachute near Point Barrow in Alaska. High temperatures during landing in June rarely exceed 7°C and are typically in the range of 2-5°C, so the environment will not be far above freezing between landing and retrieval. Precipitation (primarily rain) is minimal and snow cover is typically zero and the area receives nearly 24 hours of continuous sunlight per day, greatly aiding recovery operations [34]. The SRC contains a locator beacon and enough battery power to operate it for a full day, giving crews ample time to reach and retrieve the samples.

7.3. Internal Design

An internal schematic of the capsule is shown in Figure 7.3.A below. The uppermost portion contains the parachute and mortar system, used to decelerate the capsule to safe landing speeds during the Earth EDL phase. Surrounding this is an avionics and equipment deck that houses all the electronics required for the capsule's control systems. Below this is a conical docking adapter that houses the equipment needed to establish plumbing and electronic

connections to the sample container once it has docked. The front face of this cone contains the ports which physically connect the sample container to the capsule. Flanking this cone are two auxiliary coolant tanks, needed to provide a short-term supply of additional refrigerant to the sample cooling system during the open loop cooling phase. The sample container, once docked, occupies most of the internal space in the bottom portion of the vehicle.

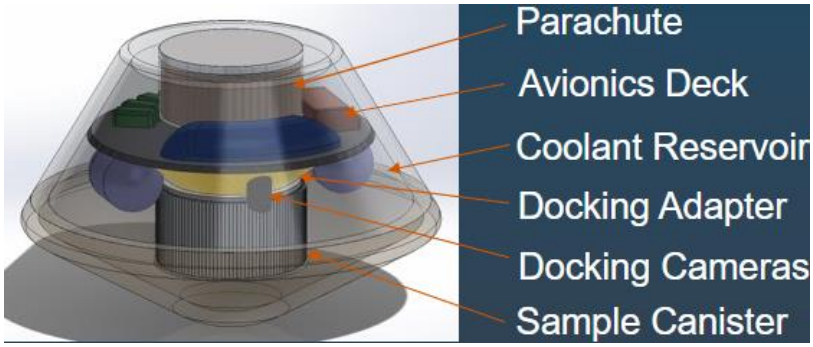

Figure 7.3.A. Schematic of SRC Internals

7.4. Docking System

The docking port is adapted from NASA's Universal Docking Port (UDP) developed for the SPHERES project on the ISS [35]. The same lance and latch design is used, but the orientation is modified such that all the lances are on the sample container in order to put the active side of the mechanism entirely on the side of the SRC. The lances also are modified to act as electrical contacts for the orbiter to supply power to the sample cooling system during cruise. A pair of central plumbing connections facilitates the flow of coolant from the auxiliary reservoirs into the sample container and from the sample container to the external vent. A mechanism within the docking adapter press-fits these plumbing connections together once the lances are latched into place. Though this design poses a relatively significant risk of some leakage, these lines are only in operation for a fleeting period of time during the open-loop cooling phase. Therefore, the threshold for acceptable leakage in this case is quite low.

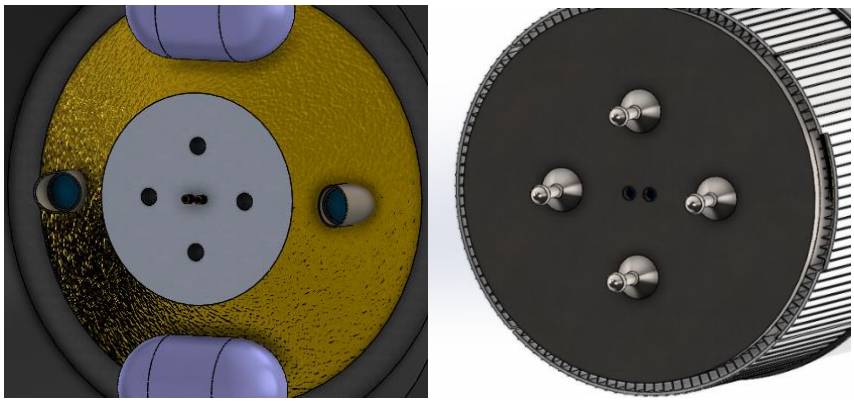

Figure 7.4.A. Details of Docking Adapter on SRC (Left) and Sample Container (Right)

8. Launch Vehicle Selection

The launch vehicle selection is constrained by the required C_3 of the Earth escape trajectory, combined wet mass of all spacecraft elements, cost of the launch, and fairing size. The minimum possible C_3 during the 2026 transfer window is 9.18 km^3/s^2. The only currently operating launch vehicle capable of meeting these requirements is the Falcon Heavy, which can carry a total of 5312 kg to a trajectory with a C_3 of 10 km^3/s^2 in its fully reusable configuration. Launching from Kennedy Space Center with a Falcon Heavy will cost a maximum of about $150 million, cheaper than any other available heavy lift launch vehicle. Because the standard fairing size offered by SpaceX is 5.2 m and the vehicle is compatible with the standard 1194 mm payload interface, no modifications will be necessary for the vehicle to launch this mission [36].

9. Mission Management

This section contains an overview of the mission's research and development schedule from concept studies to operations and sustainment. Then a risk analysis was performed detailing mission risks and mitigation. Finally, a detailed cost analysis with two cost models and breakdowns is discussed.

9.1. Mission Development and Operations Schedule

The mission schedule is constrained by the December 2030 deadline, and the R&D schedule is constrained by the Fall 2026 launch window. The deadline for this proposal is set as the end of Pre-Phase A and the beginning of the mission schedule. Because there is no new technology in this mission, there is no need for technology development schedules. Because much of the spacecrafts' designs are taken from past mission heritage, the challenges in this mission are of spacecraft integration, not of spacecraft design. The minimum length of times for each of the phases were determined, and a 33% margin of 16 months was added across the phases to allows for unexpected project delays without delaying the entire mission.

Nine months were allocated for Phase A and B each (including margin), followed by the Preliminary Design Review in November 2022. Sixteen months are allocated for Phase C to finalize the design and begin fabrication and ends with the critical design review in February 2024. Thirty-one months are allocated for Phase D for finishing fabrication, assembly and integration, and test and launch operations prior to launch. The final Assembly Test and Launch Operations readiness review is in November 2025, which can be delayed if the schedule margin is needed. The operational phase lasts from launch in Fall 2026 to Sample Return in June 2029, which is significantly before

the RFP deadline requirement. The design and operational phases and reviews before and after launch are listed in Figure 9.1.A.

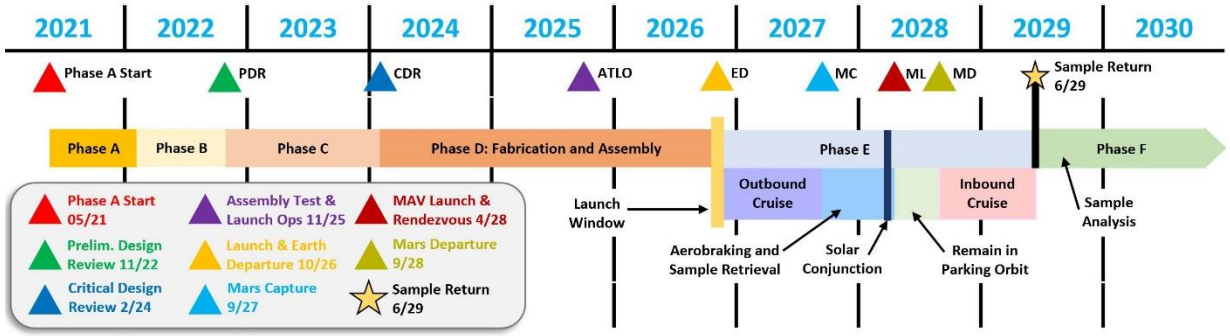

Figure 9.1.A. Mission Development and Operations Schedule

9.2. Risk Analysis

A key aspect of mission design is identifying technical and operational risks in different areas and creating strategies to mitigate them. Some risks to this mission and their associated mitigation strategies are summarized in the Table 9.2.A below. This list is not complete, but

Table 9.2.A Mission Risk Matrix

Risk	REQ #	Mitigation Strategy
Drill failure results in inability of lander to collect samples	SYS-003	Drill technology leverages development done for the Mars 2020 mission to maximize technology heritage and increase reliability.
Samples reach melting temperature during surface operations on Mars	SYS-005	Samples are placed into container with active cooling capability immediately after extraction. Lander is oriented to shade sample container from solar radiation.
Samples reach melting temperature during Earth EDL or before they can be collected after landing	SYS-006	Sample return capsule is cold soaked prior to release for lowest possible starting temperature. Active cooling system in container interfaces with SRC for open-loop cooling during EDL. Landing in cold climate with passive insulation prevents melting before retrieval.
Program costs exceed the $1B USD budget constraint	SYS-008	Systems with existing spaceflight heritage are used wherever possible to reduce cost and schedule risk.
Mass growth exceeds launch vehicle capacity	SYS-011	Current estimates show 15.8% mass margin to launch vehicle capacity. Option to expand capacity by expending center core of FH with minimal additional cost and schedule impact.
Spacecraft is not ready for 2026 launch window and sample return deadline cannot be met	SYS-010	Systems with existing spaceflight heritage are used wherever possible to reduce cost and schedule risk. The proposed development schedule includes 16 months of margin as of the beginning of Phase A.
Loss of orbiter due to solar conjunction during aerobraking phase prevents sample return	ORB-001	Aerobraking is planned to be paused during solar conjunction and resumed afterward to allow near constant monitoring.

Orbiter propulsion system fails or does not have sufficient Delta-V for sample return	ORB-003	15% margin is applied on Delta-V budget on top of conservative maneuver allocations to ensure adequate capacity. Flight-proven engine and fluid system designs are used to increase system reliability.
Orbiter HGA failure results in inability to monitor mission operations and issue commands	ORB-009	Orbiter contains redundant LGAs as well as UHF antennae that allow higher rate communications with other assets in area, so failure of HGA would be inconvenient but not a complete loss of mission.
EDL failure results in crash and complete loss of lander and mission	EDL-001	Skycrane EDL system with successful flight heritage in very similar and even more demanding conditions is used.
No ice in in reach of lander at landing location	EDL-002	Ice deposits are mapped from orbit prior to EDL and used ton construct maps which the EDL system's TRN software uses to select a landing site with access to ice.
EDL system fails to set down lander with appropriate azimuth angle	EDL-003	Margin for acceptable angle error is very large compared to accuracy of EDL ADCS sensors. MAV is capable of correcting any errors on launch using TVC.
Dust covering solar panels reduced power generation and makes mission operations impossible	LND-004	Lander can enter sleep mode during dust storms. Tilted arrays result in lower dust buildup. Relatively short operations period does not allow dust to accumulate.
Drill is trapped by ice melting and refreezing around it	LND-001	Temperature monitoring and drill speed modulation are used to ensure ice does not approach melting temperature during drilling.
Lander tips over due to mass imbalance when MAV is raised to vertical	LND-002	Landing legs are positioned such that the MAV center of mass never moves outside of the lander leg base.
Communications disruption due to shadowing of antennas.	LND-009	Landing at north side of crater prevents southern rim from significantly shadowing lander. Antennas located at back side to prevent obstruction of Earth (primarily in the south) by solar arrays.
MAV has insufficient Delta-V to reach target orbit	MAV-001	All sources of losses are considered in delta-V budget and 5% margin is applied on top of the total. Mass of samples will be measured to ensure payload capacity is not exceeded.
Samples melt or MAV runs out of power between launch and rendezvous	MAV-002	Trajectory is planned for fast rendezvous. Batteries sized for 8 hours, 4x the expected transit time of 2 hours. Passive insulation of samples gives high thermal inertia.
MAV does not have enough cold gas for rendezvous and docking maneuvers	MAV-005	The MAV is a completely passive vehicle while docking, only needing to maintain a certain attitude while the orbiter does the required maneuvering.
Samples melt from aerodynamic heating during Earth EDL	SRC-002	The SRC contains passive insulation and the ability to transition the sample container cooling system to open-loop using excess coolant reservoirs to actively reject heat from samples
SRC cannot be found before samples melt or beacon run out of power	SRC-003	Landing site is selected to be near Barrow, Alaska to provide a cold environment with long daylight hours and minimal precipitation/snow cover to aid recovery operation

9.3. Cost Analysis

NASA's Project Cost Estimating Capability (PCEC) [37] was used to cost this mission. PCEC uses NASA's library of cost estimating relationships (CERs) to develop a full cost breakdown across a mission's work breakdown structure

(WBS). The significant mission elements covered included spacecraft subsystems, assembly, integration & test, launch services, and operations. A model was also developed for comparison. This model was a Monte Carlo simulation that used CERs from Space Mission Engineering: The New SMAD [10] to develop a range of possible values for mission element cost outcomes. Cost analysis is critical to our mission because the RFP dictates our end-to-end mission cost cannot exceed $1 billion (in fiscal year 2020 US dollars).

9.3.1. Procedure

PCEC is NASA's main parametric cost estimation tool for spacecraft. It uses CERs derived from historical NASA data combined with user input about mission and spacecraft architecture to develop estimates for NASA's WBS. This program is incredibly reliable as it is heavily detailed, updated yearly, and uses NASA's vast collection of historical data for its CERs.

The important outputs for this program include subsystem, launch services, operations, and mission total cost. PCEC takes in input like mission architecture, subsystem mass, heritage ratings, and types of scientific payload to estimate cost. The mass inputs used are shown in Figures 2.3.A, 4.1.A, 5.1.A, 5.1.B, and 6.6.A. All numerical inputs such as mass and power required three inputs. The first was a point estimate, the second was a lower bound case, and the third was an upper bound case. This was so PCEC could make the best probabilistic estimate for cost.

To examine the validity of the PCEC model, two more cost estimates were made. One used CERs developed in Space Mission Engineering: The New SMAD to create a Monte Carlo simulation and another was NASA's Advanced Missions Cost Model.

The first step in the first comparison was developing the Monte Carlo simulation. Palisade's @Risk [38] was used for the simulation, which requires a model to run. The model for this cost analysis was a PERT distribution defined by the minimum, most likely, and maximum total mission costs. These were found by summing the minimum, most likely, and maximum costs for each mission element. To develop the model, cost estimating relationships were either found or generated for the following elements: spacecraft subsystems, integration, assembly, & test, launch services, and operations. The spacecraft subsystems included structural & thermal, attitude determination & control system, power system, propulsion, telemetry, tracking, & control, and communications.

The cost estimating relationships for the spacecraft subsystems and assembly, integration, & test came from Space Mission Engineering: The New SMAD. Costs were estimated for both one development & qualification unit and one

flight unit. The development & qualification unit cost relationships were found in Table 11-8. The flight unit cost relationships were found in Table 11-9. Both Tables use The Unmanned Space Vehicle Cost Model, Eighth Edition (USCM8) as the source of their cost estimating relationships. The data required to complete these estimates were mostly subsystem mass values. These mass values were obtained from the mass estimates completed for Spacecraft Systems Lab. Minimum, most likely, and maximum inputs were obtained by using mass estimates from team members. This allowed minimum, most likely, and maximum costs to be found for each element. Having these ranges of values allowed @Risk to create PERT distributions for each element.

To develop the cost estimating relationship for launch services and operations, The Planetary Society's Planetary Science Budget Dataset [39] was used to procure similar and recent Mars mission data. Determining minimum, most likely, and maximum costs for both launch services and operations allowed a PERT distribution to be made with the @Risk software.

9.3.2. Results

The cost estimate from the Project Cost Estimating Capability software is $1.009 billion. Figure 9.3.2.A shows the PCEC work breakdown structure with the total mission cost in the bottom-right cell. The most expensive elements that should be focused on are launch services, operations, spacecraft structures, and spacecraft communications.

Robotic Spacecraft

Units Conversion Factor: 1.000
FY2020 $M — Inflation Factor: 1.115

WBS #	Level	WBS Element	Non-Recurring	Design & Development	System Test Hardware	Flt Unit	Recurring Production	Non-Allocated	Operations	Total	Fee + Burden	Total w/ Fees & Burdens
0	1	System Name	$ 392.74	$ -	$ -	$ -	$ 295.09	$ 212.18	$ 109.16	$ 1,009.18	$ -	$ 1,009.18
1.0	2	Project Management	$ 6.97	$ -	$ -	$ -	$ 11.97	$ -	$ -	$ 18.94	$ -	$ 18.94
2.0	2	Systems Engineering	$ 15.79	$ -	$ -	$ -	$ 27.12	$ -	$ -	$ 42.91	$ -	$ 42.91
3.0	2	Safety and Mission Assurance	$ 7.71	$ -	$ -	$ -	$ 13.24	$ -	$ -	$ 20.95	$ -	$ 20.95
4.0	2	Science/Technology	$ -	$ -	$ -	$ -	$ -	$ 17.10	$ -	$ 17.10	$ -	$ 17.10
5.0	2	Payload(s)	$ 8.89	$ -	$ -	$ -	$ 13.01	$ -	$ -	$ 21.90	$ -	$ 21.90
5.01	3	Payload Management	$ 1.64	$ -	$ -	$ -	$ 2.41	$ -	$ -	$ 4.05	$ -	$ 4.05
5.02	3	Payload System Engineering	$ 3.72	$ -	$ -	$ -	$ 5.45	$ -	$ -	$ 9.17	$ -	$ 9.17
5.03	3	Payload Product Assurance	$ 1.82	$ -	$ -	$ -	$ 2.66	$ -	$ -	$ 4.48	$ -	$ 4.48
5.10	3	Instruments - EMPTY ROLLUP	$ -	$ -	$ -	$ -	$ -	$ -	$ -	$ -	$ -	$ -
5.x	3	Payload I&T	$ 1.70	$ -	$ -	$ -	$ 2.49	$ -	$ -	$ 4.20	$ -	$ 4.20
6.0	2	Flight System \ Spacecraft	$ 328.33	$ -	$ -	$ -	$ 155.04	$ -	$ -	$ 483.37	$ -	$ 483.37
6.01	3	Flight System Project Management	$ 3.94	$ -	$ -	$ -	$ 6.54	$ -	$ -	$ 10.47	$ -	$ 10.47
6.02	3	Flight System Systems Engineering	$ 8.92	$ -	$ -	$ -	$ 14.81	$ -	$ -	$ 23.73	$ -	$ 23.73
6.03	3	Flight System Product Assurance	$ 4.36	$ -	$ -	$ -	$ 7.23	$ -	$ -	$ 11.58	$ -	$ 11.58
6.10	3	Spacecraft	$ 307.03	$ -	$ -	$ -	$ 119.70	$ -	$ -	$ 426.73	$ -	$ 426.73
--	4	Structures & Mechanisms	$ 14.96	$ -	$ -	$ -	$ 74.95	$ -	$ -	$ 89.91	$ -	$ 89.91
--	4	Thermal Control	$ 1.91	$ -	$ -	$ -	$ 4.75	$ -	$ -	$ 6.66	$ -	$ 6.66
--	4	Electrical Power & Distribution	$ 12.43	$ -	$ -	$ -	$ 13.68	$ -	$ -	$ 26.10	$ -	$ 26.10
--	4	GN&C	$ 9.26	$ -	$ -	$ -	$ 16.68	$ -	$ -	$ 25.94	$ -	$ 25.94
--	4	Propulsion	$ 9.02	$ -	$ -	$ -	$ 9.63	$ -	$ -	$ 18.65	$ -	$ 18.65
--	4	Communications (SSPA)	$ 200.51	$ -	$ -	$ -	$ -	$ -	$ -	$ 200.51	$ -	$ 200.51
--	4	C&DH	$ 58.95	$ -	$ -	$ -	$ -	$ -	$ -	$ 58.95	$ -	$ 58.95
6.x	3	Flight System I&T	$ 4.08	$ -	$ -	$ -	$ 6.77	$ -	$ -	$ 10.86	$ -	$ 10.86
7.0	2	Mission Operations System (MOS)	$ 17.83	$ -	$ -	$ -	$ 62.31	$ -	$ 109.16	$ 189.30	$ -	$ 189.30
--	3	MOS/GDS Development (Phase B-D)	$ 17.83	$ -	$ -	$ -	$ 62.31	$ -	$ -	$ 80.14	$ -	$ 80.14
--	3	Mission Ops & Data Analysis (Phase E)	$ -	$ -	$ -	$ -	$ -	$ -	$ 109.16	$ 109.16	$ -	$ 109.16
8.0	2	Launch Vehicle/Services	$ -	$ -	$ -	$ -	$ -	$ 195.08	$ -	$ 195.08	$ -	$ 195.08
9.0	2	Ground Data System (GDS)	$ -	$ -	$ -	$ -	$ -	$ -	$ -	$ -	$ -	$ -
10.0	2	System Integration, Assembly, Test & Check Out	$ 7.22	$ -	$ -	$ -	$ 12.41	$ -	$ -	$ 19.63	$ -	$ 19.63
11.0	2	Education & Public Outreach	$ -	$ -	$ -	$ -	$ -	$ -	$ -	$ -	$ -	$ -

	Reserves %	Total w/Reserves	Total w/Fees, Burdens, & Reserves
Reserves	0%	$ 1,009.18	$ 1,009.18

Figure 9.3.2.A. PCEC Work Breakdown Structure

Figure 9.3.2.B displays the percentage cost of all Level 2 WBS elements.

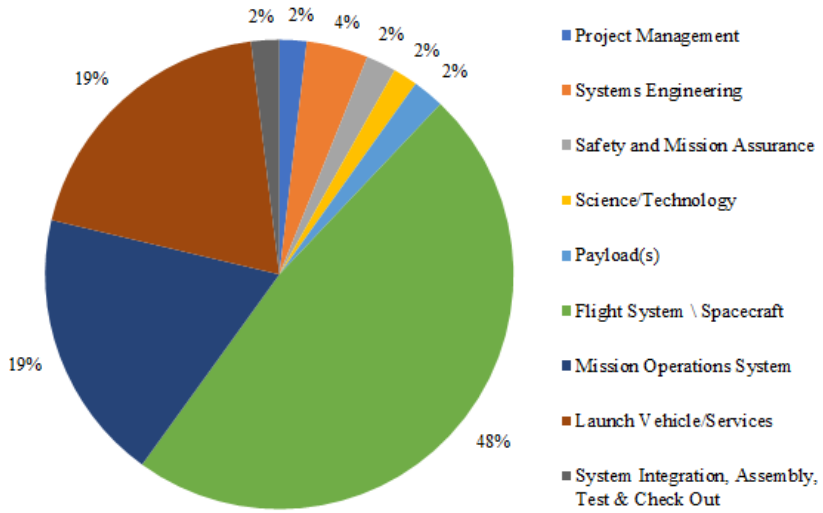

Figure 9.3.2.B. PCEC Total Cost Percentage Breakdown

Figure 9.3.2.C takes the "Spacecraft" section from the "Flight System \ Spacecraft" cost from Figure 9.3.2.B and breaks it down into its Level 4 WBS elements to display the corresponding percentage costs. These Level 4 WBS elements are the costs for the spacecraft's subsystems. It should be noted that the "Flight System Project Management", "Flight System Systems Engineering", and "Flight System Product Assurance" WBS elements are not included in this Figure but can be seen in Figure 9.3.2.A.

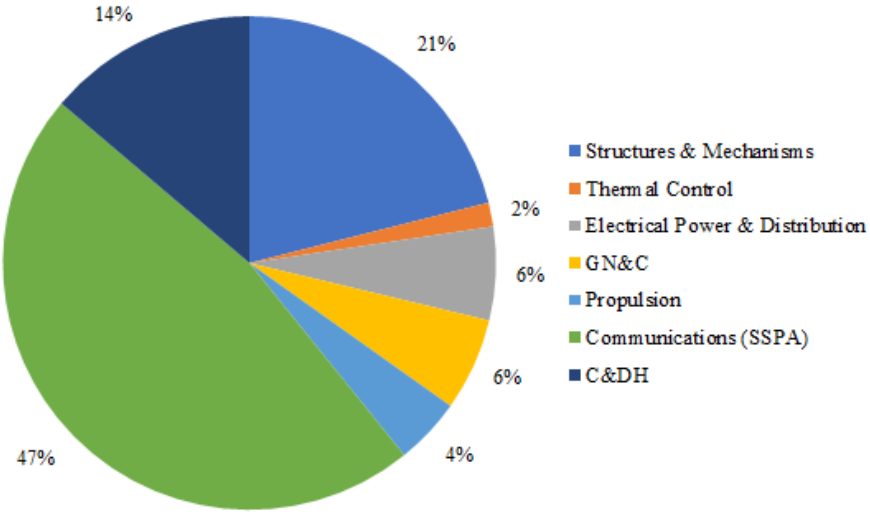

Figure 9.3.2.C. PCEC Spacecraft Cost Percentage Breakdown

The actual PCEC cost estimate should be much lower. The launch vehicle cost for this estimate is $195 million. Recent Falcon Heavy contracts from NASA have been around $120 million. The PCEC estimate is a $75 million overestimate. Therefore, the actual cost estimate for this mission is $934 million which is within budget.

For the Monte Carlo simulation, the probabilistic total cost of this mission is $847 million. Below is the completed cost model. Cost numbers in Figure 9.3.2.D are rounded to integers for ease of reading only. Actual calculations were not rounded.

Cost Component	CER Input Parameter	Minimum Value	Most Likely Value	Maximum Value	Units	Minimum Development + Qualification Unit Cost ($M)	Most Likely Development + Qualification Unit Cost ($M)
1.0 Spacecraft							
1.1 Structural & Thermal	mass	740	1108	1475	kg	59	78
1.2 ADCS	mass	143	214	285	kg	46	69
1.3 Power System	mass	501	751	1000	kg	32	48
1.4 Propulsion	devel: RCS tank volume	8860	75312	141764	cm^2	2	5
1.4 Propulsion (Continued)	flight: mass, burn time	310	465	619	kg		
1.5 TT&C	devel: none, flight: mass	167	250	332	kg	30	30
1.6 Communications	mass	95	143	190	kg	59	88
1.7 Integration, Assembly, & Test	bus + payload cost	228	318	405	2020 $M	44	62
2.0 Launch Services							
3.0 Operations							
Total Cost							

Cost Component	Maximum Development + Qualification Unit Cost ($M)	Minimum Flight Unit Cost ($M)	Most Likely Flight Unit Cost ($M)	Maximum Flight Unit Cost ($M)	Minimum Total Cost ($M)	Most Likely Total Cost ($M)	Maximum Total Cost ($M)	Probabilistic Cost ($M)
1.0 Spacecraft								
1.1 Structural & Thermal	95	17	25	33	76	103	128	103
1.2 ADCS	92	15	19	23	61	89	115	88
1.3 Power System	64	16	24	32	48	73	97	73
1.4 Propulsion	6				11	18	24	18
1.4 Propulsion (Continued)		9	13	18				
1.5 TT&C	30	12	15	17	42	45	47	45
1.6 Communications	117	18	27	36	77	115	153	115
1.7 Integration, Assembly, & Test	79	28	39	50	73	101	129	101
2.0 Launch Services					90	163	243	164
3.0 Operations					30	133	281	140
Total Cost					508	839	1218	847

Figure 9.3.2.D. The New SMAD Completed Cost Model

This probabilistic cost estimate is $87 million lower than the PCEC estimate. However, the PCEC estimate is still within this cost estimate's range. PCEC has a much higher level of detail and was updated more recently than the USCM8 that the CERs were drawn from. Therefore, the PCEC estimate should be more accurate. If PCEC is more

accurate, it points to a need for more serious mission adjustments to be made to cut costs. Thankfully, the PCEC estimate being close to this cost estimate is encouraging because this bolster's PCEC's validity. Furthermore, the similar cost elements on this estimate and the PCEC estimate were close.

The RFP for this mission dictates that the mission's max budget is $1 billion. Thus, the confidence interval is the probability that the total mission cost is between $0 and $1 billion. The confidence interval found for this range is 85.6%. Figure 9.3.2.E shows the probability density function for the total mission cost, which displays the confidence interval. Figure 9.3.2.E also shows the cumulative distribution function for the total mission cost. This Figure more easily displays the 85.6% probability of staying within budget.

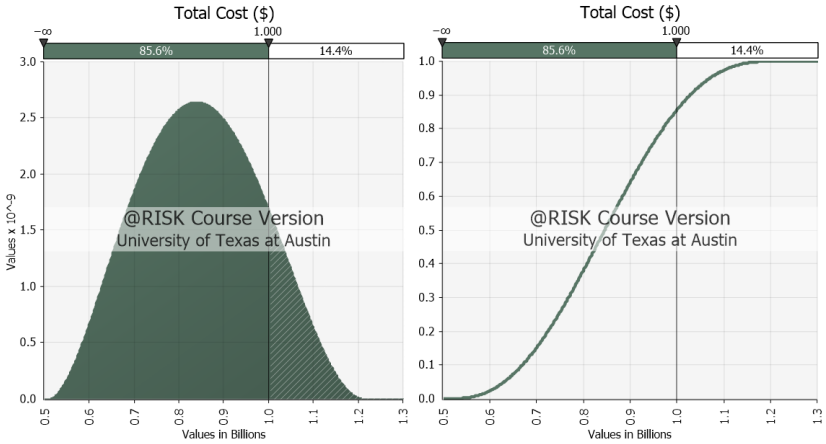

Figure 9.3.2.E. Probability Density Function & Cumulative Distribution Function of Mission Cost

9.3.3. Relevance to Mission

Cost analysis is extremely important to the design of this mission because this mission has a tight budget. Historically, NASA Mars missions have consistently been costly. For example, NASA's *Mars 2020* mission, whose *Perseverance* rover performs similar soil collecting duties to this mission, has cost almost $3 billion to date[3]. The RFP for this mission chose $1 billion as the max budget. This is extremely low and has been one of the greatest challenges of designing this mission from the start. This mission may not succeed if its funding runs out. Performing a cost analysis during mission design quantifies the cost of individual elements. Therefore, if the total predicted cost of the mission is over budget, the element estimates can show how the cost is distributed. This clarity allows mission changes to be made with confidence. As the mission details change, the confidence interval for staying within budget changes. Changes can be selected that produce a mission that is likely to be within budget.

9.3.4. Impact of Results on Design

For the PCEC estimate, a total mission cost of $934 million is encouraging. This mission can be accomplished within budget. With that said, this estimate is still close to $1 billion. Delays or errors could cause the cost to increase. Launch services, operations, spacecraft structures, and communications have the highest probabilistic costs out of all the cost elements. These mission cost elements will have to be watched closely to ensure that they don't cause the mission to go overbudget. Improvements could be made to ensure the mission doesn't exceed the budget. For the Monte Carlo simulation, a confidence interval of 85.6% for the mission budget is reassuring. However, a confidence interval of 95% or higher would be ideal. This means that costs should be cut to ensure the budget will not be exceeded. Both PCEC and the New SMAD estimates highlight where adjustments need to be made.

Launch services, operations, spacecraft structures, and communications have the highest costs out of all the cost elements. There are a few things we can do to trim cost. Using SpaceX's Falcon Heavy for this mission is the cheapest viable option, so nothing can be done to decrease launch costs at this time. To decrease operations costs, shortening the mission time span could be prudent. This could be accomplished by ensuring that less time is spent on Mars collecting samples. Using NASA's Mission Operations Cost Estimation Tool (MOCET) would be ideal to estimate a better operations cost. MOCET could help pinpoint cost elements to trim within operations cost. Decreasing the number of scientific instruments and choosing cheaper instruments could also decrease operations costs. Reducing communications weight would also greatly reduce its cost.

9.3.5. Cost Analysis Summary

The cost estimate from the Project Cost Estimating Capability software is $934 million. Our Monte Carlo simulation shows that our confidence interval for staying within a $1 billion budget is 85.6%. The most expensive mission cost elements are launch services, operations, spacecraft structures, and communications. These elements will have to be watched closely to ensure that they won't cause the mission to go over budget. Adjustments might even have to be made. This could include selecting a reducing communications weight and using MOCET. Overall, this mission is on track to stay within budget.

10. Conclusion

The *Glacies Nova* mission heavily relies on heritage to simplify the mission development process in order to stay within the restrictive one-billion-dollar budget. Most of the mission architecture is derived from previous Martian rover missions, such as *Curiosity* and *Perseverance*. The orbiter-lander system, in which the return vehicle remains in orbit, while the lander separates is derived from several older missions, including the *Viking* missions and several attempted Soviet/ESA missions. Additionally, the orbiter structure has an adapted *MRO* aerobraking architecture which allows for fuel savings and an all-in-one launch to Mars.

The key challenges faced in this mission include maintaining budget for the drill and sample handling design, integrating a reliable refrigeration system as well as adapting heritage architecture to allow for Mars ascent and Earth return. These crucial challenges do not exist in whole through heritage, rather only in concept studies or portions of missions. Sample return has been demonstrated by *Stardust* and soon by *OSIRIS-REx*, but not from a planet, which has a more substantial gravitational pull. These challenges are overcome by adapting past mission architecture and mending it to these concept studies that explore the topics in detail.

The *Glacies Nova* mission will pioneer a new leap forward in space exploration. The samples and data collected will broaden scientific understanding of the Martian environment, allowing scientist to understand its chemical makeup and the history buried beneath its soil. Future mission will be able to utilize this information to potentially create propellant and sustain ISRU systems. The area selected will provide ideal information for human exploration, and eventually colonization of Mars. The mission will also provide heritage for future missions utilizing unique concepts such as the refrigeration system, drill and sample handling system, MAV, and Earth return architecture.

11. Compliance Matrix

Table 11.A. Compliance Matrix – Design Requirements and Constraints

Req. #	Requirement	Explanation	Compliance	Page #
RFP-01	Design a robotic mission to the surface of Mars with the primary goal of returning a minimum of 2.5 kg of ice core samples back to Earth.	All relevant components for sample collection and return (lander with sampling system, MAV, sample return capsule) are defined and capable of returning at least 2.5 kg.	Yes	18-24
RFP-02	The designed system should deliver a robotic system that can land on or near Martian ice deposits.	Landing site selected in reference to known Martian surface ice distribution and EDL system is shown to be capable of delivering the lander in local worst-case conditions.	Yes	24-26, 47-52

RFP-03	The system should be capable of perform drilling operation on the Martian surface with the express purpose of retrieving ice core samples.	All critical elements of drilling and sample handling system are defined.	Yes	56-69
RFP-04	The ice core samples should be at least 25 millimeters in diameter, and 100 millimeters in length.	Sample handling system is sized for samples that meet this requirement.	Yes	62
RFP-05	The robotic system needs to be capable of storing the ice cores in a frozen state during surface operations.	Both active and passive thermal control are addressed for the sample container.	Yes	69-71
RFP-06	The system must return a minimum of 2.5 kg of ice cores in its frozen state back to Earth and accommodate the safe transfer of the ice cores to Earth-based laboratories in their frozen state.	Thermal control is addressed at each step of the sample return path from extraction to retrieval on Earth.	Yes	69-71, 79-81
RFP-07	Design and define the end-to-end mission operations, including launch, transit to Mars, entry/descent/landing, surface operation, ascent, and return to Earth.	Full concept of operations is defined for both landed and orbital segments of the mission.	Yes	18-24
RFP-08	Select a mission architecture and vehicle design that maximizes the science data return within the cost and schedule constraints.	Schedule and cost constraints drove selection of 2026 launch window. Cost considerations are mentioned throughout, and resulting cumulative cost estimated are addressed in the cost summary.	Yes	18-24, 27-35, 84-90
RFP-09	Discuss the selection of target locations and the values of the selected site, including the assessment criteria.	Landing site selection is thoroughly discussed (Section 3.3).	Yes	24-26
RFP-10	Perform trade studies on system options at the system and subsystem level to demonstrate the fitness of the chosen mission design. It is highly desirable to use technologies that are already demonstrated on previous programs or currently in the NASA technology development portfolio. Cost, schedule, and risk consideration of utilizing advanced technology must be included in proposal.	Trade studies are presented in the form of decision matrices for various systems throughout the report. Most systems are derived largely or entirely from heritage as a strategy to mitigate technical, cost, and schedule risks.	Yes	24, 30, 48, 56, 60, 69, 75
RFP-11	Discuss selection of subsystem components, including mass, power, and volume, and how the design requirements drove the selection of the subsystem.	Requirements, mass, and power budgets are presented at various levels of details for subsystems where appropriate. Volume allocation is done through detailed CAD models.	Yes	18, 35, 37, 39, 44, 46, 57, 75, 77

RFP-12	The cost for end-to-end mission shall not exceed $1 Billion US Dollars (in FY20), including launch, design development test and evaluation (DDT&E) and flight unit costs for the mission.	Cost analysis results show mission concept is within budget.	Yes	84-90
RFP-13	If advanced technology options are utilized in the design, estimation of technology advancement cost must be included.	The mission concept does not rely on advanced or underdeveloped technologies that would require significant development time, cost, or risk.	N/A	N/A
RFP-14	The ice core samples must be returned to Earth for scientific analysis no later than December 31, 2030.	The launch window and mission architecture are chosen such that samples will be returned before the end of the year 2030.	Yes	19, 83

Table 11.B. Compliance Matrix – Required Deliverables

Required Information	Page(s)
Executive Summary	11-15
Requirements Definition	17, 36, 45, 74, 79-80
Concept of Operations	18-24
Trade Studies	24, 30, 48, 56, 60, 69, 75
Design Integration and Operation	35-81
Cost Estimate	84-90
Schedule	83
References	94-97

References

[1] NASA's treasure map for water ice on Mars – NASA's Mars exploration program. (2019, December 19). Retrieved February 13, 2021, from https://mars.nasa.gov/news/8568/nasas-treasure-map-for-water-ice-on-mars/

[2] Piqueux, S., Buz, J., Edwards, C., Bandfield, J., Kleinböhl, A., Kass, D., & Hayne, P. (2019, December 17). Widespread shallow water ice on Mars at High Latitudes and Midlatitudes. Retrieved February 13, 2021, from https://agupubs.onlinelibrary.wiley.com/doi/epdf/10.1029/2019GL083947

[3] Perseverance rover Landing ellipse In Jezero CRATER – NASA's Mars exploration program. (n.d.). Retrieved May 04, 2021, from

[4] Greicius, T. (2015, February 23). Phoenix Mars lander. Retrieved February 13, 2021, from https://www.nasa.gov/mission_pages/phoenix/main/index.html

[5] Vallado, David A., and Wayne D. McClain. *Fundamentals of Astrodynamics and Applications*. Microcosm Press, 2013.

[6] Juanluis. (n.d.). Easy porkchop. Retrieved March 25, 2021, from http://sdg.aero.upm.es/index.php/online-apps/porkchop-plot

[7] You, T., Graat, E., Helsell, A., Highsmith, D., Long, S., Bhat, R., . . . Jah, M. (n.d.). Mars Reconnaissance Orbiter Interplanetary Cruise Navigation. *Jet Propulsion Laboratory, California Institute of Technology*. doi: https://ntrs.nasa.gov/api/citations/20080012702/downloads/20080012702.pdf

[8] Prince, J. L., & Striepe, S. A. (2007). Mars Reconnaissance Orbiter Operational Aerobraking Phase Assessment. *17th AAS/AIAA Space Flight Mechanics Meeting*. doi: https://ntrs.nasa.gov/api/citations/20070010460/downloads/20070010460.pdf

[9] Blau, P. (2021). OSIRIS-REx sample return Capsule – Osiris-rex: Spaceflight101. Retrieved February 12, 2021, from https://spaceflight101.com/osiris-rex/osiris-rex-sample-return-capsule/

[10] Wertz, J. R. (ed.), *Space Mission Engineering: The New SMAD*, 1st ed., Microcosm Press, Hawthorne, CA, 2015.

[11] PDF [In-Space Propulsion Data Sheets]. (2020, April 8). Aerojet Rocketdyne.

[12] Mars Reconnaissance Orbiter: The Mission. (n.d.). Retrieved February 13, 2021, from https://web.archive.org/web/20060331050959/http://mars.jpl.nasa.gov/mro/mission/sc_guide.html

[13] Martínez, G.M., Newman, C.N., De Vicente-Retortillo, A. et al. The Modern Near-Surface Martian Climate: A Review of In-situ Meteorological Data from Viking to Curiosity. Space Sci Rev 212, 295–338 (2017). https://doi.org/10.1007/s11214-017-0360-x

[14] Mars 2020/Perseverance Fact Sheet [PDF]. (2020, March). Washington D.C.: National Aeronautics and Space Administration.

[15] Way, D., Dutta, S., Zumwalt, C., & De Leon, S. S. (2020). EDL simulation results for the Mars 2020 landing Site safety assessment. *2020 IEEE Aerospace Conference*. doi:10.1109/aero47225.2020.9172525

[16] Pantano, D., Dottore, F., Tobery, E., Geng, S., Schreiber, J., and Palko, J., "Utilizing Radioisotope Power System Waste Heat for Spacecraft Thermal Management", NASA/TM, Vol. 2005, No. 213990, 2005. Prakash, R., Burkhart, P. D., Chen, A., Comeaux, K., Guernsey, C. S., Kipp, D. M., Lorenzoni, L. V., Mendeck, G. F., Powell, R. W., Rivellini, T. P., San Martin, A. M., Sell, S. W., Steltzner, A. D., & Way, D. W. (2008). Mars Science Laboratory Entry, Descent, and Landing System Overview. Jet Propulsion Laboratory, NASA Johnson Space Flight Center, NASA Langley Research Center.

[17] Johnson, A., Et. al. (n.d.). The Lander Vision System for Mars 2020 Entry, Descent, and Landing. *Jet Propulsion Laboratory*. doi: http://hdl.handle.net/2014/46186

[18] Weiss, J. M., & Guernsey, C. S. (2014). Design and Development of the MSL Descent Stage Propulsion System. In 2014 IEEE Aerospace Conference: Big Sky, Montana, USA, 1-8 March 2014. Piscataway, NJ: IEEE. doi: http://hdl.handle.net/2014/44893

[19] Sengupta, A., Steltzner, A., Steltzner, A., Rowan, J., & Cruz, J. (2008). Overview of the Mars Science Laboratory Parachute Decelerator Subsystem.

[20] Way, D. W., Powell, R. W., Chen, A., Steltzner, A. D., San Martin, A. M., Burkhart, P. D., & Mendeck, G. F. (2006, March). Mars Science Laboratory: Entry, Descent, and Landing System Performance. IEEE Aerospace Conference, Big Sky, MT

[21] Drake, Bret. (2009, July). Human Exploration of Mars Design Reference Architecture 5.0. Retrieved November 15, 2020, from https://www.nasa.gov/pdf/373665main_NASA-SP-2009-566.pdf.

[22] Bhandari, P., Birur, G., Bame, D., Mastropietro, A., Karlmann, P., Liu, Y., and Miller, J., "Performance Of The Mechanically Pumped Fluid Loop Lander Heat Rejection System Used For Thermal Control Of The Mars Science Laboratory Curiosity Lander On The Surface Of Mars", 43rd International Conference on Environmental Systems, 2013.

[23] Werner, J., Johnson, S., Dwight, C., and Lively, K., "Cost Comparison in 2015 Dollars for Radioisotope Power Systems -- Cassini and Mars Science Laboratory", 2016.

[24] "Final Environmental Impact Statement for the Mars 2020 Mission", Mars.nasa.gov Available: https://mars.nasa.gov/mars2020/files/mep/Mars2020_Final_EIS.pdf.

[25] "The Cost of Perseverance, in Context", The Planetary Society Available: https://www.planetary.org/articles/cost-of-perseverance-in-context.

[26] Levine, J., Kraemer, D., and Kuhn, W., "Solar radiation incident on Mars and the outer planets: Latitudinal, seasonal, and atmospheric effects", *Icarus*, Vol. 31, No. 1, 1977, pp. 136-145.

[27] Zacny, K., and Cooper, G., "Considerations, constraints and strategies for drilling on Mars", Planetary and Space Science, Vol. 54, No. 4, 2006, pp. 345-356.

[28] "Tungsten Carbides - an overview | ScienceDirect Topics", Sciencedirect.com Available: https://www.sciencedirect.com/topics/earth-and-planetary-sciences/tungsten-carbides.

[29] Staehle, Robert. (1976). Mars polar ice sample return mission. I. Spaceflight. 18. 383-390.

[30] Mellor, M., and Sellmann, P., General considerations for drill system design, Hanover, N.H.: Corps of Engineers, U.S. Army Cold Regions Research and Engineering Laboratory, 1975.

[31] Zacny, K., Bar-Cohen, Y., Brennan, M., Briggs, G., Cooper, G., Davis, K., Dolgin, B., Glaser, D., Glass, B., Gorevan, S., Guerrero, J., McKay, C., Paulsen, G., Stanley, S., and Stoker, C., "Drilling Systems for Extraterrestrial Subsurface Exploration", *Astrobiology*, Vol. 8, No. 3, 2008, pp. 665-706.

[32] Mars 2020 Communications. (n.d.). National Aeronautics and Space Administration, Jet Propulsion Laboratory Retrieved May 14, 2021, from https://mars.nasa.gov/mars2020/spacecraft/rover/communications/

[33] Home - Northrop Grumman. (n.d.). Retrieved February 13, 2021, from https://www.northropgrumman.com/wp-content/uploads/NG-Propulsion-Products-Catalog.pdf

[34] Thomas, B. (2010-2020). [Barrow Observatory Atmospheric Data]. Unpublished raw data. NOAA global Monitoring Laboratory

[35] LeVasseur, D. (2015, April 09). Universal docking PORT (UDP). Retrieved April 02, 2021, from https://www.nasa.gov/content/universal-docking-port-udp

[36] Performance website - home. (n.d.). Retrieved February 13, 2021, from https://elvperf.ksc.nasa.gov/Pages/Results.aspx

[37] Project Cost Estimating Capability, Software Package, Ver. 2.0, NASA, Washington, D.C., 2017.

[38] @Risk, Software Package, Ver. 8.0, Palisade, Ithaca, NY, 2020.

[39] Dreier, C., “Mars Missions,” *Planetary Science Budget Dataset* [online database],URL: https://docs.google.com/spreadsheets/d/e/2PACX-1vSngWs2AJa9KoPByrpX-XUgqD6UcMdjl3IW1xAW-m3yCvjreNM6d9KFWkshhxE_sPW9JmgmsaV0NwbG/pubhtml# [Retrieved 29 December 2020]

Additional Software Used

- AGI Systems Tool KIT (STK): https://www.agi.com/products/stk
- MathWorks MATLAB: https://www.mathworks.com/products/matlab.html
- Dassault Systemes Solidworks: https://www.solidworks.com/